universität wien

DISSERTATION / DOCTORAL THESIS

Titel der Dissertation /Title of the Doctoral Thesis

„To bundle or not to bundle F-actin?
Mechanism of calcium-regulation of α-actinin-2 from *Entamoeba histolytica*“

verfasst von / submitted by

mgr. Karolina Krystyna Zielinska

angestrebter akademischer Grad / in partial fulfilment of the requirements for the degree of

Doctor of Philosophy (PhD)

Wien, 2018 / Vienna 2018

Studienkennzahl lt. Studienblatt / degree programme code as it appears on the student record sheet:	A 794 685 490
Dissertationsgebiet lt. Studienblatt / field of study as it appears on the student record sheet:	Molekulare Biologie
Betreut von / Supervisor:	Univ.-Prof. Dipl.-Ing. Dr. Kristina Djinovic-Carugo

“Beyond a certain point there is no return.

This point has to be reached.”

Franz Kafka

ACKNOWLEDGEMENTS

I would like to express my profound gratitude to Prof. Kristina Djinović-Carugo for giving me the opportunity to join her research group and a fascinating project to work on. In her group I finally found a place where I could complete my Ph.D. I am grateful for all kind of support and constructive criticism I was given and for all our endless and stimulating scientific discussions. I am thankful for the trust she put in me and for the time she gave me to learn and to become a better researcher. Not to mention her stimulating me to run my first half-marathon :)

I appreciate that Dr. Tim Clausen (IMP), Dr. Thomas Marlovits (IMBA) and Dr. Ivan Yudushkin (MFPL), all agreed to invest their time to be my Ph.D. committee members.

I am grateful to Prof. Roberto Dominguez and Prof. Jari Ylänne for reviewing my thesis.

I would like to thank Dr. Thomas Leonard, Prof. Sasha Martens and Prof. Jari Ylänne to invest their time in being my PhD examiners.

During my Ph.D. I went through all the phases depicted in "The Last Judgement" of Hieronymus Bosch, from elation to deep desperation, back and forth. I am indebted to my colleagues for creating a wonderful working atmosphere which helped to protect my sanity during those four years. My special thanks go to Dr. Joan Lopez Arolas for being my supervisor for over three years, for his guidance, many useful tips, stimulating discussions, his valuable help with writing the manuscript as well as for the proof-reading of my thesis. And for sharing the passion for BARÇA! I would like to express my gratitude to our always cheerful Actin Expert Dr. Julius Kostan for his time, huge dose of patience and looooooong discussions. I am thankful to Claudia Schreiner for providing actin for my experiments. Thank you Dr. Martin Puchinger for being my Fluorescence Mate and also occasionally, running partner.

I consider myself lucky to have worked with and to share office with Antonio Sponga, Eneda Höllerl and Tobias Thöni who was also my lunch mate. I was blessed to work and share expertise with Sara Sajko, Dr. Georg Mlynek, Valeria Stefania, Tamara Sijacki, Eduardo Bezerra, Dr. Gustavo Arruda Bezerra, Dr. Euripedes de Almeida-Ribeiro, Dr. Irina Grishkovskaya, Dr. Dalibor Milić, Dominic Pühringer, Miriam Pedron, Tamás Hatfaludi, Tamara Sijacki, Slobodan Vujin and Thomas Pühringer. You all created fantastic (although sometime quirky) atmosphere.

Though I prefer to run alone, in some cases relay is better, as it was in the case of this project. Crystallography work was started by Claudia Schreiner, who purified ABD and rod domains of α-actinin-2 from *Entamoeba histolytica* (*Eh*Actn2), which were subsequently crystallized by Dr. Muhammad Bashir Khan, who also crystallized and solved the structure of Ca^{2+}-bound *Eh*Actn2 in tetragonal space group. Ca^{2+}-bound *Eh*Actn2 was crystallized in orthorhombic space group by Dr. Eirini Gkougkoulia and the structure was solved by Dr. Nikos Pinotsis. Dr. Joan Lopez Arolas solved the structure of ΔCa variant. In all cases final refinement of the structures was performed by Dr. Nikos Pinotsis. Although I have never worked directly with Prof. Alok Bhattacharya and Dr. Mrigya Babuta (Jawaharlal Nehru University, New Delhi), all the *in vivo* experiments were done thanks to uplifting collaboration we had together. It was my pleasure to work with Dr. Luciano Ciccarelli from Thomas Marlovits lab, who provided us with high quality EM micrographs.

Special thanks go to Gerlinde Aschauer for her understanding, time and help with straightening my chaotic paper work.

I am indebted to my parents Małgorzata and Tomasz. They gave me more than could be contained in one sentence and even more so as I was not an easy kid.

And of course – thank you my Zarghoon, for everything.

Without the help I received all the way through until here I would not be in this place now. I apologize if I did not list everybody who contributed to my success and helped me to grow.

PREFACE

The project presented in this thesis is the continuation of the work started by some colleagues before I joined Kristina Djinovic's group. Before my arrival the crystal structure of Ca^{2+}-bound α-actinin-2 from *Entamoeba histolytica* (*Eh*Actn2) had been solved by Dr. Nikos Pinotsis. Moreover, Dr. Eirini Gkougkoulia had generated an *Eh*Actn2 Ca^{2+}-insensitive variant (ΔCa). In order to explain how *Eh*Actn2 is regulated by Ca^{2+}, I first obtained diffracting crystals of the ΔCa variant, whose structure was solved by Dr. Joan Lopez Arolas and further refined by Dr. Nikos Pinotsis. Next, I generated and purified a large collection of *Eh*Actn2 constructs and performed most of the biochemical and biophysical assays presented here, such as Ca^{2+}-binding assays, protein stability measurements, circular dichroism spectroscopy, static light scattering experiments, actin co-sedimentation assays, etc. In this thesis I present my findings in the context of Ca^{2+}-bound *Eh*Actn2 and ΔCa variant crystal structures. Time-resolved fluorescence measurements were conducted by Dr. Martin Puchinger and negative staining microscopy images were collected by Dr. Luciano Ciccarelli (Thomas Marlovits lab, IMBA). Finally, biochemical and biophysical data were supported by *in vivo* experiments performed by Dr. Mrigya Jnu in the group of Prof. Alok Bhattacharya (Jawaharlal Nehru University, New Delhi).

TABLE OF CONTENTS

LIST OF ACRONYMS

ABD	actin-binding domain
ABP	actin-binding protein
ABS	actin-binding site
Actn	α-actinin
ADF	actin-depolymerizing factor
AMP	adenosine 5′-monophosphate
ADP	adenosine 5′-diphosphate
ATP	adenosine 5′-triphosphate
Bis-tris	2-bis(2-hydroxyethyl)amino-2-(hydroxymethyl)-1,3-propanediol
CaBP	Ca^{2+}-binding protein
CBP40	Ca^{2+}-binding protein 40
CaM	calmodulin
CD	circular dichroism
CD2	cluster of differentiation 2
CH	calponin homology domain
DLS	dynamic light scattering
DSF	differential scanning fluorimetry
DTT	dithiotreitol
EDTA	ethylenediaminetetraacetic acid
EFhd2	EF-hand domain-containing protein D2
EGTA	ethylene glycol-bis(2-aminoethylether)-N,N,N′,N′-tetraacetic acid

*Eh*Actn2	α-actinin-2 from *Entamoeba histolytica*
*Eh*C2PK	C2-domain-containing protein kinase from *Entamoeba histolytica*
EM	electron microscopy
ESRF	European Synchrotron Radiation Facility
FSGS	focal segmental glomerulosclerosis
GA	Gibson assembly
GDP	guanosine 5’-monophosphate
GFAP	glial fibrillary acidic protein
GSSG	oxidized glutathione
GTP	guanosine 5’-triphosphate
ϒTuRC	ϒ-tubulin ring complex
HEPES	4-(2-Hydroxyethyl)piperazine-1-ethanesulfonic acid
IF	intermediate filament
ITC	isothermal titration calorimetry
LM	ligand mimic helix
MALLS	multiangle laser light scattering
MS	mass spectrometry
MW	molecular weight
NMR	nuclear magnetic resonance
PCR	polymerase chain reaction
PDB	Protein Data Bank
PEG	polyethylene glycol
PI3K	phosphatidylinositol-4,5-bisphosphate 3-kinase

PIP_2	phosphatidylinositol 4,5-bisphosphate
QC	QuikChange site-directed mutagenesis
SDM	site-directed mutagenesis
SDS-PAGE	sodium dodecyl sulfate polyacrylamide gel electrophoresis
SEC	size exclusion chromatography
SLS	static light scattering
TCEP	tris(2-carboxyethyl)phosphine hydrochloride
Tm	melting temperature
TnC	troponin C
TEV	Tobacco Etch Virus
WT	wild-type

ABSTRACT

α-Actinin is a major cytoskeletal protein found in almost all organisms with the exception of plants and prokaryotes, which belongs to the spectrin superfamily of proteins that crosslink actin filaments into extended networks or bundles. Although it was first reported in 1981 that bundling ativity of non-muscle α-actinin is negatively regulated by Ca^{2+} ions (Burridge & Feramisco, 1981), the molecular mechanism behind this event has not been unraveled until now. This work aims at understanding the molecular basis of α-actinin function inhibition by Ca^{2+}, with focus on α-actinin isoform 2 from *Entamoeba histolytica* (*Eh*Actn2), a dangerous human pathogen that causes more than 10,000 deaths annually. *Eh*Actn2 shows 30% sequence identity with human non-muscle homologs, but contains a shorter rod domain (two central spectrin-like repeats (SR) *vs*. four in human proteins), thus representing a common ancestor of eukaryotic α-actinins (Virel, Addario et al., 2007, Virel & Backman, 2007).

The crystal structure of Ca^{2+}-bound *Eh*Actn2 revealed an overall antiparallel dimeric topology similar to that of human α-actinins, which allows the protein to crosslink actin filaments. Accordingly, each protomer comprises an N-terminal actin binding domain (ABD) followed by a continuous α-helix known as the neck, a central rod domain built by spectrin-like repeats, and a C-terminal calmodulin-like (CaM) domain comprising four EF-hand motifs separated into two distinct lobes (EF1-2 and EF3-4). In contrast to human α-actinins, in *Eh*Actn2 EF1-2 is sandwiched between SRs. In addition, and similarly to the human counterpart, EF3-4 wraps around the neck from the adjacent protomer *via* hydrophobic interactions and regulates in this way the position of ABD. A twist embedded in the rod domain positions ABDs on the opposite end of the molecule perpendicular to each other in the Ca^{2+}-bound form, resulting in a protein which cannot bundle F-actin.

In order to further enlighten the impact of Ca^{2+} on *Eh*Actn2, a Ca^{2+}-insensitive *Eh*Actn2 variant (ΔCa) was designed and its crystal structure determined, revealing increased flexibility of ABD and EF-hands. Comparison of Ca^{2+}-bound and Ca^{2+}-free structures solved in the same space group and at comparable resolution, together with differential scanning fluorimetry and limited proteolysis, demonstrated that Ca^{2+}-binding to *Eh*Actn2 stabilizes the protein structure.

Isothermal titration calorimetry experiments were used to assess Ca^{2+}-affinity of *Eh*Actn2 EF1-2, which was found to be extremely high (low nanomolar range). Subsequently, it was shown that *Eh*Actn2 can also bind Mg^{2+}, albeit with lower affinity, and that the competition between both ions would, therefore, enable

*Eh*Actn2 to be regulated *in vivo*. Moreover, using static light experiments (SLS) we found that ion binding exerts very subtle changes in the protein structure in solution.

Subsequently, F-actin bundling experiments were used to assess the impact of Ca^{2+} and Mg^{2+} ions on *Eh*Actn2 function. As reported before, Ca^{2+} reduces *Eh*Actn2 bundling (Virel et al., 2007), whereas we here showed that Mg^{2+} does not, which implies that this α-actinin is indeed a truly Ca^{2+}-regulated protein. Moreover, the mutant in which EF3-4/neck contact was abrogated, resulting in a highly flexible ABD, as assessed by SLS, was not able to bundle F-actin, which highlights the subtlety behind *Eh*Actn2 regulation. Similarly, removal of CaM domain completely abolished actin bundling by *Eh*Actn2, which could be rescued in a Ca^{2+}-dependent manner by the presence of an integral CaM domain. Furthermore, effective cross-talk between EF1-2 and EF3-4 requires that the former is positioned between SRs, as evinced by using a chimeric construct where the rod domain from *Eh*Actn2 was substituted with the closed rod from *h*Actn2, resulting in the loss of Ca^{2+}-dependence in *Eh*Actn2.

Taken together, this work provides the first structure of a Ca^{2+}-regulated α-actinin and uncovers the mechanism of its regulation in a human parasite. We prove that *Eh*Actn2 function requires multi-domain communication. Accordingly, Ca^{2+} binding to EF1-2 affects EF3-4/neck interaction and ultimately modulates the position of ABD, which in turn affects the protein capacity to bundle actin filaments. Although this molecular mechanism may partially apply to human Ca^{2+}-regulated α-actinins, *Eh*Actn2 has unique features, namely its high affinity for Ca^{2+} ions and an open rod domain resulting from the insertion of EF1-2. Since *Eh*Actn2 is a cytoskeletal protein, we envision that it might play a crucial role in the mobility and pathogenicity of *E. histolytica*.

ZUSAMENFASSUNG

α-Actinin ist ein wichtiges Zytoskelett-Protein, das in fast allen Organismen, mit Ausnahme von Pflanzen und Prokaryoten, vorkommt. Es gehört zur Superfamilie der Spektrine, die Aktinfilamente zu ausgedehnten Netzwerken oder Bündeln quervernetzen. Obwohl 1981 erstmals berichtet wurde, dass die Bündelung die Aktivität von Nichtmuskel-α-Actinin durch Ca^{2+}-Ionen negativ reguliert (Burridge & Feramisco, 1981), wurde der molekulare Mechanismus dahinter bisher nicht entschlüsselt. In dieser Arbeit wird die molekulare Basis der α-Actinin-Regulation durch Ca^{2+} mit Schwerpunkt auf α-Actinin-Isoform 2 aus *Entamoeba histolytica* (im Folgenden *Eh*Actn2), einem gefährlichen menschlichen Parasit, der jährlich mehr als 10 000 Todesfälle verursacht, untersucht. *Eh*Actn2 zeigt 30% Sequenzidentität mit humanen Nicht-Muskel-Homologen, enthält aber eine kürzere „rod domain" (zwei zentrale Spektrin-ähnliche Repeats (SR) *vs*. vier in menschlichen Proteinen), stellt also einen gemeinsamen Vorfahren eukaryotischer α-Actinine (Virel, Addario et al., 2007, Virel & Backman, 2007) dar.

Die Kristallstruktur von Ca^{2+}-gebundenem *Eh*Actn2 zeigte eine antiparallele Dimer-Topologie auf, die jener von menschlichen α-Actininen ähnlich ist und die dem Protein die Vernetzung von Aktinfilamenten ermöglicht. Dementsprechend umfasst jedes Protomer eine N-terminale Aktinbindungsdomäne (ABD), gefolgt von einer kontinuierlichen α-Helix, bekannt als „neck", einer zentralen „rod domain", die aus spektrinartigen Wiederholungen (SRs) aufgebaut ist, und einer C-terminalen Calmodulin-ähnlichen (CaM) Domäne. Diese wiederrum besteht aus vier EF-Hand-Motiven, die in zwei unterschiedliche Lappen (EF1-2 und EF3-4) unterteilt sind. Im Gegensatz zu menschlichen α-Actininen befindet sich EF1-2 in *Eh*Actn2 zwischen den SRs. Darüber hinaus, und ähnlich dem menschlichen Gegenspieler, umwickelt EF3-4 über hydrophobe Wechselwirkungen den „neck" des benachbarten Protomers und reguliert auf diese Weise die Position der ABD. Durch einen in der „rod domain" eingebetten Twist positionieren sich die ABDs am gegenüberliegenden Ende des Moleküles senkrecht zueinander in Ca^{2+} -gebundener Form, was ein Protein formt, das F-Aktin nicht bündeln kann.

Die Kristallstruktur von Ca^{2+}-gebundenem *Eh*Actn2 zeigte eine antiparallele Dimer-Topologie auf, die jener von menschlichen α-Actininen ähnlich ist und die dem Protein die Vernetzung von Aktinfilamenten ermöglicht. Dementsprechend umfasst jedes Protomer eine N-terminale Aktinbindungsdomäne (ABD), gefolgt von einer kontinuierlichen α—Helix, bekannt als „neck", einer zentralen „rod domain", die aus spektrinartigen Wiederholungen (SRs) aufgebaut ist, und einer C-terminalen Calmodulin-ähnlichen (CaM) Domäne. Diese wiederrum besteht aus vier EF-Hand-Motiven, die in zwei unterschiedliche Lappen (EF1-2

und EF3-4) unterteilt sind. Im Gegensatz zu menschlichen α-Actininen befindet sich EF1-2 in *Eh*Actn2 zwischen den SRs. Darüber hinaus, und ähnlich dem menschlichen Gegenspieler, umwickelt EF3-4 über hydrophobe Wechselwirkungen den „neck" des benachbarten Protomers und reguliert auf diese Weise die Position der ABD. Durch einen in der „rod domain" eingebetten Twist positionieren sich die ABDs am gegenüberliegenden Ende des Moleküles senkrecht zueinander in Ca^{2+} -gebundener Form, was ein Protein formt, das F-Aktin nicht bündeln kann.

Um die Auswirkungen von Ca^{2+}-auf *Eh*Actn2 zu entschlüsseln, wurde die *Eh*Actn2-Mutante (im Folgenden ΔCa) produziert und ihre Kristallstruktur bestimmt. Diese ergab eine erhöhte Flexibilität von ABD- und EF-Händen. Der Vergleich von Ca^{2+} -gebundenen zu Ca^{2+} -freien Strukturen, mit selbiger „space group" und bei vergleichbarer Auflösung gelöst, zeigte, zusammen mit Differential-Scanning-Fluorimetrie und begrenzter Proteolyse, dass die Ca^{2+} -Bindung an *Eh*Actn2 die Proteinstruktur stabilisiert.

Isotherme Titrationskalorimetrie-Experimente wurden durchgeführt, um die Ca2+ -Affinität von EhActn2 EF1-2 zu bestimmen. Diese ewies sich als extrem hoch (niedriger nanomolarer Bereich). Anschließend wurde gezeigt, dass *Eh*Actn2 auch Mg^{2+} binden kann, wenngleich mit geringerer Affinität, und dass die Konkurrenz zwischen beiden Ionen es daher ermöglicht, *Eh*Actn2 *in vivo* zu regulieren. Darüber hinaus wurde mithilfe von statischer Lichtstreuung (SLS) herausgefunden, dass die Ionenbindung sehr subtile Veränderungen der Proteinstruktur zeigt.

Anschließend wurde der Einfluss von Ca^{2+} - und Mg^{2+} -Ionen auf die *Eh*Actn2-Funktion mittels F-Actin-Bündelungsexperimente untersucht. Wie bereits berichtet, reduziert Ca^{2+} die *Eh*Actn2-Bündelung (Virel et al., 2007), während hier gezeigt wurde, dass Mg^{2+} dies nicht tut, was impliziert, dass dieses α-Actinin tatsächlich ein Ca^{2+} -reguliertes Protein ist. Die Mutante mit durch aufgebrochenen EF3-4 /„neck"-Kontakt hochflexiblen ABD (durch SLS und FA festgestellt), war nicht in der Lage F-Aktin zu bündeln, was die Subtilität hinter der *Eh*Actn2-Regulation unterstreicht. In ähnlicher Weise ging durch die Deletion der CaM-Domäne die Aktinbündelung durch *Eh*Actn2 vollständig verloren, welche aber bei integraler CaM-Domäne und im Beisein von Ca^{2+} gerettet werden konnte. Effektives Zusammenspiel zwischen EF1-2 und EF3-4 erfordert darüber hinaus, dass ersteres zwischen SRs positioniert ist, wie durch Verwendung eines chimären Konstrukts gezeigt wurde, wobei die „rod domain" von *Eh*Actn2 durch den geschlossenen „rod" von hActn2 ersetzt wurde, was zu einem Verlust der Ca^{2+} -Abhängigkeit von *Eh*Actn2 führte.

Zusammengefasst liefert diese Arbeit die erste Struktur von Ca^{2+}-reguliertem α-Actinin und erklärt den Mechanismus seiner Regulation in einem menschlichen Parasiten, E. histolytica, der

Multidomänenkommunikation in *Eh*Actn2 erfordert. Die Bindung von Ca^{2+} an EF1-2 beeinflusst die EF3-4 / „neck“-Interaktionen und moduliert schließlich die Position der ABD, was wiederum ihre Fähigkeit beeinflusst Aktinfilamente zu bündeln. Obwohl dieser Mechanismus teilweise auf menschliche Ca^{2+} -regulierte α-Actinine anwendbar ist, hat EhActn2 einzigartige Eigenschaften, nämlich seine hohe Affinität für Ca^{2+} -Ionen und die offene „rod domain“. Da es sich bei *Eh*Actn2 um ein Zytoskelett-Protein handelt, nehmen wir an, dass es eine entscheidende Rolle bei der Mobilität und Pathogenität von *E. histolytica* spielen könnte.

1. INTRODUCTION

1.1 How to study the inside of the cell?

I would like to start this Dissertation with a quote from the lecture of cell and developmental biologist P. Weiss, which was given 58 years ago: "… the cell is not just an inert playground for a few almighty masterminding molecules, but is a *system*, a hierarchically *ordered* system, of mutually interdependent species of molecules, molecular groupings, and supramolecular entities; and that life, through cell life, depends on the *order* of their interactions" (Allen, 1962). Although this statement dates back to 1960 it stays relevant even today, as when we focus on studying single molecules we tend to neglect their interplay with other components of the cell. The question is, therefore, how to study and understand the function of biomolecules within the cell. In this thesis we uncover how Ca^{2+} ions regulate actin cytoskeleton by binding to α-actinin. We combine complementary techniques, namely structural biology, biochemistry and *in vivo* experiments (not shown in this thesis). I believe that the combination of different methods is the proper way to look at the cell as a system.

1.2 Few words about cytoskeleton

What would be of our body without a skeleton? We can extend this analogy to the cell, with one important difference, namely that cytoskeleton is not a static structure, it is in fact a very dynamic network of proteins and organelles which control the spatial organization of the cell as well as its shape, motility and stress resistance. Fletcher und Mullins conveniently compare cytoskeleton building blocks to LEGO, as they can create diverse set of structures and the monomers can be reshuffled to make new polymers (Fletcher & Mullins, 2010). There are three major components of cytoskeleton, namely F-actin networks, microtubules and so-called intermediate filaments, with microtubules being the thickest and the stiffest element and the actin the thinnest one. Actin and tubulin polymers display molecular polarity, a feature that is critical for the action of molecular motors, which move along polymers only in one direction. Intermediate filaments are the most fragile components of cytoskeleton, yet they can make networks with actin filaments and microtubules due to crosslinking molecule, called plectin. They are, however, not polarized and therefore do not interact with molecular motors. Although initially the presence of

cytoskeleton was ascribed only to *Eukaryotes* it became clear in the past several years that bacteria and *Archae* do have homologues of actin, tubulin and intermediate filaments (Shih & Rothfield, 2006). Fascinating property of the constituents of cytoskeleton is their ability to form elastic structures *in vitro*, when mixed together. There are therefore two ways to study the behavior of cytoskeletal components: *in vivo* and *in vitro.* In this thesis the latter approach was used to understand the dynamic of actin crosslinking by α-actinin, as further discussed below.

1.3 Microtubules

Microtubules are long tubes (up to 50 μm) formed by polymerization of αβ-tubulin heterodimers, which are organized head-to-tail, resulting in a polar structure, where β subunits are exposed on plus (growing) end and α subunits on a minus end (**Fig. 1**). Microtubules are dynamic structures, undergoing continuous growing and disassembly and although they can spontaneously nucleate *in vitro* in the presence of guanosine 5'-triphosphate (GTP) and Mg^{2+} ions, the exact molecular mechanism behind their nucleation *in vivo* has not been yet completely understood (Roostalu & Surrey, 2017). ϒ-Tubulin ring complex (ϒTuRC), a multi-protein assembly, has been shown to be indispensable platform for microtubules assembly in the cell (Kollman, Merdes et al., 2011). Recently, it has been demonstrated that microtubules can start nucleation on the side of existing filaments, a process driven by augmin-mediated recruitment of ϒTuRC complex (Petry, Groen et al., 2013). Nucleation precedes elongation of microtubules, where 13 protofilaments of tubulin associate laterally to create a hollow tube, 25 nm in diameter (Desai & Mitchison, 1997). During polymerization β-subunit hydrolyzes bound GTP molecule, which results in polarity of the filament, namely the growing end of the microtubule is GTP-bound and minus end contain GDP. GTP hydrolysis is accompanied by conformational changes in tubulin molecule (Ravelli, Gigant et al., 2004). Consequently, loss of stabilizing GTP cap leads to a catastrophe and shrinking of the filament.

Microtubules control a vast range of molecular processes, such as intracellular transport, chromosome separation during cytokinesis, cell polarity regulation. They are major components of cilia and flagellum and regulate the position of cell nucleus and other organelles (Roostalu & Surrey, 2017).

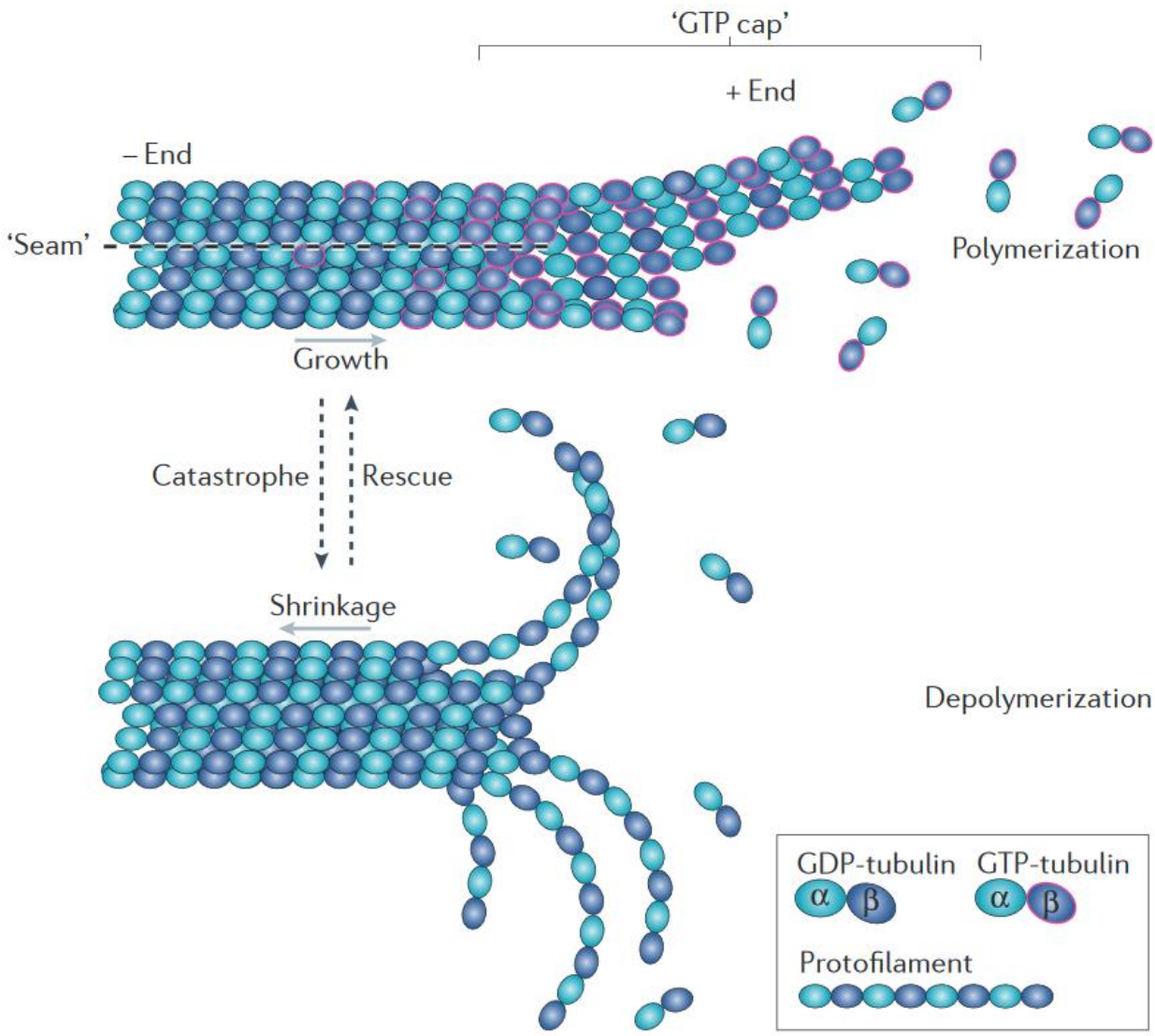

Figure 1. Microtubules dynamics. GTP-bound tubulin dimers subunits are incorporated into growing end of microtubules. Loss of GTP-cap on the pointed end of the filament results in a catastrophe and rapid depolymerization of microtubules. Figure adapted from (Roostalu & Surrey, 2017).

1.4 Intermediate filaments

Intermediate filaments (IFs) are dynamic cytoskeletal structures with diameter (10 nm) between microtubules (25 nm) and actin microfilaments (7 nm). In contrast to the latter ones, IFs do not bind nucleotides, do not show polarity and display much higher stability. In humans there are at least 65 genes encoding for IFs proteins, often with cell type specific expression pattern, which can be classified into five

groups: acidic keratins (type 1), basic keratins (type 2), vimentin, desmin, Glial fibrillary acidic protein (GFAP) (type 3), neurofilament proteins (type 4), and nuclear lamins (type 5) (Herrmann, Bar et al., 2007). IF proteins share structural conservation, where central, 45 nm-long α-helical domain (rod) is flanked by globular domain (head and tail, respectively) (Fig. 2). Central rod domain mediates head-to-head dimerization *via* coiled-coil formation. Dimers associate with each other in a head-to-tail fashion to create tetramers, which associate end to end, forming protofilament, a building block of protofibrils. Four protofibrils pack together laterally form a 10 nm IF (**Fig. 2**) (Lodish, Berk et al., 2013).

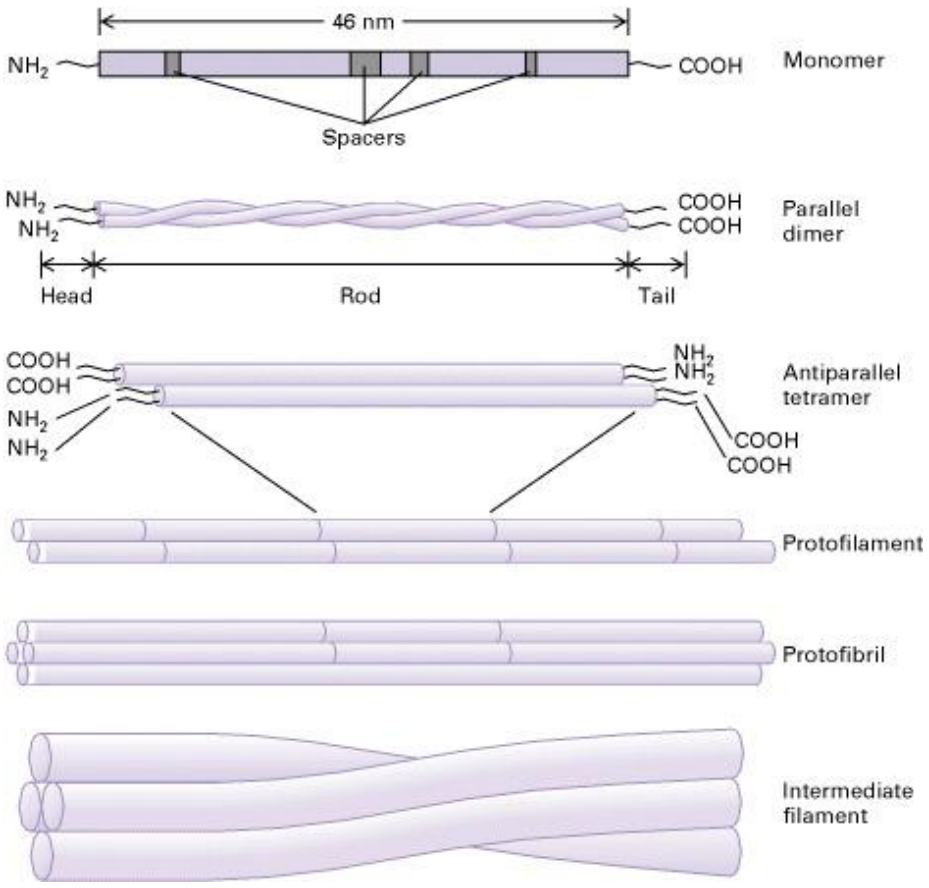

Figure 2. Organisation of intermediate filaments. IF proteins contain long central rod domain, which mediates dimerization. Dimers associate with each other to form tetramers, which end-to-end association gives rise to protofilament. Protofilaments further associate to form protofibril, a building block of IFs. Figure adapted from (Lodish et al., 2013).

IFs are localized at the nucleus (lamins), where they organize heterochromatin, at the cytoplasm, where they are involved in organization of some of the organelles and complexes, such as Golgi, mitochondria, or at the cell membrane, where they participate in formation of desmosomes, hemidesmosomes and focal

adhesions (Godsel, Hobbs et al., 2008). Mutations in IF proteins are linked to many skin blistering diseases, which highlights their importance in cell mechanics (Godsel et al., 2008).

1.5 Actin and actin filaments

Actin is the second most abundant protein in eukaryotic cells which can exist in the cell either in a monomeric form (G-actin) or as filamentous actin (F-actin). In vertebrates three actin isoforms have been reported – α, β and ϒ, with minor differences in sequence between each of them. Monomeric actin is composed of four subdomains (1-4), which form two distinct lobes, divided by two clefts. The upper cleft binds Mg^{2+} ions and nucleotides, whereas the lower, more hydrophobic one, is a major site for actin binding proteins (Dominguez & Holmes, 2011) (**Fig. 3**).

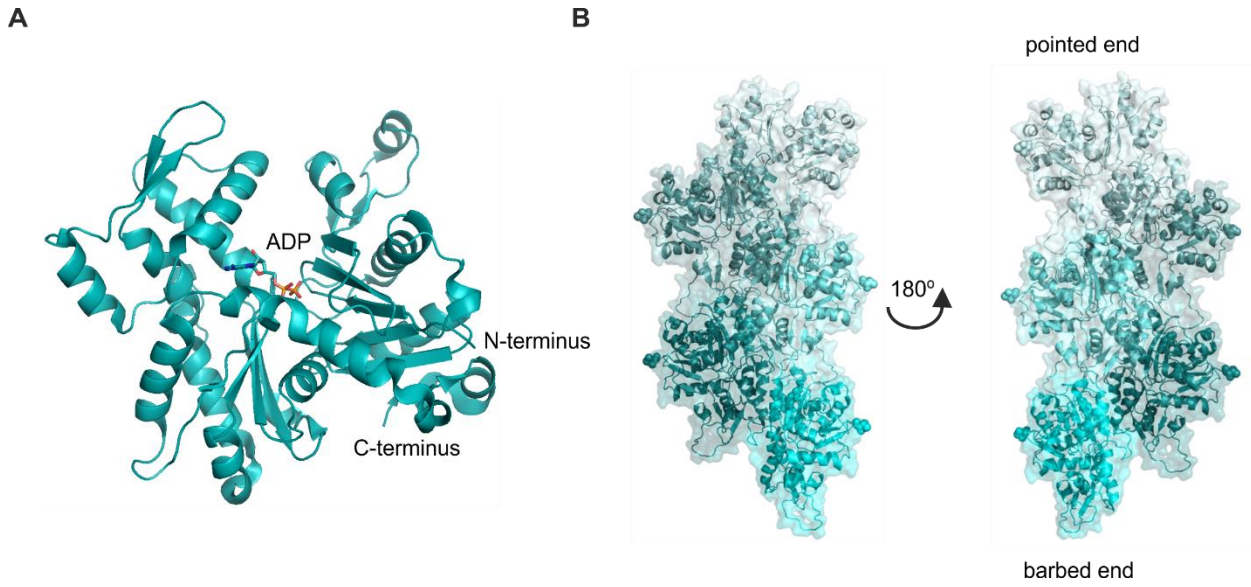

Figure 3. Structure of actin. (A) Ribbon plot of ADP-bound G-actin. Figure was made in PyMOL using PDB code 1J6Z. (B) Structure of F-actin. Figure was made in PyMOL from five actin monomers using PDB code 5JLF (von der Ecken, Muller et al., 2015) .

The transition between G- and F-actin is determined by the concentration of free monomers, temperature and ionic strength, and is regulated by a plethora of actin binding proteins. Formation of actin polymers begins with an energetically unfavorable nucleation step encompassing initial formation of actin dimers and subsequently higher oligomers.

Electron microscopy structure of actin-tropomyosin is the highest resolution structure of F-actin until now (at 3.7 Å resolution) (von der Ecken et al., 2015). Interestingly, actin adopts very similar conformations in monomeric and filamentous forms (**Fig. 3**), with the latter one being partially flattened with a 20° twist between both lobes. Additionally, a loop on the top of the outer domain (so-called D-loop) has a different orientation in the polymer. Actin filament forms right-handed long-pitch helix in which both ends show different dynamic, namely barbed and pointed end, respectively. Actin monomers bind either adenosine 5'-monophosphate (ATP) or adenosine 5'-diphosphate (ADP), however they cannot hydrolyze ATP, whereas F-actin possesses this property. ATP-actin dissociates from the filament slower than ADP-actin, therefore ATP-actin monomers at the top of actin filament (barbed end) effectively slow down actin dissociation, whereas ADP-actin from the pointed end can be removed faster. The constant recycling of actin monomers in the filament is referred to as 'treadmilling' (Stossel, Chaponnier et al., 1985).

Although cytoskeleton was believed to be an eukaryotic structure, it becomes clear that prokaryotes also possess filamentous proteins with high structural similarity to eukaryotic tubulin and actin, including MreB and ParM (Shih & Rothfield, 2006). MreB forms antiparallel filaments which are single stranded and straight (Oda, Iwasa et al., 2009), similar to ParM filaments, which are also single stranded, but left-handed (Bharat, Murshudov et al., 2015). Recently, an actin homologue, crenactin, was found in *Archae* (Izore, Kureisaite-Ciziene et al., 2016), which points towards common ancestry of *Archae* and *Eukaryota* (Merino & Raunser, 2016).

1.6 Actin binding proteins

Organization of actin cytoskeleton requires coordinated action of many actin-binding proteins (ABPs) and is controlled by small signaling molecules, such as Ca^{2+} ions, phosphatidylinositols and other factors, such as local changes in cellular pH. ABPs can be classified into few groups, described below (dos Remedios, Chhabra et al., 2003, Stossel et al., 1985, Winder & Ayscough, 2005):

1. Actin monomers binding proteins: profilin, DNAse-I, thymosin β-4.

The major function of these proteins is maintaining a pool of monomeric ATP-bound actin ready to assemble into filaments and preventing actin from unwanted nucleation. Therefore, they play mainly a buffering role.

2. Proteins regulating higher-order structures of actin filaments (e.g. α-actinin, fimbrin, filamin).

This group of proteins can be divided into two separate classes: actin cross-linkers and actin bundling proteins. The difference between them lie in their molecular composition: cross-linkers form loose and branched connections between actin filaments due to their branched structure, whereas actin filaments in bundle are organized parallel or antiparallel to each other, which is usually achieved by symmetrical architecture of bundling proteins, where ABDs lie opposite each other on both ends of the protein (**Fig. 4A**).

3. Actin nucleating factors (Arp 2/3 complex, formins).

Those factors stimulate the growth of actin on its barbed end from the pool of free actin. They help to overcome the actin nucleation energy barrier. (**Fig. 4B**). Arp2/3 complex is composed of seven proteins, showing molecular mimicry to actin.

4. Actin side-binders (e.g. tropomyosin, nebulin).

Those ABPs stabilize mechanically actin filament and act as molecular rulers (**Fig. 4C**).

5. Actin severing proteins (e.g. cofilin, gelsolin).

Those ABPs disrupt actin filaments. Cofilin binds to the sides of the filaments and distorts the actin filament leading to a break in a place which is not blocked by cofilin. Gelsolin breaks the filaments at the site of interaction. Activity of cofilin and gelsolin is controlled by Ca^{2+} ions, PiP_2 and pH. Actin severing proteins regulate the gel-to-sol transition of actin (**Fig. 4D**).

6. Actin-filaments end-blockers (e.g. Cap-Z, gelsolin, tropomodulin).

Capping proteins usually bind to the barbed end of the actin filament. Tropomodulin is an exception and protects the pointed end (**Fig. 4D**).

7. Actin filament depolymerizing proteins (e.g. actin-depolymerizing factor (ADF) and cofilin).

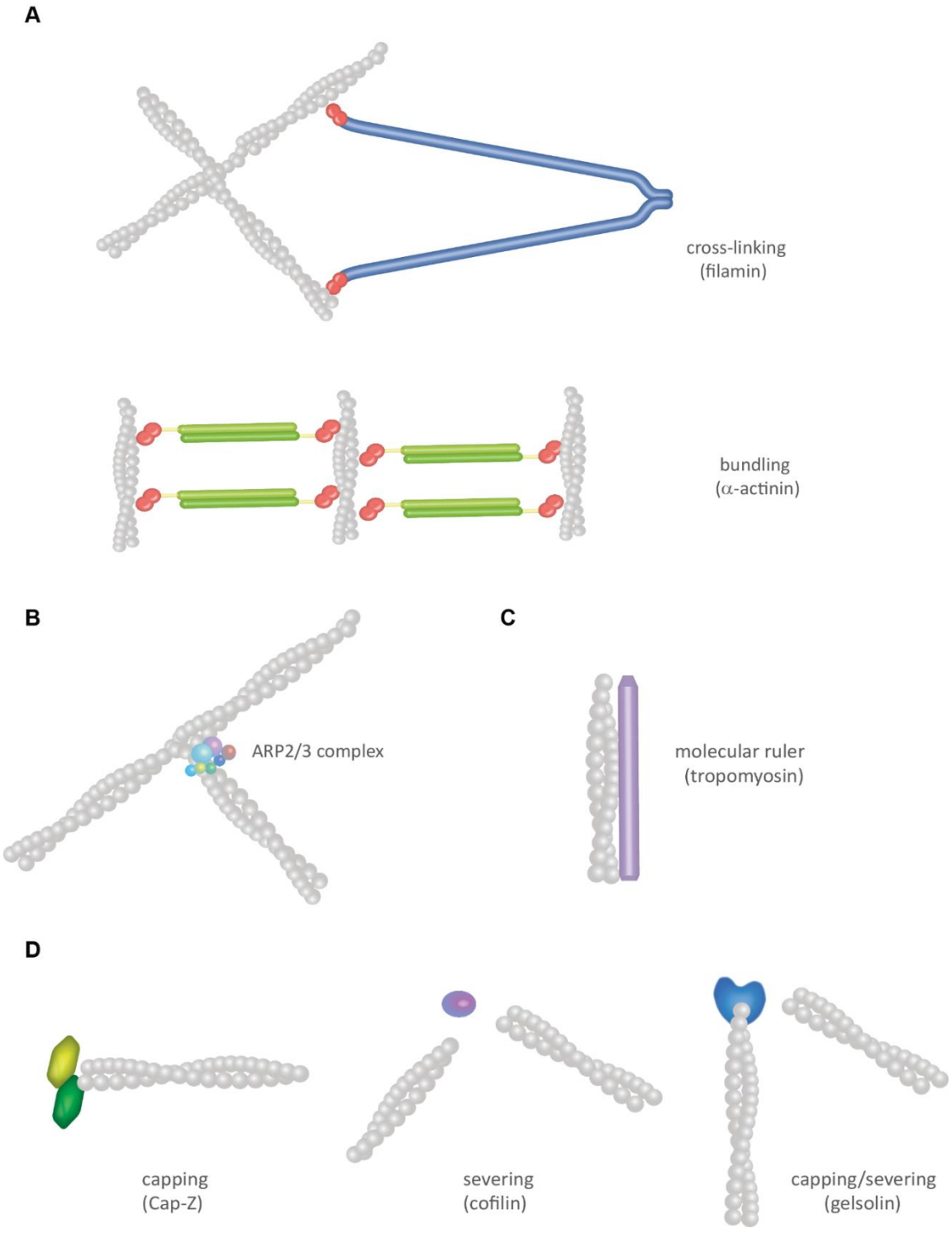

Figure 4. Actin binding proteins. (A) Actin cross-linking and bundling proteins (filamin and α-actinin). (B) ARP2/3 complex is composed of seven molecules and initiates actin nucleation. (C) Actin side-binders proteins stabilize mechanically actin filament and act as molecular rulers. (D) Capping protein (Cap-Z) and actin severing proteins keep the pool of shorter actin filaments.

8. Motor proteins (e.g. myosins).

All known myosins use actin as a 'track' on which they transport their cargo using force generated by ATP hydrolysis.

9. ABPs linking F-actin to cell membrane and other cytoskeletal components (e.g. microtubule associated proteins, which link actin with microtubules).

Control of intracellular actin network requires coordinated interplay of ABPs. In fact, many of them exert their functions together (like tropomodulin and tropomyosin), whereas others compete with each other for binding to actin, like e.g. DNAse I and cofilin or DNAse I and gelsolin (dos Remedios et al., 2003, Stossel et al., 1985, Winder & Ayscough, 2005).

1.7 Keeping it in the (spectrin) family

Members of the spectrin family constitute an important group of of actin bundling and membrane-anchoring proteins (Liem, 2016). Common characteristic of those proteins is the presence of 106-amino acid long spectrin repeats (SRs) and often calponin homology (CH) domains and EF-hands (**Fig. 5**). Most important members of this superfamily are spectrin, dystrophin, utrophin, α-actinin as well as spectraplakins and nesprins (Liem, 2016). Spectrin molecule is an antiparallel tetramer formed by head to tail association of dimer formed by α and β-spetrin molecules (**Fig. 5**). Spectrin is a membrane-associated cytoskeleton-organizer. Dystrophin plays a similar function in muscle sarcolemma. Utrophin is more ubiquitously expressed member of the family with a similar role. α-Actinin is believed to be an ancestral predecessor of spectrin family members. Increased number of SRs in other proteins from the family is the result of gene duplication events (Pascual, Castresana et al., 1997). Based on the sequence analysis SR1 and SR2 of α-actinin are homologous to β-spectrin SR2 and SR3, respectively, whereas SR3 and SR4 of α-actinin is most closely related to α-spectrin SR20 and SR21 (Viel, 1999). Conservation of those domains drives antiparallel association of α-actinin monomers and α-and β-spectrin molecules.

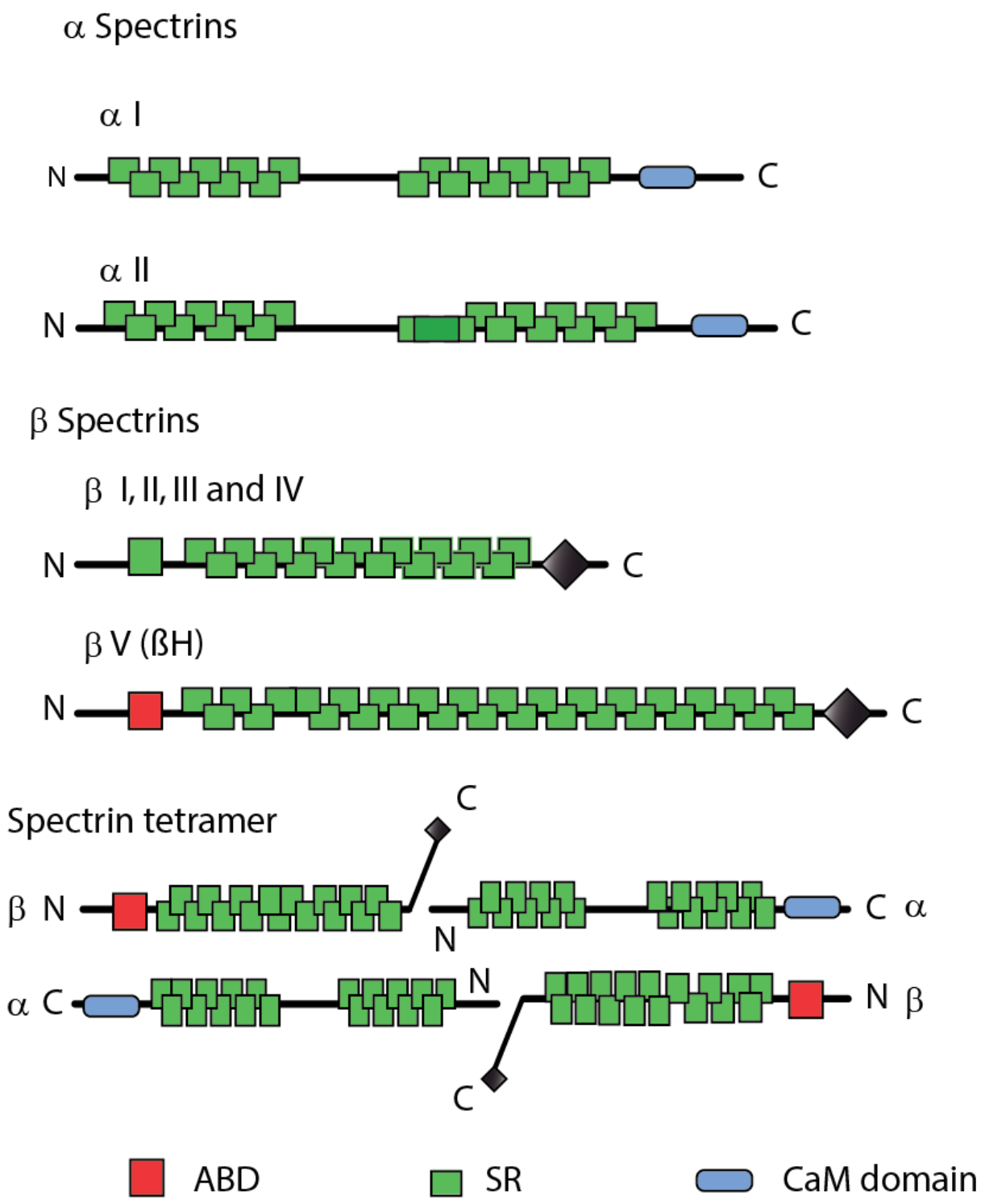

Figure 5. Domain architecture of spectrins. Spectrin is a tetramer formed by head-to-head association of α and β spectrin dimer. ABD is shown in red, SRs in green, CaM domain in blue. Figure adapted from (Bennett & Healy, 2009).

1.8 α-Actinins – ancestral actin cross-linkers

α-Actinin genes can be found in organisms as different as amoebas, fungi and yeast, which made them ancestral organizers of actin cytoskeleton. Notably α-actinin genes are not present in plants. Genetic conservation of α-actinins is highlighted in the common domain organization, with rod domain being the only variable one (e.g. displaying variable length due to different number of SRs). Tellingly, invertebrates usually express only one α-actinin isoform, whereas in vertebrates there are three or four (Murphy & Young, 2015), indicating that duplication events occurred in α-actinin genes during the evolution (Virel & Backman, 2007). α-Actinin genes in metazoans are also more intron rich, which facilitates alternative splicing (Lek, MacArthur et al., 2010). Also, the C-terminal PDZ-domain binding site is present only in metazoans with the exception of nematodes (Lek et al., 2010). Vertebrate α-actinins can be either Ca^{2+}-sensitive or insensitive, which is the result of alternative splicing of exon 19, restricted to *Chordata*. In case of Ca^{2+}-sensitive α-actinins binding of this ion diminishes their capacity to bundle F-actin through hitherto unknown mechanism. Alternative splicing of exon 8 in human α-actinin 2 (*h*Actn2) gene creates a brain specific isoform (Lek et al., 2010).

Studies of α-actinins from model organisms demonstrate that some of their functions are conserved within the tree of life and some are very specialized in particular organisms. α-Actinin from *S. pombe* is Ca^{2+}-insensitive, contains two SRs and is a relatively poor actin bundler (Addario, Sandblad et al., 2016) , but it is important for the process of cytokinesis in this organism under certain stress conditions (Wu, Bahler et al., 2001). In *Dictyostelium discoideum* α-actinin regulates cell growth and mobility, but its deletion causes cell defects only under stress condition or when combined with deletion of other actin-binding proteins, similarly to fission yeast α-actinin.

Oddly enough, deletion of α-actinin in more complex organisms like *Drozophila melanogaster* and *Caenorhabditis elegans* causes severe defects only in the muscle tissue. As α-actinin deletion mutants lack any specific non-muscle phenotypes in fruit flies and worms, it suggests that in non-muscle cells of those organisms α-actinin function is either not crucial or can be substituted by other proteins (Murphy & Young, 2015).

In mammals four isoforms of α-actinin are differentially expressed. Ca^{2+}-sensitive isoforms 1 and 4 show ubiquitous pattern of expression, whereas Ca^{2+}-insensitive isoforms 2 and 3 are expressed in muscle tissues and are regulated by phosphatidylinositol 4,5-bisphosphate (PIP_2) (Ribeiro Ede, Pinotsis et al., 2014). Moreover, Ca^{2+}-sensitive variants of isoforms 1 and 4 (containing exon 19b) are expressed in

smooth muscle cells and in the brain (Foley & Young, 2013). Furthermore, it was demonstrated that heterodimers formed by non-muscle isoforms seem to constitute predominant α-actinin dimers, followed by an interpretation that those may confine new functions of α-actinins due to the unique protein-protein interactions involving both monomers (Foley & Young, 2013).

1.9 Molecular architecture of α-actinin

α-Actinin is an elongated, thin, cylindrical molecule with central rod domain and ABDs located opposite to each other (**Fig. 6A**). For many years structure of full-length (FL) protein was missing and structural information about α -actinins was limited to its single domains. The first low-resolution EM structure of *h*Actn1 from negatively stained specimens was reported in 2001 (Tang, Taylor et al., 2001). So far only one crystal structure of FL Ca^{2+}-insensitive *h*Actn2 has been published (Ribeiro Ede et al., 2014). This is to date the highest resolution structure of human α-actinin (3.5 Å). In agreement with the structure from Taylor's lab, in *h*Actn2 EF3-4 wraps itself around the neck region (**Fig. 6B**). Taylor's model suggested some flexibility of ABD and EF-hands, which is not observed in the crystal form.

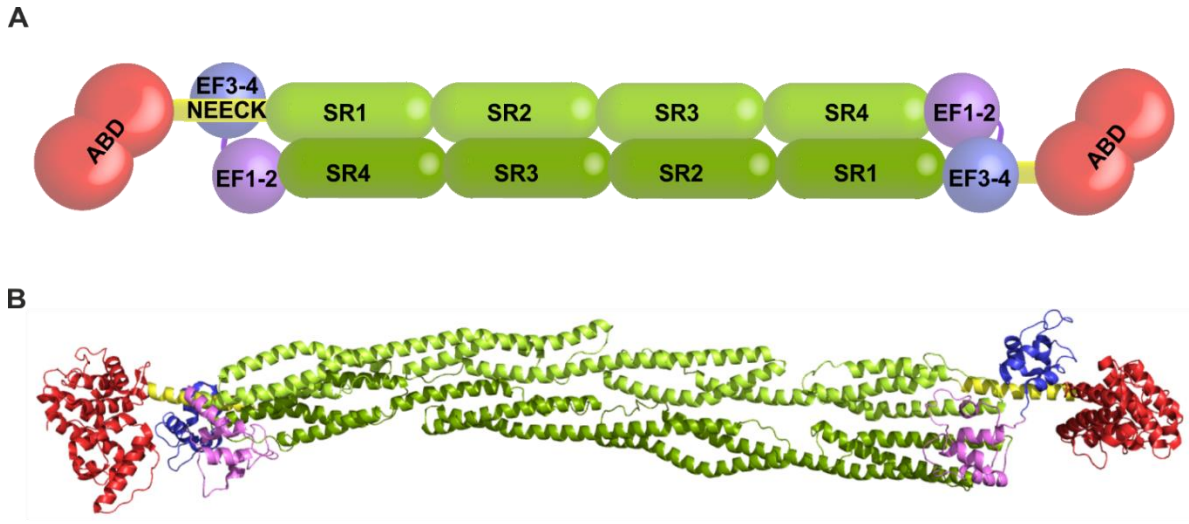

Figure 6. Schematics and crystal structure of hActn2. (A) Scheme of human a-actinin. ABD is colored in red, neck region in yellow, rod domain in green, EF1-2 in violet, and EF3-4 in blue. (B) Crystal structure of *h*Actn2. Colors like in (A). In this representation the twist in the rod domain is clearly visible. Figure was generated in PyMOL using PDB code 3D1E (Ribeiro Ede et al., 2014).

1.9.1 Actin binding domain

Actin binding domain (ABD) is the most conserved domain among different actin binding proteins (Banuelos, Saraste et al., 1998). It consists of a pair of CH domains, each of which is built by four major helices (A, C, E and G) and two or three shorter ones (**Fig. 7A**). In all reported crystal structures of isolated ABDs, except from *Arabidopsis thaliana* fimbrin, which has mutations on the CH1/CH2 interface, this domain adopts a closed conformation, where CH1 and CH2 are in an intimate contact achieved by packing of helices A and G from CH1 against helices F and G of CH2, creating an interaction interface of about 700-900 Å (Borrego-Diaz, Kerff et al., 2006, Franzot, Sjoblom et al., 2005). Open ABD conformation in the case of utrophin and dystrophin crystal structures is a result of domain swapping, a crystallographic artifact, however in the solution both ABDs also adopt closed conformations (Singh & Mallela, 2012, Winder, 1996). EM studies of F-actin decorated with ABDs from α-actinin and utrophin demonstrate that both interact with filamentous actin in an open conformation (Galkin, Orlova et al., 2010, Galkin, Orlova et al., 2002), in agreement with localization of actin binding site (ABS) 1 on the ABD surface. Namely, there are three ABSs on the surface of ABD (**Fig. 7A,B**) (Bresnick, Janmey et al., 1991, Corrado, Mills et al., 1994, Fabbrizio, Bonet-Kerrache et al., 1993, Kuhlman, Hemmings et al., 1992, Levine, Moir et al., 1990, Levine, Moir et al., 1992). ABS1 is located on N-terminal helix A of CH1 domain and is obstructed in a closed conformation, therefore ABD needs to open in order to exhibit this site. ABS2, the major ABS, encompasses the G-helix of CH1, which continues to ABS3 formed by N-terminal helix of CH2.

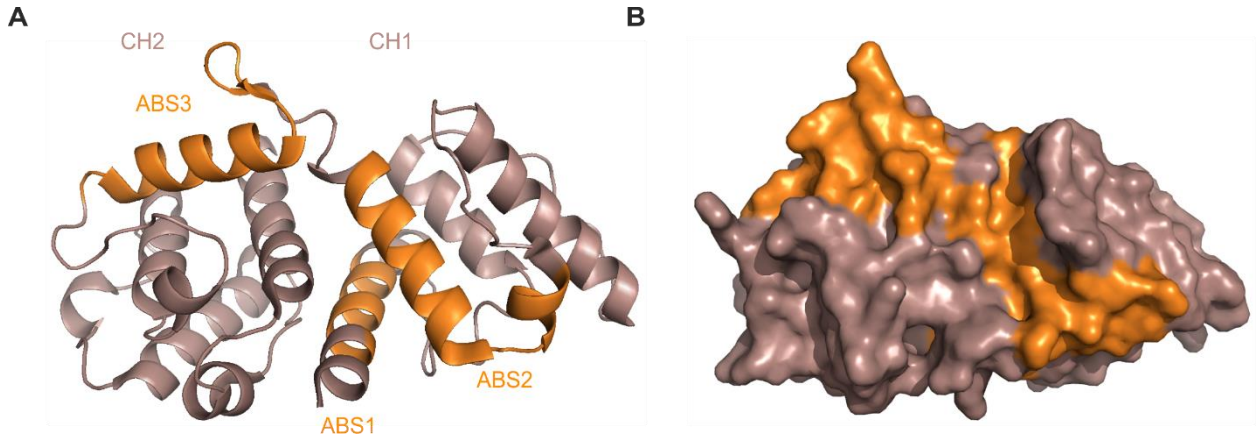

Figure 7. Actin binding domain from hActn3. (A) Crystal structure of *h*Actn3 ABD. (B) Surface representation of *h*Actn3 ABD. Figure was generated in PyMOL using PDB code 1TJT (Franzot et al., 2005). CH domains are colored in dark salmon, ABSs in orange.

Consistently, CH1 has stronger affinity to F-actin, having two ABSs, whereas CH2 is not able to bind actin on its own (Banuelos et al., 1998). Effective interaction between ABDs and F-actin requires tandem CH domains.

1.9.2 Rod domain

Rod mediates dimerization in α-actinin and is the least conserved domain, as the number of its building blocks (SRs) is variable between species (Lek et al., 2010). The structure of the rod from *h*Actn2 reveals that it forms an antiparallel dimer with the length of 240 Å and the width of 40-50 Å (Ylanne, Scheffzek et al., 2001). Dimer interface encompasses 11% of its solvent accessible area and is mainly maintained by electrostatic and hydrophobic interactions, resulting in a very tight association of both monomers, with a reported K_d of 10 pM (Flood, Rowe et al., 1997). Electrostatic potential of SRs shows a gradient, being most basic in SR1 and most acidic in SR4, which additionally facilitates dimer formation (Djinovic-Carugo, Young et al., 1999) The most striking feature of this domain is its left-handed torsional twist along long axis (**Fig. 8**), as a result of which ABDs on the opposite ends of the molecule are rotated by 90° in respect to each other (Ylanne et al., 2001). Additionally, rod surface is acidic, which has been suggested to have implications in its interaction with plasma membrane as well as transmembrane receptors (Ylanne et al., 2001).

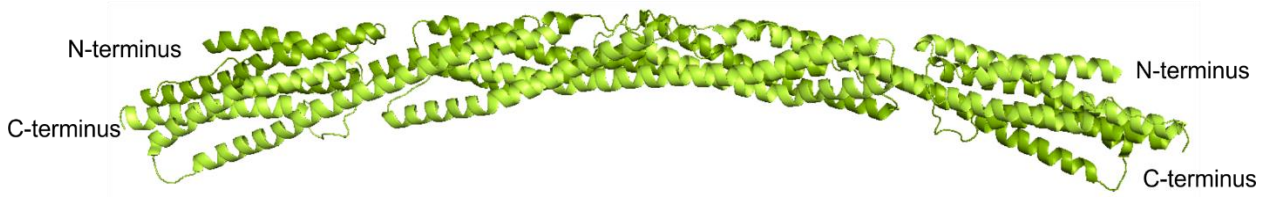

Figure 8. Rod domain of hActn2. Rod domain in human α-actinins is formed by head-to-tail association of monomers containing four SRs. A characteristic feature of the rod is its left-handed torsional twist. Figure was generated in PyMOL using PDB code 1HCI (Ylanne et al., 2001).

1.9.3 Calmodulin-like domain

C-terminal CaM domain in α-actinins can be Ca^{2+}-sensitive or insensitive. At this point it is worth to highlight the fact that in human α-actinins this domain makes an intimate contact with neck region. Features of CaM domains are described in more detail below.

1.10 One ion does it (almost) all

Ca^{2+} is involved in the regulation of virtually all vital biological processes, including the fast ones, like muscle contraction, exocytosis, synaptic transmission and ion channel modulation, which are events in the range of ms-s (Verkhratskiĭ & Toescu, 1998). On the other end of the time scale are delayed responses regulated by Ca^{2+}, involving shaping the enzymatic activity, regulation of gene expression, growth and ultimately cell death (Verkhratskiĭ & Toescu, 1998).

Ca^{2+} ion has some unique chemical properties which enable it to exert its functions as universal second messenger. First of all, Ca^{2+} has a double positive charge which explains why it would be preferentially bound to negatively charged proteins instead of monovalent cations, like K^+ or Na^+. Moreover, Ca^{2+} interacts with many inorganic substrates, including phosphate, with which it makes poorly soluble salts. This requires that Ca^{2+} concentration within the cell has to be kept at very low level. Cells maintain a gradient of Ca^{2+} over the cell membrane. Intracellular Ca^{2+} concentration in a resting state is about 30-150 nM, whereas the extracellular one is about 10,000-fold higher (Celio, Pauls et al., 1996). This creates an ideal environment for Ca^{2+} to act as a signaling molecule ensuring also good signal to noise ratio (Verkhratskiĭ & Toescu, 1998). The same principle implies existence of efficient Ca^{2+} removal systems in the cytosol in order to maintain cell homeostasis. Ca^{2+} ions bind to a plethora of targets, including protein kinases, and have broader spectrum of effects than other signaling molecules, including cyclic adenosine 5'-monophosphate (AMP) or diacyloglycerol. Specificity of the effects exerted by Ca^{2+} is defined by spatio-temporal organization of signaling and is driven by the fact that Ca^{2+}-binding proteins display a huge range of Ca^{2+} affinities, ranging from hundreds of micromolar (e.g. calpain) to nanomolar (e.g. calbindin D9k) (Celio et al., 1996).

1.11 EF-hand – a professional Ca^{2+} binding unit

EF-hand is the most common Ca^{2+}-binding motif in protein structures (Pidcock & Moore, 2001). Its name was first mentioned by Robert Kretsinger to describe a helix-loop-helix motif found in carp parvalbumin (Kretsinger & Nockolds, 1973). Since then EF-hand motif was found in many other proteins, including model Ca^{2+}-binding proteins like CaM, troponin C, light chains of myosins, calbindin D9k etc. (Kawasaki, Nakayama et al., 1998). A pair of EF-hands forming a stable four-helix bundle is the most basic structural motif in Ca^{2+}-regulated proteins, even if one of the domains lost its Ca^{2+}-binding ability. Although proteins with a single EF-hand were reported, they are rare, and isolated EF-hands tend to be less stable than a paired-domain (Gifford, Walsh et al., 2007). An example of EF-hand is shown in **Fig. 9A**, where the structural elements are denoted after Strynadka & James (Strynadka & James, 1989) as a following sequence: helix A- loop I- helix B – helix C – loop II – helix D. **Fig. 9B** shows CaM domain from *h*Actn1.

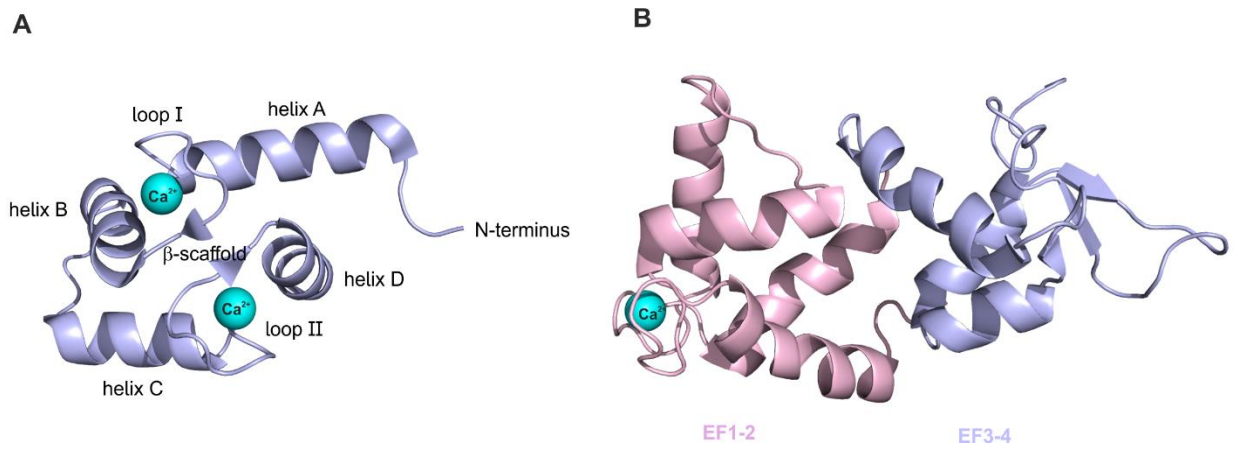

Figure 9. Structure of EF-hands. (A) N-lobe of holo-CaM from *Paramecium tetraurelia*. β-scaffold formed by two adjacent Ca^{2+}-binding loops is visible. (B) CaM domain from *h*Actn1 in Ca^{2+}-bound form. Figure was generated in PyMOL using PDB code 1EXR (A) (Wilson & Brunger, 2000) and pdb code 2N8Y (B) (Drmota Prebil, Slapsak et al., 2016).

Helices flank Ca^{2+}-binding loops, which are composed typically of 12 amino acids. Pair of EF-hands is stabilized by intra-domain interactions. Amphipathic nature of the helices drives packing of their aliphatic residues inside the core of the domain inducing a network of hydrophobic interactions. On the other hand, charged residues on the surface of the EF-hand unit promote faster Ca^{2+}-association (Martin, Linse et al., 1990). Paired EF-hands are stabilized additionally through a short stretch of antiparallel β-sheet (β-scaffold) (**Fig. 9**), formed by residues 7, 8 and 9 of loops from the neighboring EF-hands (Grabarek, 2006).

EF-hand motifs from various proteins display huge diversity in their domain organization, conformational states and responses to Ca^{2+}.

1.12 Keeping it traditional: canonical EF-loops and Ca^{2+} coordination

In most EF-hands the Ca^{2+}-binding loop is formed by 12 residues, the first one being Asp and the last one Glu. Ca^{2+} ion is coordinated by seven oxygen atoms arranged as pentagonal bipyramid, provided by six loop residues (**Fig. 10**). Ca^{2+}-chelating amino acids have assigned specific numbering, namely X (residue 1), Y (residue 3), Z (residue 5), -Y (residue 7), -X (residue 9) and –Z (residue 12). Three to four oxygen atoms coordinating Ca^{2+} come from side-chain carboxyl groups, whereas central amino acid from the loop (-Y position) contributes the carbonyl oxygen from its main chain. The last residue (-Z) is a bidentate ligand as it provides 2 oxygen atoms from its ϒ-carboxyl group. Often one of the loop residues is found to be too distant to directly coordinate Ca^{2+} ion, and there this interaction is mediated by a bridging water molecule.

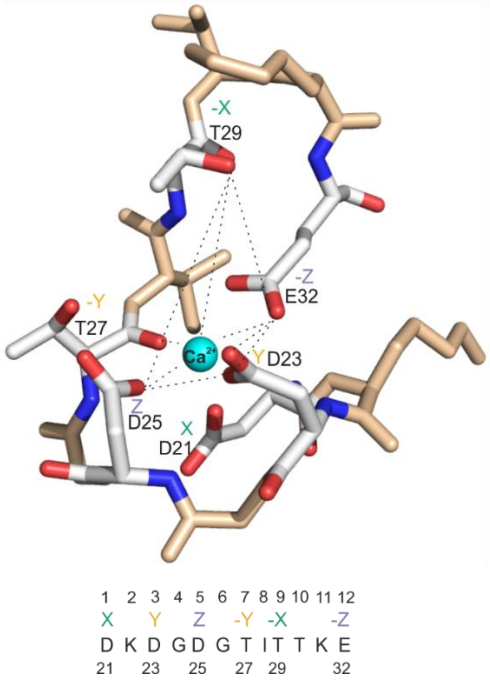

Figure 10. Example of Ca^{2+}-coordination in EF-hand. Ca^{2+} coordinating residues of EF-1 from chicken calmodulin (shown in grey). Ca^{2+} ion is coordinated in pentagonal bipyramidal fashion. Numbers above the amino acid sequence refer to amino acid position in the Ca^{2+}-binding loop, number below amino acid sequence denote amino acid residue in the protein sequence. Figure was made in PyMOL using PDB code 1UP5 (Rupp, Marshak et al., 1996).

Stability of the loop is additionally enhanced by an extensive network of hydrogen bonds between loop residues, which moreover help to neutralize the unfavorable electrostatic contributions from negatively charged residues coordinating Ca^{2+} (Grabarek, 2006). Although the amino acid composition of the loops can vary significantly, some positions are occupied more selectively (**Table 1**).

Accordingly, the first position is always filled by Asp residue. One of its carboxylate groups directly coordinates Ca^{2+} whereas the second one makes a hydrogen bond with amine group of invariable Gly in positon 6. This conserved residue provides the necessary flexibility for other residues in the loop to rotate in order to facilitate Ca^{2+}-binding. The eighth position is occupied by a bulky, hydrophobic amino acid which engages in hydrophobic interaction with the corresponding residue from the neighboring EF-hand. The last, bidentate ligand at position 12 (-Z) is crucial for pentagonal bipyramid coordination of Ca^{2+}. This residue is also involved in forming a network of hydrogen bonds with amine groups of amino acids in positions 2, 3 and 7, which are the least conserved positions in Ca^{2+}-binding loop (Gifford et al., 2007, Strynadka & James, 1989).

Table 1. Amino acid composition of EF-hands.

EF-loop residue	1	2	3	4	5	6	7	8	9	10	11	12
Coordinating ligand	**X**		**Y**		**Z**		**-Y**		**-X**			**-Z**
	sc*		sc		sc		bb**		sc			sc2
Most common amino acid	**Asp**	**Lys**	**Asp**	**Gly**	**Asp**	**Gly**	**Thr**	**Ile**	**Asp**	**Phe**	**Glu**	**Glu**
	100%	29%	76%	56%	52%	96%	23%	68%	32%	23%	29%	92%
Other observed amino acid		Ala	Asn	Lys	Ser		Phe	Val	Ser	Tyr	Asp	Asp
		Gln		Arg	Asn		Lys	Leu	Thr	Ala	Lys	
		Thr		Asn			Gln		Glu	Thr	Ala	
		Val					Tyr		Asn	Leu	Pro	
		Ile					Glu		Gly	Glu	Asn	
		Ser					Arg		Gln	Lys		
		Glu										
		Arg										

**sc –side chain, **bb- backbone.* Table adapted from (Gifford et al., 2007).

1.13 Closed or open? Conformational changes in EF-hands

The mechanism behind the conformational changes occurring in EF-hands upon Ca^{2+} binding has been proposed to be a two-step process centered around so-called EFβ—scaffold. Binding of an ion starts within the N-terminal part of the loop and then propagates into its C-terminal part, which involves movement of exiting helix, accompanied by ~2 Å movement of the Glu in position –Z, which closes the Ca^{2+}-binding loop. More precisely, the role of N-terminal part of the loop would be to trap the ion, whereas the movement of the C-terminal part is responsible for the conformational change of the loop (Grabarek, 2006). According to this model, the partial Ca^{2+} coordination by only N-terminal part of the loop, captured e.g. in CaM41/75 with engineered disulfide bond between residues 41 and 75 (Grabarek, 2005), is proposed to be an intermediate state in ion binding with Ile in position 8 of the loop being the critical hinge residue. The role of the Glu in position 12 is crucial for driving the conformational change in EF-hands, as evidenced by studies of E104Q and E140Q mutants of CaM, where replacing a bidentate with monodentate ligands not only nearly completely reduces Ca^{2+}-binding, but also forces the C-terminal lobe of CaM to oscillate between closed and open conformations due to the lack of formation of hydrogen bonds of those residues with amine groups of amino acids in positions 2 and 9 (Evenas, Malmendal et al., 1998, Evenas, Thulin et al., 1997). Similar results were obtained for E41A mutant of troponin C, which remains closed despite Ca^{2+} binding (Gagné, Li et al., 1997). Those findings underline the role of the conserved 12th position in the EF-loop in a conformational changes occuring upon Ca^{2+} binding at least in Ca^{2+} sensors (see below).

Initially, conformational changes in EF-hands caused by Ca^{2+}-binding were described by the differences in the interhelical angles of CaM domains (Ikura, 1996). Although this approach might help to distinguish between regulatory and sensor proteins, it is not complete, as it does not allow to describe the movement of helices with respect to each other. A more advanced method of classification of conformational changes in EF-hands was proposed by Yap et al (Yap, Ames et al., 1999), where authors compare the positions of exiting end entering helices of particular EF-hand and use three angles to describe the geometry of exiting helix (**Fig. 11A**). This method takes into account rotation about the axis of exiting helix, which describes better conformational changes in EF-hands. Nevertheless, the method proposed by Yap et al. was based on arbitrary superposition of studied EF-hand with the reference structure (N-lobe of apo-calmodulin), which was questioned by Kawasaki and Kretsinger, who introduced a defined coordinate system with a pseudo-two fold axis between each EF-hand lobe to more precisely describe the conformation of CaM domains (**Fig. 11B**) (Kawasaki & Kretsinger, 2012) .

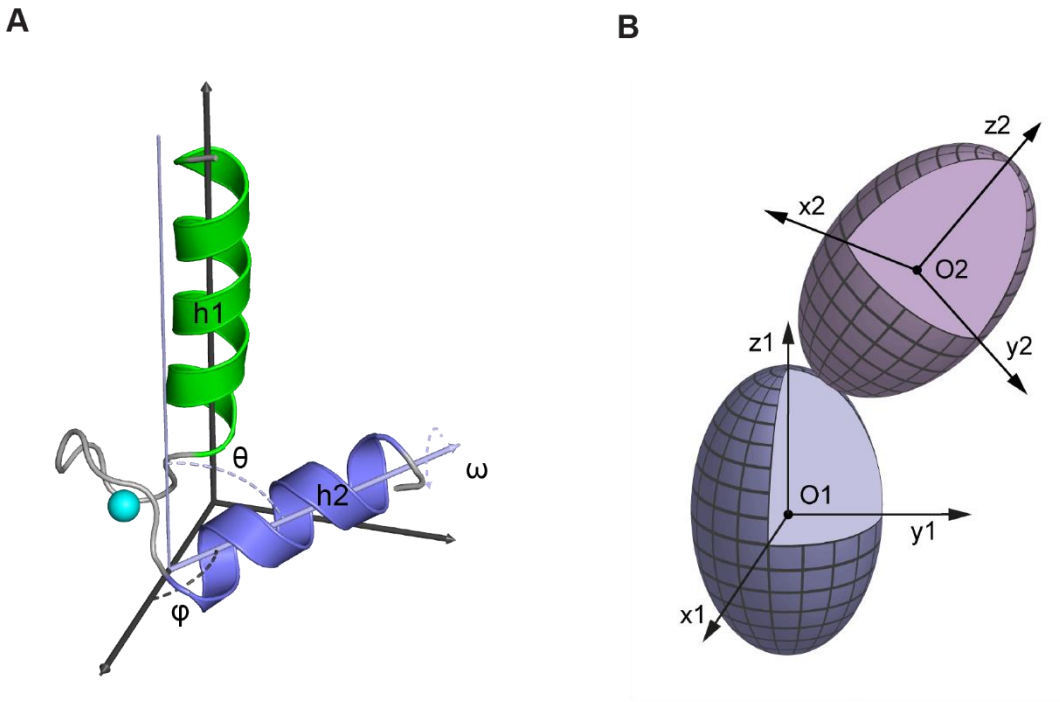

Figure 11. Geometrical models explaining conformational changes occurring in EF-hands upon Ca^{2+} binding. (A) Method of Yap *et al* (Yap et al., 1999) introduces three angles to describe the position of exiting helix (h2) in respect to entering helix (h1). (B) Method of Kawasaki and Kretsinger introduces coordinates system to allow for monitoring changes in the relative orientation of N- and C-lobes (Kawasaki & Kretsinger, 2012). O stands for the center of mass of the respective EF-hand lobe. Figure made by Dr. Julius Kostan.

Independently of the classification used it becomes clear that EF-hands can adopt a wide range of conformations. Most commonly CaM domains are described as either open, closed or semi-open (Yap et al., 1999). Ca^{2+} sensors display the biggest conformational changes upon Ca^{2+}binding (**Fig. 12A,B**). In those EF-hands, entering and exiting helix are antiparallel in apo structures, whereas the bottoms of both helices open to an inverted V-shape, which results in the change in interhelical angle from around 120° to nearly 90°. In model Ca^{2+} sensors (e.g. CaM and TnC), ion binding causes also loss of the contacts between helices B and D, whereas interfaces between helices A and D and B and C are not affected by Ca^{2+} binding. Such changes are, on the contrary, not seen in EF-hands acting as Ca^{2+} buffers (**Fig. 12C,D**) (Nelson & Chazin, 1998). Importantly, disruption of interhelical contacts upon Ca^{2+}-binding results inevitably in exposure of hydrophobic patches in CaM and other sensors (**Fig. 12A,B**). Although it is necessary for the biological function of those proteins, such a conformational change is not favorable from the thermodynamic point of view. How binding of Ca^{2+} can overcome those negative energetic contributions is further discussed below.

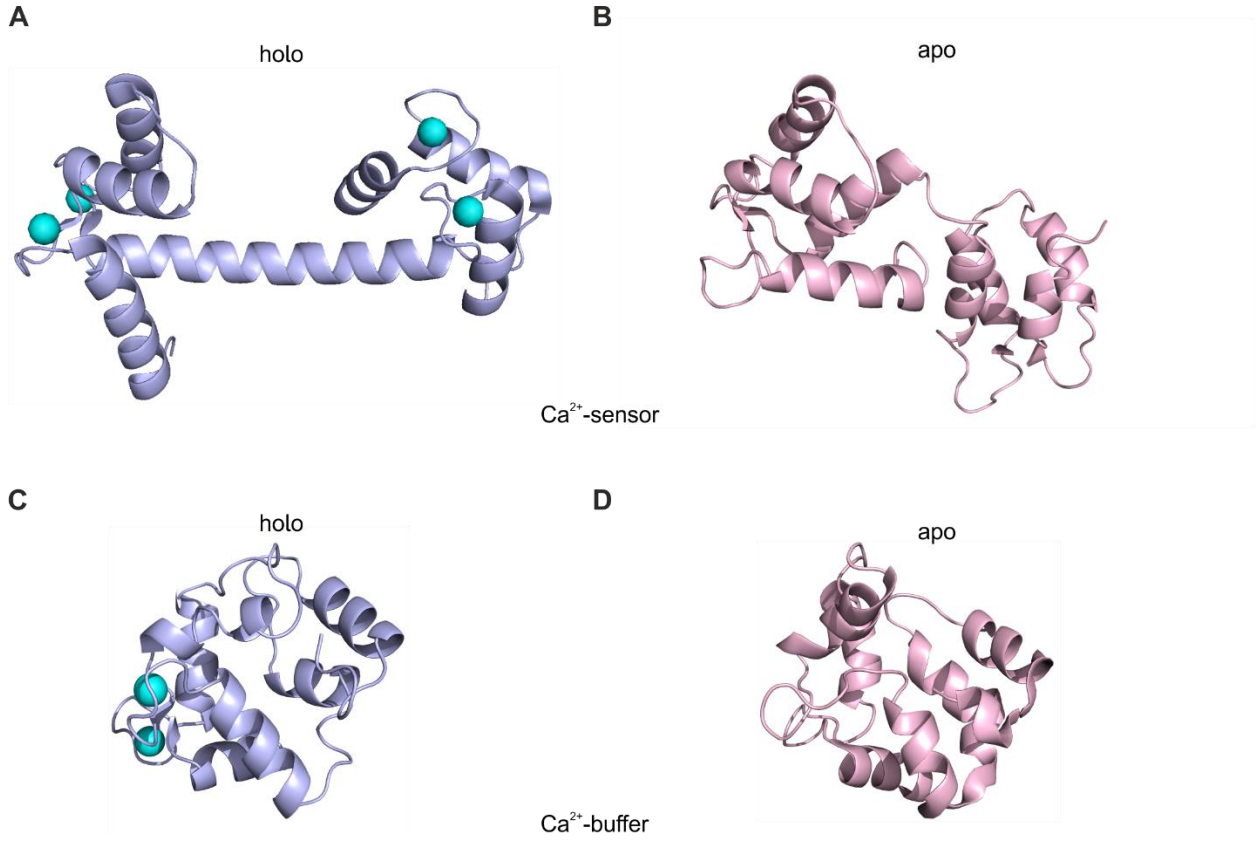

Figure 12. Conformational changes in EF-hand upon Ca^{2+} binding. *(A)* 1-Å crystal structure of holo-CaM from *Paramecium tetraurelia*. Figure was generated in PyMOL using PDB code 1EXR (Wilson & Brunger, 2000). Ca^{2+} ion is shown as cyan sphere. (B) NMR model of apo CaM from *Xenopus leavis*. In this structure N-and C-lobe are connected by a flexible linker, unlike in (A), where the linker forms a continuous α-helix. Figure was generated in PyMOL using PDB code 1DMO (Zhang, Tanaka et al., 1995). (C) Crystal structure of Ca^{2+}-bound parvalbumin from *Cyprinus carpio*. Figure was generated in PyMOL using PDB code 1B8R (Cates, Berry et al., 1999). (D) NMR structure of Ca^{2+}-free parvalbumin from *Rattus norvegicus*. Figure was generated in PyMOL using PDB code 2JWW (Henzl & Tanner, 2008).

1.14 How to choose the correct ion? Selectivity of EF-hands for Ca^{2+}

Ca^{2+} belongs to spherical, 'hard' metals, which prefer ionic interactions over covalent ones, with oxygen atom being Ca^{2+} favorite ligand and nitrogen, chloride, bromide and sulfur being less preferred ones. Coordination number of Ca^{2+} ion differs, but in proteins most commonly six to eight oxygens stabilize the bound ion (Falke, Drake et al., 1994). The preferred ligands are carboxylate, carbonyl, water and finally, hydroxyl oxygen. The distance between carboxyl and carbonyl oxygens and ion is typically between 2.3

and 2.5 Å (Katz, Glusker et al., 1996), and it is bigger when a water molecule bridges the coordinated Ca^{2+}. Crystal ionic radius of Ca^{2+} equals 1.20 Å and dehydration energy of this ion is 363 kcal/mol. In comparison, Mg^{2+} is smaller (ionic radius of 0.86 Å), has higher dehydration energy (439 kcal/mol), prefers a 6-fold coordination and shows shorter ion-oxygen distances (between 2.0 and 2.2 Å), which explains why EF-hands would prefer Ca^{2+} over the latter ion (Falke et al., 1994).

Although intracellular concentration of Na^{+} and K^{+} is 10^{3}-10^{5} times higher than Ca^{2+}, those cations are not bound by EF-hands because single positive charge cannot sufficiently neutralize negative charges present in the EF-loop. The size of the loop has important consequences also for ion specificity of EF-hands. Mutational analysis shed new light into ion selectivity of EF-hands. Engineering Gln in the position 9 of EF-loop from *Escherichia coli* D-galactose and D-glucose receptor for a smaller amino acid promotes binding of bigger ions, whereas substitution with negatively charged residues changed selectivity of the loop, enhancing binding of trivalent cations (Falke, Snyder et al., 1991). Lanthanide ions have very similar ionic radius to Ca^{2+} (1.28 Å for Tb^{3+}, 1.21 Å for Eu^{3+} and 1.27 Å for Sm^{3+}, respectively) and they can therefore be used as fluorescent probes to study EF-hands (Falke et al., 1994). Lanthanides can additionally serve as heavy metals in X-ray crystallography, example of which is given in the following publication where Sm^{3+} was used (Iwasaki, Sasaki et al., 2003).

1.15 Which ion is better? Why do EF-hands bind Mg^{2+}?

If we consider that Mg^{2+} concentration in the cell lies between 0.5 and 2.0 mM, it will be 10^{2}-10^{4} higher than the concentration of Ca^{2+}. Under those conditions many EF-hands will be at least partially occupied with Mg^{2+}, but what would be the physiological role of the competition between both divalent cations for the binding to EF-hands? In case of CaM, affinity for Ca^{2+} is reduced in the presence of physiological concentrations of Mg^{2+}, as Ca^{2+} off-rate increases at increasing Mg^{2+}concentration (Malmendal, Linse et al., 1999). This result also suggests that binding of Ca^{2+} to the N-terminal lobe will not take place until CaM interacts with its targets. Moreover, significant decrease of affinity towards CaM targets has been reported in the presence of Mg^{2+} (Ohki, Ikura et al., 1997). The same paper shows using fluorescence techniques that structural changes caused upon binding of Mg^{2+} are very subtle and localized only to ion-binding loops, in contrast to significant structural changes caused by Ca^{2+} binding. Clearly, in case of CaM, competition of both ions will modulate the biological response of this Ca^{2+} sensor and it seems to be a more general mechanism, applying to many EF-hands.

On the other hand, Mg^{2+} binding to some proteins has been proposed to stabilize their apo state. Moreover, examples of proteins in which EF-hands can exert different functions when bound to either Ca^{2+} or Mg^{2+} have also been reported (Gifford et al., 2007).

1.16 Affinity of EF-hands for Ca^{2+}

Several factors decide how strong a given EF-loop will coordinate Ca^{2+}. The number and respective position of oxygen ligand was shown to contribute significantly to binding affinity. Initially, the acid-pair hypothesis was proposed, stating that increasing the number of acidic residues facing each other in EF-loop increases the affinity for Ca^{2+} (Reid, 1990). This prediction was true for CaM site III and suggested moreover that introduction of an additional, fifth dentate ligand would reduce Ca^{2+} affinity due to destabilization of the loop. The acid-pair hypothesis was further challenged, as introduction of acid-pairs in N-lobe of CaM increases Ca^{2+} affinity. However, in this case the presence of the fifth chelating ligand did not decrease affinity (Black, Tikunova et al., 2000). According to the authors, an additional acid pair on Z-axis should increase Ca^{2+} association since it stabilizes planar pentagonal coordination of the ion, whereas introducing acid pair on X-axis slows down Ca^{2+} dissociation, in agreement with the gateway hypothesis (see below). More recently, the 'charge-ligand-balanced-model' was proposed, suggesting that what determines the Ca^{2+} affinity is not only the number of acidic residues in the loop, but also the contributions of residues not involved in Ca^{2+} coordination, whose role would be balancing the repulsive interactions coming from negatively charged residues (Ye, Lee et al., 2005). In addition, residue in position 9 of the loop has a special role, being a gate-keeping residue. It was shown that negatively charged (and not neutral) residue in position –X should slow down ion dissociation due to favourable electrostatic interactions (Drake, Lee et al., 1996, Renner, Danielson et al., 1993). Similarly, long side chains in this position slow down dissociation due to purely steric hindrance. If there is Glu or Gln in 9^{th} position it will directly coordinate Ca^{2+} ion, whereas if there is a shorter residue, coordination will involve auxilliary water oxygen atom. This residue will therefore decide whether EF-hands will be "rapid", like in troponin C or CaM, or "slow", like paravalbumins, which have always Glu in position 9 (Renner et al., 1993).

Charged residues on the surface of EF-hands affect additionally ion binding affinity, since their removal in case of calbindin D9k resulted in reduced k_{on} for Ca^{2+} binding (Martin et al., 1990). Additionally, binding of CaM to its targets was also shown to increase its affinity for Ca^{2+} ions (Ohki et al., 1997, Peersen, Madsen et al., 1997). Another important factor determining Ca^{2+} affinity is the protein context. Grafting the EF-

loops from CaM on a scaffold made from domain 1 of the cluster of differentiation 2 protein (CD2) reversed the affinities of four Ca^{2+}-binding loops (Ye et al., 2005).

1.17 Thermodynamic challenge – Ca^{2+} binding to EF-hands

Two major forces determine the final free energy of Ca^{2+} binding and therefore Ca^{2+} affinity: entropy and enthalpy. Binding of metal ions to proteins requires removal of coordinating water molecules that is entropically favorable. The gain in solvent entropy is a dominating factor in total free energy of ions binding and is roughly constant for each Ca^{2+} ion bound (Gifford et al., 2007). Here the identity of the ligands involved in ion coordination will play a decisive role. Since the unfavorable entropic contributions can result from rearrangement of the loop upon Ca^{2+} binding, a hypothesis was proposed, which suggests that 'pre-formed' loops, that are already structured in the absence of Ca^{2+} would have lower positive entropy contributions. Important entropically costly contribution stems from the exposure of hydrophobic residues to the solvent, as seen in Ca^{2+} sensors. It was proposed that an increased number of hydrophobic residues in non-sensor EF-hands would inhibit transition from closed to open conformation. Accordingly, replacement of buried or polar amino acids from the N-lobe of CaM with corresponding nonpolar residues from calbindin D9k resulted in lower affinity for Ca^{2+} and in a closure of this subdomain even in the presence of Ca^{2+} (Ababou & Desjarlais, 2001). Entropy costs related with opening of Ca^{2+}-sensors upon binding of the cation counteract the favorable entropic contributions coming from water release which reduces significantly the theoretical maximal affinity of EF-hand loops for Ca^{2+} (Nelson & Chazin, 1998).

On the other hand, Ca^{2+} binding to EF-hands results in the formation of a network of coordination bonds, which implicates major favorable enthalpic contribution to ion chelation. Additional enthalpic effects stem from the formation of bonds stabilizing the loop and overall EF-hand architecture. Asp1 (residue in position X) is particularly important in providing hydrogen bonds network in Ca^{2+} binding loop. Its carbonyl oxygen of carboxylate group which directly coordinates the ion makes at the same time two hydrogen bonds with backbone NH groups of amino acids 4 and 5 in the loop, whereas non-coordinating oxygen is involved in a hydrogen bond with Gly in position 6 (Falke et al., 1994).

Although it has been suggested that affinity for Ca^{2+} can also be regulated by the differences in stability between apo and holo states (Gifford et al., 2007), this hypothesis does not hold true, taking into account

that proteins acting as Ca^{2+} buffers (e.g. calbindin D9k, parvalbumins) exhibit minimal changes in their conformation upon ion binding.

1.18 Molecular gymnasts versus yoga practitioners: differences between Ca^{2+} sensors and buffers

The concept of regulatory and structural sites was first suggested by Potter and Gergely (Potter & Gergely, 1975) and further discussed by Ikura (Ikura, 1996), where conformational changes in CaM and calbindin D_{9k} were compared. It was proposed that EF-hand domains in Ca^{2+}-binding proteins change conformation (Ca^{2+} sensors) only when this is needed for the biological activity, whereas proteins with buffering role (hereafter Ca^{2+} buffers) would display very minimal structural changes. Apart from minor changes occurring in buffering proteins upon Ca^{2+} binding, they have very high affinity for this cation due to the presence of many oxygen ligands in the loop and are also able to bind Mg^{2+}, albeit with lower affinity. It has also been proposed that the number of Met residues in CaM domains could help to distinguish whether a protein is Ca^{2+}sensor or buffer, respectively (Nelson & Chazin, 1998). Methionine is a special amino acid, because although being hydrophobic it is still polarizable due to the presence of a sulfur atom. This residue is also more flexible than other aliphatic residues. The number of methionines should be higher in sensors, as it will be on one hand energetically less costly to expose it into aqueous environment and it should be also able to stabilize the closed state due to its hydrophobic nature. Presumably, the most important factor determining to which class of EF-hands a protein belongs to will be the difference in the thermodynamic cost that a protein has to pay in order to change conformation from closed to open. Accordingly, sensors would prefer open conformation because the geometric restraints caused by ion binding would be higher than the cost of the exposure of hydrophobic residues to the environment (Nelson & Chazin, 1998).

1.19 When nature goes awry – mutations in human α-actinin genes

Since *h*Actn2 is heavily expressed is skeletal and cardiac muscles where it maintains the integrity of Z-disc and controls the mechanical strength generated in the sarcomere, it is not surprising that dominant

mutations found in this gene are often detrimental to muscle function and inevitably linked to myopathies (Ribeiro Ede et al., 2014). *h*Actn3 is expressed in fast-twitch muscle fibers and is dispensable in humans. About 1.5 billion people worldwide lack this protein as a result of the presence of premature stop codon polymorphism, R577X (Lee, Houweling et al., 2016). Lack of *h*Actn3 is higher in endurance elite female runners, whereas presence of *h*Actn3 allele is most common in sprint runners (Yang, MacArthur et al., 2003). Similarly, knockdown of Actn3 gene in mice increases its aerobic capacity and makes them 33% more fatigue resistant (MacArthur, Seto et al., 2007). Presumably, in those cases *h*Actn2 can compensate for the loss of *h*Actn3.

It was proposed that cells tend to express multiple variants of the same proteins to enhance their survival potential (Otey & Carpen, 2004). Although expression pattern of non-muscle isoforms usually overlaps, *h*ACTN1 is not expressed in kidney cells. Therefore, mutations in *h*Actn4 gene in human population are associated with defects in podocytes, specialized kidney cells, and subsequently result in a serious clinical condition, focal and segmental glomerulosclerosis (FSGS). α-Actinin-4 deficient mouse displays similar symptoms, despite the fact that mouse podocytes show expression of both α-actinin isoforms (Kos, Le et al., 2003). Moreover, increased expression levels of *h*Actn4 have been found in many tumor types and they correlate positively with infiltrating phenotypes (Honda, Yamada et al., 1998). A possible role of *h*Actn1 in colon tumorogenesis has been demonstrated. Namely, phosphorylation of *h*Actn1 has an effect on pressure-stimulated colon cancer cell adhesion to collagen I, a function important for tumor cell implanatation and metastasis due to its involvement in focal adhesion remodeling (Craig, Haimovich et al., 2007), which makes it a potential therapeutic target in colon cancer.

Mutations in *h*Actn1 gene, on the other hand, cause defects in one particular cell type, namely platelets, although those cells express *h*Actn4. In case of congenital macrocytopenia (CMPT), *h*Actn4 cannot substitute for *h*Actn1 deficiency. All mutations found in patients with CMPT localize in ABD and CaM domain, but interestingly not in the rod (Murphy & Young, 2015).

1.20 Role of Ca^{2+}-sensitive α-actinins in mammalian cells

Simultaneous studies of Ca^{2+}-insensitive α-actinins are rare. Although the cellular distribution of *h*Actn1 and *h*Actn4 is different, they may have overlapping functions in some cell types. It has been shown that both non-muscle α-actinin isoforms contribute to mobility and rigidity sensing of glioma cells, which may

be related to invasiveness of those tumor cells *in vivo*. Moreover, partial knockdown of each isoform resulted in an increase of vinculin expression and decrease in the level of non-muscle myosin II, which correlates with focal adhesion remodeling in those cells (Sen, Dong et al., 2009).

The role of *h*Actn1 in the determination of left-right asymmetry has been addressed in focal adhesions in cells plated on circular adhesive islands. Overexpression of GFP-tagged *h*Actn1 resulted in change of cell asymmetry, although this result should be treated with caution due to possible toxic effects related to overexpression of GFP-tagged protein, especially due to the fact that *h*Actn1 knockdown did not affect left-right asymmetry (Tee, Shemesh et al., 2015).

So far the role of Ca^{2+}-sensitivity of non-muscle α-actinins has not been thoroughly addressed. According to Burridge and Feramisco, micromolar concentrations of Ca^{2+} reduce actinin bundling activity *in vitro* (Burridge & Feramisco, 1981). However, the Ca^{2+} affinity of CaM domain from *h*Actn1 is between 50 and 100 μM (Backman, 2015, Drmota Prebil et al., 2016), which questions whether human Ca^{2+}-sensitive α-actinins are Ca^{2+} regulated, taking into account that levels of this ion in eukaryotic cells, are around 0.1 μM in a resting state and 1-100 μM during a signaling event (Verkhratskiĭ & Toescu, 1998). It can be assumed that Ca^{2+} regulation of *h*Actn1 and *h*Actn4 might take place *in vivo*, despite their low affinity for this ion, provided they are localized around cell membrane, where the local concentration of Ca^{2+} during signaling cascade might be locally more elevated than in the cytoplasm and might reach concentration of up to 100 μM (Verkhratskiĭ & Toescu, 1998). So far only one study has been published in which the function of Ca^{2+}-insensitive mutant of α-actinin during cell cytokinesis has been addressed. Authors did not find significant changes in the duration of cytokinesis in cells overexpressing GFP-Ca^{2+}-insensitive α-actinin mutant, although the level of α-actinin and actin in cleavage furrow was reduced in those cells (Jayadev, Kuk et al., 2012).

1.21 *Entamoeba histolytica* – a dangerous pathogen

Entamoeba histolytica is a protozoan, which can infect different species, including human. Under normal conditions this amoeba inhabits human intestine and feeds on bacteria present there; in some cases, though, the protozoan becomes invasive (Nozaki & Bhattacharya). In fact amebiasis caused by *E. histolytica* is the third most common parasitic disease, right after malaria and schisostomiasis, causing up to 100, 000 deaths annually as a result of either amoebic colitis or amoebic liver abscess (Stanley, 2003).

The reason why this disease still affects so many individuals is lack of proper diagnostic tests and inaccessibility of antibiotics in developing countries and lack of vaccine. Metronidazole is often used to cure the infection, but is has toxic side effects and it is plausible that *E. histolytica* will soon develop resistance towards it, so there is a need for the discovery of new anti-amebic drugs (Ralston, 2015). There are two life cycle forms of this organism, namely highly mobile amoebic trophozoites and infectious cystic form (**Fig. 13**), both colonizing host large intestine (Nozaki & Bhattacharya). *E. histolytica* is an eukaryotic organism; however, it is a very primitive one, as it lacks many organelles typical for *Eucaryotes*, such as mitochondria, Golgi and endoplasmic reticulum. The genome of *E. histolytica* was sequenced in 2005 and it allowed to uncover metabolic adaptations in this protozoan to colonize human intestine, e.g. presence of bacterial-like fermentation enzymes (Loftus, Anderson et al., 2005). Likewise, release of its genome should assist the generation of new, specific drugs against this parasite. One question seems to be particularly interesting – why is *E. histolytica* actually a pathogen? Theoretically it does not have any benefit in killing a human host, as trophozoites cannot survive outside of human body. Why is this organism not just a simple commensal, like *Entamoeba dispar*? It has been proposed that pathogenicity of *E. histolytica* might be a result of coincidental evolution, where the parasite utilizes the same mechanisms to kill enteric bacteria, host red blood cells and epithelial cells (Ghosh & Samuelson, 1997). Anyway, the line between being a commensal and pathogen is in this case very thin, as *E. histolytica* is symptomatic in only about 10% of the infected population (Stanley, 2003), and factors determining invasiveness have not been hitherto determined.

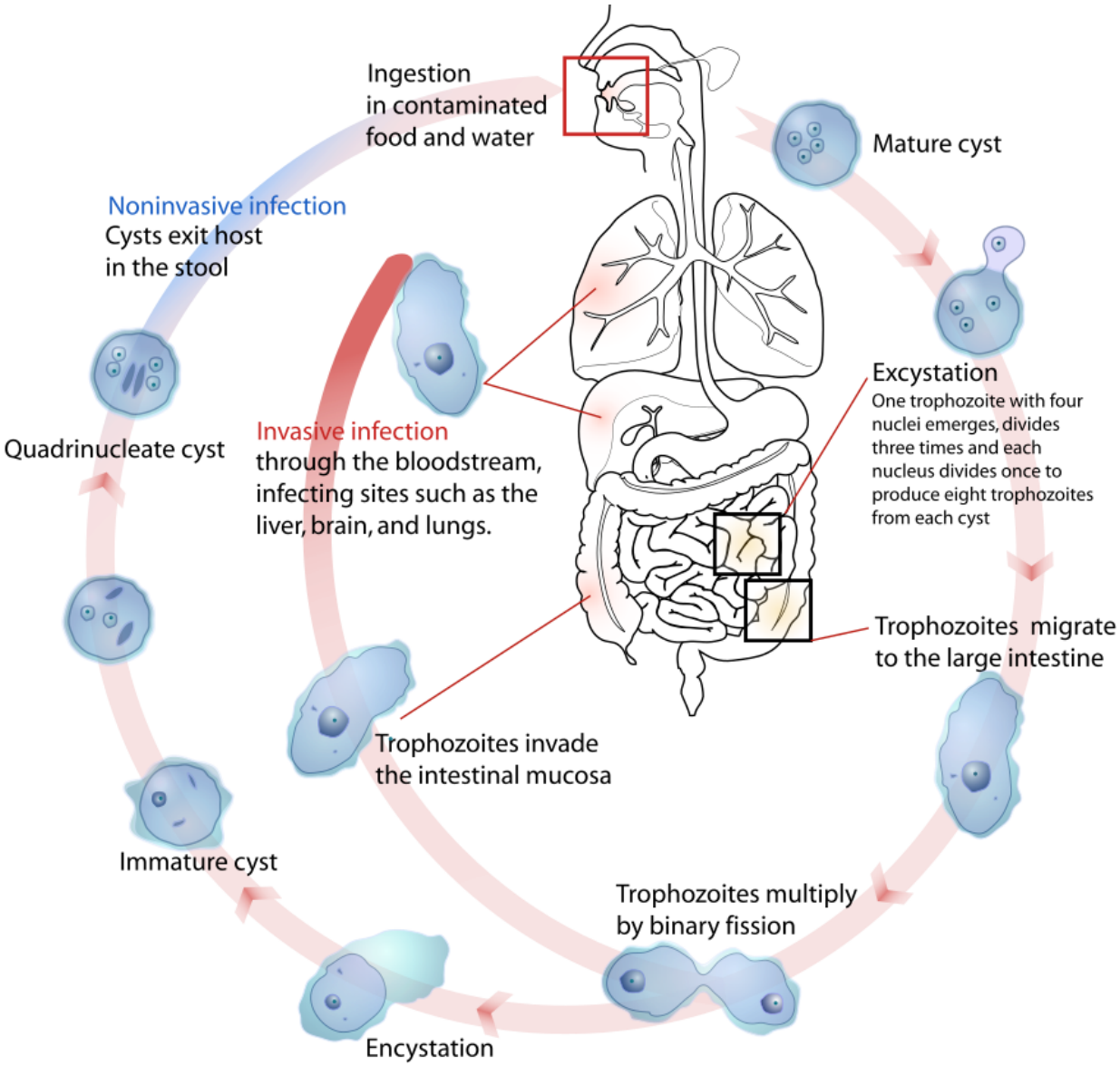

Figure 13. Life cycle of Entamoeba histolytica. Cystic form of the parasite can exist outside of the host organism and can be ingested by consumption of contaminated food or water. Upon encystation, mobile trophozoites colonize the large intestine. In some cases, *E. histolytica* colonization can progress towards invasive infection, where trophozoites are transported from the bloodstream to other organs, like brain, liver and lungs. Figure adapted from www.wikipedia.org.

1.22 Actin cytoskeleton of *Entamoeba histolytica*

Trophozites of *E. histolytica* are in constant movement and are able to form surface projections facilitating pinocytosis, phagocytosis and adhesion. Mobility of this cellular form is thought to control invasiveness

and requires the presence of an advanced form of dynamic cytoskeleton. In 1982 it was reported that cytochalasin B interferes with phagocytosis and virulence in this organism (Sabanero & Meza, 1982); *E. histolytica* actin was subsequently isolated in 1983 (Meza, Sabanero et al., 1983). Since then, the cytoskeleton of this parasite has been extensively studied and many actin-binding proteins have been identified, including profilin, α-actinin, myozins I and II, vinculin, and many others (reviewed in (Meza, Talamas-Rohana et al., 2006)).

1.23 *Entamoeba histolytica* in action – fascinating way of host cell killing

E. histolytica virulence has been related to its ability to interact with host cells and subsequently phagocytose them (Orozco, Guarneros et al., 1983). Mutants in which phagocytosis is impaired *in vitro* are also less virulent *in vivo* (Hirata, Que et al., 2007, Katz, Ankri et al., 2002, Rodriguez & Orozco, 1986). Phagocytosis requires drastic rearrangements of actin cytoskeleton and is, to some extent, regulated by Ca^{2+}, a process which is described below and might involve α-actinin.

Phagocytosis begins with the adherence of amoeba to host cells, a process mediated by a dimeric D-galactose/*N*-acetyl-d-galactosamine (Gal/GalNAc)-specific amebic lectin (Petri, Smith et al., 1987, Ravdin, Murphy et al., 1985b) and glycoproteins present on host cell surface (Chadee, Petri et al., 1987). Genome analysis revealed more specialized molecules involved in the adherence of the parasite to human cells and helped to identify amebic proteins involved in cell killing (Loftus et al., 2005). The most striking repertoire of pathogen molecules involved in cell killing are amoebapores, peptides which get inserted in host cell membrane (or bacterial cell wall) and are capable of forming ion channels. *E. histolytica* escapes the activity of its own membrane-penetrating peptides due to unique composition of its cell membrane, which is cholesterol rich (Andra, Berninghausen et al., 2004). Cysteine proteinases are yet another weapon used by the protozoan to destroy the target. Genome analysis reveals that *E. histolytica* is a very specialized killer, equipped with multiple homologues of cell killing proteins (Loftus et al., 2005). Upon contact with host cells pathogen continues its deadly actions by initiation of their apoptosis (Sateriale & Huston, 2011). Subsequently, the parasite can devour the hijacked cell in a process of phagocytosis (**Fig. 14**).

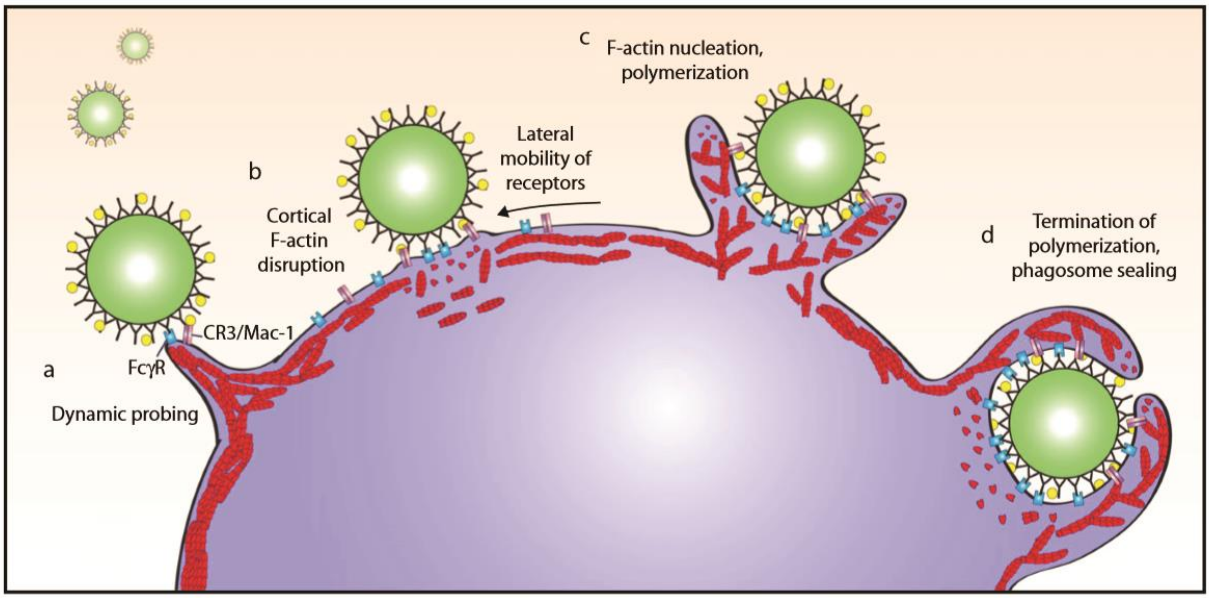

Figure 14. Schematic representation of phagocytosis in macrophages. (A) Opsonized molecule (green ball) interacts with cell surface receptors mediating phagocytosis (shown in blue and purple). (B) In the initial step of phagocytosis actin network (in red) needs to be depolymerized in order to allow for cell membrane invagination (C) Subsequently actin in the vicinity of the cell membrane polymerizes to facilitate the formation of phagocytic cup (D) To terminate phagocytosis and in order to close the cell membrane actin filaments are again disassembled. Figure adapted from (Freeman & Grinstein, 2014).

Some from over 90 transmembrane kinases present in this organism are proposed to act as receptors of apoptosis (Sateriale & Huston, 2011). Phagocytosis in *E. histolytica*, similarly to mammalian cells, requires significant remodeling of actin-myosin cytoskeleton. In order to create a pseudopod extension actin close to amebic membrane must quickly depolymerize and monomeric actin needs to now polymerize again (**Fig. 14B,C**). Deformation of the membrane, together with actin-myosin contraction, results in a closure of the phagocytic cup (**Fig. 14C**). As the last step of this process, actin filaments need to be again depolymerized to allow engulfment of the phagosome, a process regulated by Ca^{2+} ions (**Fig. 14D**) (Freeman & Grinstein, 2014, Marion & Guillen, 2006). Not surprisingly, the process of phagocytosis in *E. histolytica* has been studied extensively, as a hallmark of its virulence. As expected, many actin-binding proteins and signaling proteins (small GTP-ases) participate in this process (reviewed in (Mansuri, Bhattacharya et al., 2014)). Interestingly, this simple pathogen expresses 27 Ca^{2+}-binding proteins (Bhattacharya, Padhan et al., 2006), many of which were subsequently linked to actin cytoskeleton (Sahoo, Labruyère et al., 2004) and/or phagocytosis (Aslam, Bhattacharya et al., 2012, Kumar, Aslam et al., 2014). Recently, a new way of host cell killing by *E. histolytica* was discovered, called trogocytosis

(Ralston, Solga et al., 2014). In this case the parasite does not encapsulate the whole host cells, but rather bits off and ingests smaller parts of it. Phagocytosis and trogocytosis are compared in **Fig. 15**. The latter process usually involves bigger material and preferably living cells, whereas in phagocytosis *E. histolytica* feeds on dead cells (Ralston, 2015). Both processes require physiological temperature, significant rearrangement of actin cytoskeleton near the cell membrane and are mediated by the overlapping set of molecules, involving e.g. Gal/Gal-Nac lectin, C2-domain-containing protein kinase (*Eh*C2PK) and phosphatidylinositol-4,5-bisphosphate 3-kinase (PI3K), however some proteins are crucial only for phagocytosis, e.g. myosin and calreticulin (Ralston, 2015). Trogocytosis might be particularly important for *E. histolytica* virulence in the intestine, where the epithelial cells adhere to each other and where phagocytosis might be an impossible scenario.

1.24 Does Ca^{2+} regulate virulence of *Entamoeba histolytica*?

Ca^{2+} levels were demonstrated to be important for pathogenicity of some protozoan pathogens, including *Trypanosoma cruzi*, *Toxoplasma gondii*, *Leischmania amazonensis* and *Plasmodium falciparum* (Bhattacharya et al., 2006). Therefore, it is tempting to think that a similar mechanisms may be at work in *E. histolytica*. Exposure of the trophozoites of the latter to fibronectin results in an increase of intracellular Ca^{2+}, which is furthermore required to regulate their adhesion (Carbajal, Manning-Cela et al., 1996). This result is in a stark contrast with the results of Mandel *et al* (Ravdin, Moreau et al., 1988), who claim that there is no increase in intracellular Ca^{2+} levels in trophozoites upon contact with CHO cells, but Ca^{2+} levels increase instead in the latter one. Independently of those two contradictory results, chelation of Ca^{2+} ions was shown to interfere with cytolytic activity of *E. histolytica* (Ravdin, Murphy et al., 1985a). Similarly, Ca^{2+} antagonists were further shown to slow down the growth and encystation of *E. histolytica* and *E. invadens*, which were moreover reported to be CaM-like protein dependent (Makioka, Kumagai et al., 2001). All these findings indicate that Ca^{2+} does regulate the virulence of E. *histolytica;* however, the exact mechanism behind it has not been uncovered and most likely requires the coordinated action of many amebic Ca-binding proteins (CaBP)s.

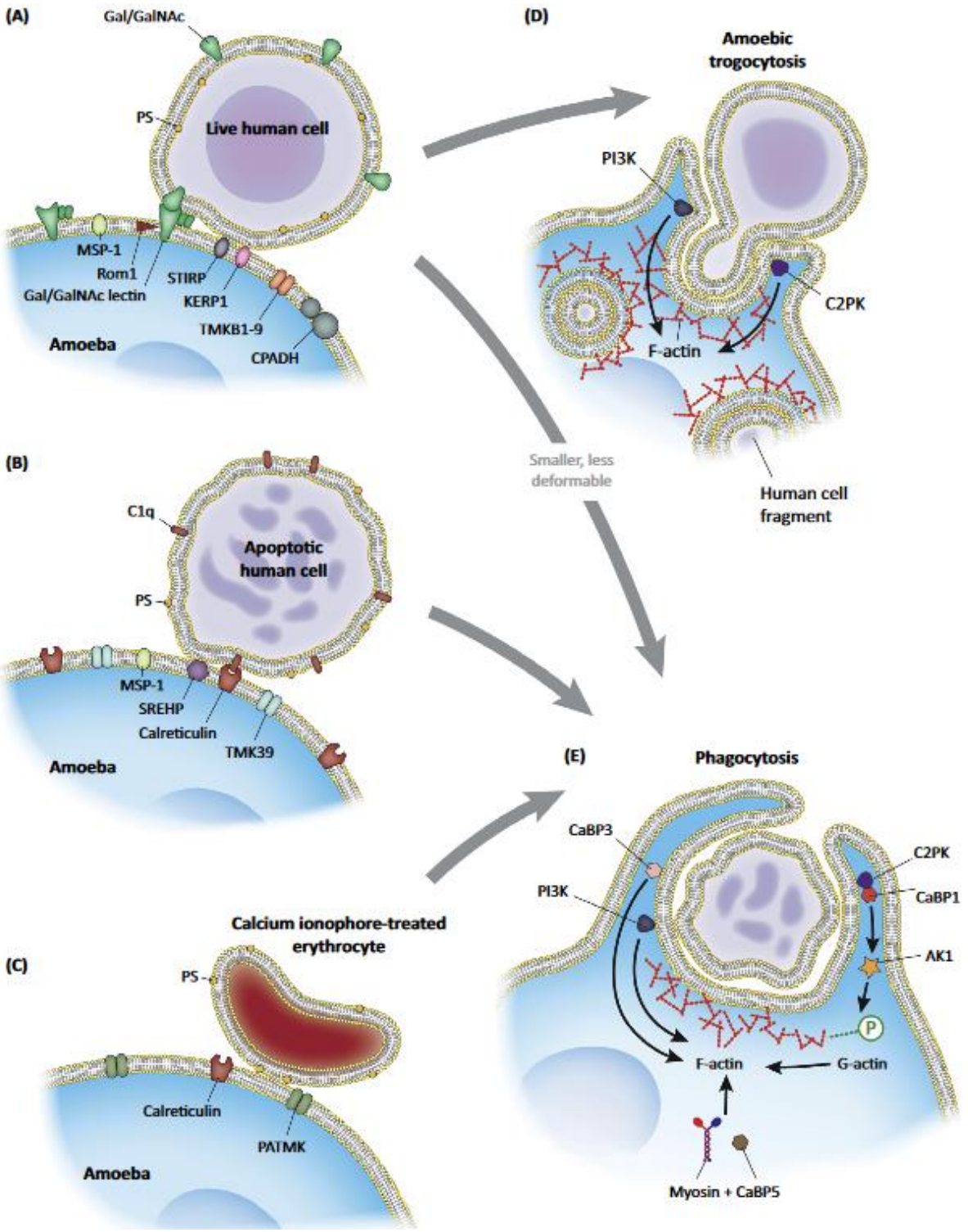

Figure 15. Comparison of trogocytosis and phagocytosis in Entamoeba histolytica. (A) Attachment of parasite to host cell is mediated by Gal/Gal-Nac lectin. (B) Host cell undergoing apoptosis is directed to undergo phagocytosis. (C) Calcium ionophore-treated erythrocyte. (D) Bigger and live material is preferentially ingested by trogocytosis. (D,E) Phagocytosis and trogocytosis are mediated by similar set of molecules. Figure adapted from (Ralston, 2015).

1.25 α-Actinin 2 from *Entamoeba histolytica*

The presence of α-actinin-like proteins in *E. histolytica* was suggested in 1992, as some proteins isolated from this parasite were shown to cross-react with anti-α-actinin antibodies (Bailey, Shen et al., 1992). In 2002, two Ca^{2+}-binding molecules (most likely only protein fragments) were discovered and called granins, due to its presence in cytoplasmic granules of amoeba (Nickel, Jacobs et al., 2000). In 2004 it was suggested that the earlier described protein is an α-actinin, which was further corroborated when Ca^{2+}-binding proteins from this organism were compared based on genomic analysis and granin 2 was indeed found out to be α-actinin (Bhattacharya et al., 2006). Simultaneously, α-actinin isoform 2 from *E. histolytica* (hereafter *Eh*Actn2, UniProt code C4LWU6) was cloned, expressed and characterized (Virel et al., 2007). The discovered 69-kDa protein is shorter than human α-actinins and was predicted to contain ABD, followed by a shorter rod domain, with presumably only two SRs and three putative EF-hands (**Fig. 16**). Importantly, it was able to bind Ca^{2+} and to bundle actin filaments in a Ca^{2+}-dependent way. This protein was proposed to be an ancestral α-actinin, preceding the ones present in higher *Eukaryotes* (Virel et al., 2007). Since then α-actinin was reported to be enriched in *E. histolytica* phagosomes, which suggests its possible role in phagocytosis and virulence (Okada, Huston et al., 2005). In 2004 it was shown that a protein from spectrin family with molecular weight (MW) of 70 kDa is able to interact with *E. histolytica* Gal/GalNac lectin (Marion & Guillen, 2006). Although it was not possible to identify and clone this protein at that time, it was envisioned that it might have been α-actinin. In this work the authors used a polyclonal rabbit antibody raised against human spectrin, which theoretically might cross-react with amebic α-actinin.

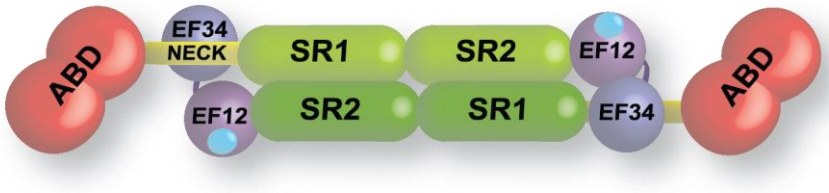

Figure 16. Scheme of α-actinin-2 from Entamoeba histolytica. In comparison to human α-actinins, *Eh*Actn2 has a shorter rod domain composed of only two SRs.

2 AIMS

α-Actinins are universal actin bundlers found in all *Eukaryota* except plants. The activity of non-muscle α-actinins is reported to be modulated by Ca^{2+}, as first demonstrated in 1981 (Burridge & Feramisco, 1981), but the molecular mechanism behind this regulation has not been hitherto unraveled.

The main goal of this thesis is to understand the mechanism of Ca^{2+}-regulation of α-actinins. α-Actinin-2 from *E. histolytica* was chosen as a model protein due to its smaller size compared to human variants, its relatively moderate sequence identity to non-muscle human counterparts (30%), and its amenability for crystallization. Also, *E. histolytica* is a common human pathogen and is therefore an interesting model organism from an epidemiological point of view.

The existing structure of Ca^{2+}-bound *Eh*Actn2, previously solved by Dr. Nikos Pinotsis (Gkougkoulia, 2014), was used as a starting point for this project. We hypothesized that Ca^{2+} binding to *Eh*Actn2 EF-hands inhibits protein activity by causing conformational changes that propagate to ABD and ultimately result in diminished F-actin bundling ability. ΔCa variant (Ca^{2+}-free *Eh*Actn2 previously designed by Dr. Eirini Gkougkoulia (Gkougkoulia, 2014)) was crystallized for comparison with Ca^{2+}-bound *Eh*Actn2. A number of biochemical and biophysical assays were employed to study protein stability in the presence and absence of Ca^{2+} as well as protein-ion and protein domains interactions. Biochemical assays were additionally used to characterize protein activity in the presence and absence of Ca^{2+}. Altogether, this research prepared the ground for further *in vivo* experiments (not shown in this thesis).

Our results on *Eh*Actn2 may pave the way to understand Ca^{2+}-regulation of human α-actinins, as *Eh*Actn2 is considered to be an ancestral variant of this protein family (Virel et al., 2007). Moreover, uncovering how the cytoskeleton is regulated in *E. histolytica* might help us not only to better understand the biology of this pathogen but also to expand the general view of amoeba-host interactions, which might, in turn, have potential therapeutic benefits.

3 EXPERIMENTAL PROCEDURES

3.1 Molecular cloning

The coding sequence of FL *Eh*Actn2 wild-type (WT) (619 residues, containing two differences with respect to UniProt code C4LWU6; F247L and E435G, for details on constructs, see **Table 2**) was kindly provided by Lars Backman (Umeå University, Sweden) and cloned into a modified pET19b vector (Novagen) for recombinant expression in *Escherichia coli*. This vector confers resistance towards ampicillin and attaches an N-terminal deca-histidine tag (His_{10}-tag) followed by a tobacco etch virus (TEV) protease cleavage site. This construct was used as template to generate other variants of the protein in the same vector, with the exception of the rod domain, which was cloned into pETM14 vector. Quikchange mutagenesis (Agilent Technologies) was used for the introduction of point mutations. Site-directed mutagenesis (Hemsley, Arnheim et al., 1989) was implemented for the creation of deletions (i.e. to clone ΔEF-hands constructs). A chimeric construct was generated using Gibson assembly (Gibson, Young et al., 2009). All cloned constructs were verified by DNA sequencing (Eurofins Genomics). ΔCa, ΔEF1-4, ΔEF3-4 and rod constructs were cloned by Dr. Eirini Gkougkoulia (Gkougkoulia, 2014). SS1 and SS2 mutations were introduced in rod, ΔEF3-4 and *Eh*Actn2 constructs, whereas SS3 was additionally introduced in rod and ΔEF3-4. Primers used for molecular cloning are listed in **Table 3**.

3.2 Protein production and purification

All constructs were overexpressed using auto-induction medium (Studier, 2005) in *E. coli* strain Rosetta2(DE3)pLysS except EF-hands, which were expressed in *E.coli* BL21(DE3)pLysS strain. Cells were typically incubated for 6 h at 37°C and then overnight at 20°C in the media containing either 100 μg/ml carbenicillin (constructs in pET19b vector) or 50 μg/ml kanamycin (pETM14 vector) plus 34 μg/ml chloramphenicol. Cells were harvested by centrifugation at 5,000x*g* for 20 min and resuspended in buffer A (see buffer composition in **Table 4**) plus protease inhibitors cocktail, which was usually supplemented with 20 mM imidazole, 5% (v/v) glycerol, 0.1% (v/v) Triton X-100 and 0.5 mM EDTA.

Table 2. Constructs used in this work.

Name	Sequence	MW* (kDa)	Mutations	Vector / Protein tag	Additional N-t residues
*Eh*Actn2 WT	1-619	140		pET19b / N-t His_{10}-tag	G-S
ΔCa	1-619	140	D497N+N499G+D501N	pET19b / N-t His_{10}-tag	G-S
NEECK	1-619	140	A241E+L245E	pET19b / N-t His_{10}-tag	G-S
$NEECK_b$	1-619	140	A241E	pET19b / N-t His_{10}-tag	G-S
ΔEF3-4	1-561	127		pET19b / N-t His_{10}-tag	G-S
ΔEF1-4	1-480	108		pET19b / N-t His_{10}-tag	G-S
ΔEF3-4 SS1	1-561	127	S322C+Q473C	pET19b / N-t His_{10}-tag	G-S
ΔEF3-4 SS2	1-561	127	G326C+Q473C	pET19b / N-t His_{10}-tag	G-S
ΔEF3-4 SS3	1-561	127	Q319C+Y469C	pET19b / N-t His_{10}-tag	G-S
HA-*Eh*Actn2	1-619	142		pET19b / N-t His_{10}-tag & C-t HA-tag	G-S
ABD	3-231	26		pETM14 / N-t His_6-tag	G-P-A-M
ABD-SR1	1-367	42		pET19b / N-t His_{10}-tag	G-S
ABD-SR1 NEECK	1-367	42	A241E+L245E	pET19b / N-t His_{10}-tag	G-S
rod	240-480	55		pETM14 / N-t His_6-tag	G-P-A-M
rod SS1	240-480	55	S322C+Q473C	pETM14 / N-t His_6-tag	G-P-A-M
rod SS2	240-480	55	G326C+Q473C	pETM14 / N-t His_6-tag	G-P-A-M
rod SS3	240-480	55	Q319C+Y469C	pETM14 / N-t His_6-tag	G-P-A-M
EF1-2	480-561	9		pET19b / N-t His_{10}-tag	G-S
EF3-4	565-619	7		pET19b / His_{10}-tagG-S	G-S
EF1-4	480-619	16		pET19b / N-t His_{10}-tag	G-S
EF1-4 ΔCa	480-619	16	D497N+N499G+D501N	pET19b / N-t His_{10}-tag	G-S
EF1-4 D501N	480-619	16	D501N	pET19b / N-t His_{10}-tag	G-S
EF1-4 D505N	480-619	16	D505N	pET19b / N-t His_{10}-tag	G-S
chimActn2	1-245 (*Eh*Actn2) +272-742 (hActn2) +457-619 (*Eh*Actn2)	202		pET19b / N-t His_{10}-tag	G-S

*MW (molecular weight) corresponds to the oligomeric state of the protein (i.e. monomer or dimer).

Table 3. Primers used in this work.

Construct	Forward primer	Reverse primer	Cloning method
NEECK	5'GAAAAAGCTGGTAAAAGAGAGGGTAATTTC GAAGATTTCCTTAGAGCTACAG	5'CTGTAGCTCTAAGGAAATCTTCGAAATTACCCT CTCTTTTACCAGCTTTTTC	QC*
NEECK$_b$	5'GAAAAAGCTGGTAAAAGAGAGGGTAATTTC CTTGATTTC	5'GAAATCAAGGAAATTACCCTCTCTTTTACCAGC TTTTTC	QC
^{4}*Eh*Actn2 WT	5' GTGAGTTAGTTGCTCAATGG	5' TTCCCTGAAAATAAAGATTCTCAG	SDM
SS1	**S322C** 5'GCTACATTATTTGGTCAAATTAATTGTAAATT AAGAGGAATGAAAAGACCAG **Q473C** 5'GAAGATTGTTTATATTGAAGCCTGCATTAAT GAAGCATCTAGTGGAG	**S322C** 5'CTGGTCTTTTCATTCCTCTTAATTTACAATTAATTT GACCAAATAATGTAGC **Q473C** 5'CTCCACTAGATGCTTCATTAATGCAGGCTTCAA TATAAACAATCTTC	QC
SS2	**G326C** 5'GGTCAAATTAATTCAAAATTAAGATGCATGA AAAGACCAGTTTATGTTGC **Q473C** 5'GAAGATTGTTTATATTGAAGCCTGCATTAAT GAAGCATCTAGTGGAG	**G326C** 5'GCAACATAAACTGGTCTTTTCATGCATCTTAAT TTTGAATTAATTTGACC **Q473C** 5'CTCCACTAGATGCTTCATTAATGCAGGCTTCAA TATAAACAATCTTC	QC
SS3	**Q319C** 5'TTAATGCAACCAAATAATGTAGCAAGATCAC CTTG **Y469C** 5'GATTGTTTGTATTGAAGCCCAAATTAATG	**Q319C** 5'TTTGGTTGCATTAATTCAAAATTAAGAGGAAT GAAAAG **Y469C** 5'CTTCAATACAAACAATCTTCTTTTCAAACATAC	QC
ABD-SR1	5'TGATGTCTTATTGCACTTAGAAAAGCATTTGC	5'CTAATTTCTCATAGCAGTATTTAATTTAGATC	SDM
EF1-2	5'TAACTAGCATAACCCCTTGGGGCCTCT	5'ATTTTCATCGTTCTTTTCTTTCATGTATTGG	SDM
EF3-4	5'CCAGGGGCCCGCCGAACAACTTAATGAAATC TTCTCTACTATTG	5'GACCCGACGCGGTTAATTATCTTAACCCAAGC AGCATAATC	SDM
EF1-4	5'CCAGGGGCCCGCCAGTGGAGTTACTGCTGA ACAAATG	5'GACCCGACGCGGTTAATTAGTCTTAACCCAAG CAGCATAATC	SDM
EF1-4 D501N	5'CATTTGATGGAAATCATAATGGAATTCTTGA TAAAC	5'GTTTATCAAGAATTCCATTATGATTTCCATCAA ATG	QC
EF1-4 D505N	5'GAAATCATGATGGAATTCTTAATAAACTTGA ATTTAGATC	5'GATCTAAATTCAAGTTTATTAAGAATTCCATCA TGATTTC	QC
chimActn2	**INSERT PCR** 5'GCTGGTAAAAGAGCTGGTAATTTCCTT GCTGTGAATCAAGAGAATGAGAGGC **VECTOR PCR** 5'GCCTCTCATTCTCTTGATTCACAGC AAGGAAATTACCAGCTCTTTTACCAGC	**INSERT PCR** 5' GCAGTAACTCCACTAGATGCTTCATT GATCTGAGTCTCCACCTCATTGATG **VECTOR PCR** 5'CATCAATGAGGTGGAGACTCAGATC AATGAAGCATCTAGTGGAGTTACTGC	GA

*QC states for QuikChange Mutagenesis, SDM for site-directed mutagenesis, GA for Gibson assembly. Introduced mutations are indicated in red. Blue-colored fragments in Gibson assembly indicate complementary DNA sequences between PCR products of vector and insert.

Cells were disrupted at 4°C by sonication and the cell debris was removed by centrifugation at 50,000x*g* for 30 min at 4°C. Supernatant was subsequently loaded onto a 5-ml His-Trap FF crude column (GE Healthcare) previously equilibrated with buffer A plus 20 mM imidazole, and the sample was eluted with the same buffer plus 300 mM imidazole. The N-terminal His-tag was next cleaved using either TEV (pET19b vector) or 3C (pETM14 vector) protease by overnight dialysis at 4°C against buffer A. The digested sample was loaded onto a Ni Sepharose 6 Fast Flow column (GE Healthcare) previously equilibrated with buffer A to remove un-cleaved protein and His_6-tagged protease. Flow-through fractions were pooled and diluted with 20 mM Tris-HCl, pH 7.6 to 20 mM NaCl concentration, loaded onto a Resource Q column (GE Healthcare), and further eluted with a 0-100% gradient of the same buffer plus 1 M NaCl. Protein fractions were pooled and finally loaded onto a Superdex 200 26/600 or Superdex 75 16/60 column (both GE Healthcare) previously equilibrated with buffer A. For crystallographic studies ΔCa was methylated as published elsewhere (Rauert, Eddine et al., 2007) and further polished by size-exclusion chromatography (SEC) as described above.

Protein samples were dialyzed against specific buffers (**Table 4**) and concentrated by ultrafiltration before each experiment. Protein identity and purity were analyzed by Coomassie-stained 12%-15% Glycine-SDS-PAGE. Protein concentration was determined by measuring absorbance at 280 nm in a NanoDrop spectrophotometer using the calculated absorption coefficients $E_{0.1\%}$=0.886 (*Eh*Actn2 WT, ΔCa, NEECK), $E_{0.1\%}$=0.817 (ΔEF3-4 and ΔEF3-4-SS variants), $E_{0.1\%}$=1.246 (ABD), $E_{0.1\%}$=0.454 (rod and rod-SS variants), $E_{0.1\%}$=1.044 (EF1-4 variants), and $E_{0.1\%}$=0.634 (EF1-2), $E_{0.1\%}$=1.200 (chimActn2). For estimation of molar protein concentration proteins were considered in their respective oligomeric state (i.e. monomer or dimer). To verify the presence of disulfide bonds, samples at protein concentration of 1 mg/ml were incubated at room temperature (RT) for 1 h in the absence and presence of 0.5 mM oxidized glutathione and next analyzed by Coomassie-stained 7-12.5% Glycine-SDS-PAGE using loading buffer with and without 2-mercaptoethanol. The presence of Ca^{2+} in *Eh*Actn2 WT and EF1-4 was assessed by intact mass spectrometry at the Mass Spectrometry Service Facility (MFPL, Vienna).

Table 4. Composition of the most common buffers used in this work.

Buffer name	Chemical composition
Buffer A	50 mM Tris-HCl, pH 7.6, 150 mM NaCl
Buffer B	20 mM Tris, pH 8.0, 100 mM KCl
Buffer C	20 mM HEPES, pH 8.0, 100 mM KCl
Buffer D	20 mM HEPES, pH 6.7, 150 mM NaCl, 1 mM TCEP
G-buffer	2 mM Tris-HCl, pH 8.0, 0.2 mM $CaCl_2$, 0.2 mM ATP, 2 mM 2-mercaptoethanol
10x F-buffer	50 mM Tris-HCl, pH 8.0, 0.5 M KCl, 20 mM $MgCl_2$, 20 mM ATP

3.3 Static and dynamic light scattering

Sample dispersity was assessed by both static and dynamic laser light scattering. The former was performed at RT by SEC coupled to multi-angle static laser light scattering (MALLS) using a Superdex 200 10/300 column (GE Healthcare) previously equilibrated with buffer A plus either 5 mM EGTA or 5 mM $CaCl_2$. Samples were loaded at protein concentration of 4 mg/ml using an Agilent Technologies 1260 Infinity HPLC system coupled to a MiniDawn Treos detector (Wyatt) with a laser emitting at 690 nm. The refractive index was measured with a Shodex RI-101 detector (Shodex). Samples for dynamic laser light scattering were prepared at protein concentration of 0.5-5 mg/ml in buffer A and measured at RT using a DynaPro Nanostar instrument (Wyatt Technology) with a laser wavelength of 658 nm. Data were analyzed with DYNAMICS software (Wyatt Technology).

3.4 Circular dichroism spectroscopy

Far-UV circular dichroism spectra were acquired using a Chirascan Plus spectrophotometer (Applied Photophysics). Samples were prepared in buffer A and diluted to a final protein concentration of 10 µM in the presence of either 1 mM EGTA or 1 mM $CaCl_2$. Spectra were collected in triplicate at 260-200 nm using a 0.1 mm path-length quartz cuvette and 1 nm intervals. Secondary structure content was analyzed using K2D server (http://dichroweb.cryst.bbk.ac.uk/html/links.shtml).

3.5 Differential scanning fluorimetry

Proteins were first dialyzed against buffer B and then mixed (4 µl at 2 mg/ml) in the same buffer with 1 µl of 20x SYPRO Orange protein gel stain (ThermoFisher Scientific) to a final volume of 25 µl. Measurements were carried out in triplicate in the presence of either 1 mM EGTA, 1 mM $CaCl_2$, or 0.2 mM EGTA plus 2 mM $MgCl_2$. Fluorescent signal was measured using iQTM5 multicolour Real-Time PCR Detection System (Bio-Rad) and data analyzed using Bio-Rad CFX Manager software.

3.6 Limited proteolysis experiments

Limited proteolysis of *Eh*Actn2 WT and ΔCa (both at 1 mg/ml) was performed in buffer B plus 5 mM $CaCl_2$ using bovine pancreatic trypsin, bovine pancreatic chymotrypsin, proteinase K from *Engyodontium album*, subtilisin from *Bacillus licheniformis*, and thermolysin from *B. thermoproteolyticus* (all from Sigma-Aldrich). Reactions were incubated at RT for 1 h at protease:substrate weight ratios of 1:50 and 1:100. Samples were subsequently precipitated with trichloroacetic acid and analyzed by Coomassie-stained 12.5% Glycine-SDS-PAGE. Selected bands were identified by peptide mass fingerprinting at the Mass Spectrometry Service Facility.

3.7 Isothermal titration calorimetry

Isothermal titration calorimetry of WT EF1-2 and WT and mutant EF1-4 was conducted using a MicroCal iTC200 (Malvern Instruments) at both 25°C and 37°C in buffer C. ΔCa EF1-4 was used as negative control. Prior to measurements samples were incubated with 10 mM EGTA in order to remove completely Ca^{2+} from the protein and subsequently polished by SEC in Chelex-resin treated buffer C. Absence of EGTA/EDTA in EF1-2 and EF1-4 preparations was confirmed by intact mass spectrometry at the Mass Spectrometry Service Facility. Ca^{2+} binding affinity was quantified at 20, 100 and 500 µM protein concentration using, respectively, 0.2, 1 mM and 5 mM $CaCl_2$, which was titrated in 2 µls injections. Mg^{2+} binding affinity was determined by titrating 100 µM EF1-4 with 1 mM $MgCl_2$ in buffer C. For competition experiments 100 µM EF1-4 was titrated with 1 mM $CaCl_2$ in buffer C supplemented with 1 mM $MgCl_2$. Each measurement was performed at least in triplicate. To account for the heat of dilution, Ca^{2+} or Mg^{2+},

respectively, were titrated into the reaction buffer and this signal was substracted from the signal obtained for protein titration with the ions. Interactions between ABD-SR1 and EF-hands was performed as described above. Binding parameters were obtained using a single-site model of Origin software (Origin Lab). Data from competition experiment were analyzed using AFFINImeter software (Malvern Panalytical). Experiments performed using *Eh*Actn2 WT and ΔCa at 10-30 µM protein concentration did not render significant signal to proceed with Ca^{2+} binding quantification.

3.8 Fluorescence assays

The amount of Ca^{2+} bound to *Eh*Actn2 WT and WT EF1-4 was measured using the fluorescent dye Quin-2 (Sigma-Aldrich). ΔCa and ΔCa EF1-4 were used as negative controls. Quin-2 was serially diluted in buffer C previously treated with Chelex 100 resin (BioRad) to a final concentration of 88 µM. Dye concentration was determined by measuring absorbance at 240 nm using the extinction coefficient ε=4.2 x 10^4 M/cm. Ca^{2+} standards and boiled protein samples were prepared in buffer C plus 4 M urea and subsequently diluted 1:10 with Quin-2. Fluorescence measurements were performed at 20°C using a 10 mm path-length cuvette and a Perkin Elmer LS50B fluorimeter at λ_{ex}=331 nm and λ_{em}=500 nm.

Ca^{2+}-dye competition assays were carried out using Oregon Green 488 BAPTA-5N dye (Thermo Fisher Scientific), which was initially dissolved in dimethylformamide and later diluted in buffer C previously treated with Chelex 100 resin to a working concentration of 6.5 µM. Dye concentration was determined spectrophotometrically at 494 nm using the extinction coefficient ε=7.65 x 10^4 M/cm. Affinity of dye for Ca^{2+} in buffer C was found to be 4 µM in good agreement with the manufacturer's specifications. In the assays, increasing concentrations of proteins (*Eh*Actn2 WT, ΔCa, WT EF1-4, and ΔCa EF1-4) were added to Chelex-treated buffer C containing 2.5 µM Ca^{2+}. Dye at final concentration of 260 nM was next added to protein- Ca^{2+} mixtures, and fluorescence was measured at 20°C using a 10 mm path-length cuvette and a Perkin Elmer LS50B fluorimeter at λ_{ex}= 494 nm and λ_{em}=520 nm. Normalized fluorescence intensity values were fitted using a one-site competition model in SigmaPlot software (Systat Software).

3.9 Co-sedimentation assays for F-Actin binding

G-actin purified from rabbit skeletal muscle acetone powder was kindly provided by Matthias Rief (Technische Universität München, Germany). Prior to assays, G-actin was polymerized into F-actin by

addition of 1/10th volume of 10x F-buffer and subsequently depolymerized by extensive dialysis against G-buffer to ensure the presence of polymerizable actin only. The different *Eh*Actn2 constructs (*Eh*Actn2 WT, ΔCa, NEECK, and ΔEF3-4, all at 3 µM) in buffer B were mixed with increasing concentrations of G-actin in G-Buffer in the presence of either 1 mM EGTA or 1 mM $CaCl_2$. G-actin was then polymerized into F-actin by addition of 1/10th volume of 10x F-Buffer. Samples were incubated for 1 h at RT and centrifuged at 125,000x*g* for 30 min at 22°C. Supernatant was subsequently transferred to new tubes and diluted with 2x loading buffer. Equivalent amount of 1x loading buffer was added to pellet fractions. *Eh*Actn2 in supernatant and pellet fractions was quantified using a LabChip GX II Touch HT instrument (PerkinElmer) according to the manufacturer's instructions. All experiments were performed at least in triplicate. Quantification was performed assuming a 1:1 actin: *Eh*Actn2 stoichiometry. For comparison, selected samples were analyzed by Coomassie-stained 12.5% Glycine-SDS-PAGE and protein bands quantified by gel scanning. Binding curves were generated using SigmaPlot software assuming a one-site saturation model.

3.10 Co-sedimentation assays for F-Actin bundling

Prior to assays, G-actin was dialyzed overnight at 4°C against G-Buffer while *Eh*Actn2 constructs (*Eh*Actn2 WT, ΔCa, NEECK, $NEECK_b$, ΔEF3-4) were prepared in buffer B. All proteins were then centrifuged at 125,000x*g* for 1 h at 4°C. G-actin was polymerized into F-actin by addition of 1/10th volume of 10x F-Buffer. F-actin (4 µM) was mixed with increasing concentrations of *Eh*Actn2 constructs ranging from 0.01875 µM to 3 µM in the presence of either 1 mM EGTA or 1 mM $CaCl_2$. To assess the effect of Mg^{2+} on bundling, the assay was performed in the presence of 1 mM EGTA plus 2 mM $MgCl_2$. For rescue experiments EF-hands 3-4 or 1-4 in 20-fold molar excess were first incubated for 10 min with 1 mM $CaCl_2$ or 1 mM EGTA, next mixed with ΔEF1-4 or ΔEF3-4, respectively, and finally incubated for 1h at room temperature. Next F-actin was added to the mixture and incubated for additional 1 h at RT. F-actin was added to the mixture and incubated for additional 1 h at RT. Samples were centrifuged at 18,000x*g* for 20 min at 20°C. Supernatant was subsequently transferred to new tubes and diluted with 2x loading buffer. Equivalent amount of 1x loading buffer was added to pellet fractions. Actin in supernatant and pellet fractions was quantified using a LabChip GX II Touch HT instrument according to the manufacturer's instructions. All experiments were performed at least in triplicate. For comparison, selected samples were analyzed by Coomassie-stained 12.5% Glycine-SDS-PAGE and protein bands quantified by gel scanning.

In additional F-actin bundling experiments, 0.25 µM of *Eh*Actn2 construct (*Eh*Actn2 WT, ΔCa, NEECK, and ΔEF3-4) was mixed with 4 µM F-actin, incubated for 1 h at RT, and analyzed by negative staining electron microscopy. Samples were prepared by applying 3 µl of protein solution on previously glow discharged carbon-coated copper grids and further negatively stained with 2% uranyl acetate. Dilutions were optimized to ensure a good distribution of the sample across the grid. Grids were imaged under low dose conditions with a Tecnai Morgani 80 KV electron microscope at a defocus range of 2.0-5.0 µm and at a nominal magnification of 15,200x resulting in a pixel size of 5.89 Å on the specimen.

3.11 Protein crystallization and X-ray data collection

Initial crystallization screens of ΔCa were performed by the sitting-drop vapor-diffusion technique using 96x2-well plates (Molecular Dimensions) and mixing equal volumes of protein solution (at 5 mg/ml) and precipitant with a nanodrop Phoenix RE robot (Art Robins Instruments). Crystallization plates were stored in Minstrel DT UV devices (Rigaku) at 4°C and 22°C. Successful hits were scaled up to the microliter range using 24-well plates (Hampton Research). The best crystals of ΔCa were obtained at 20°C within 1-2 weeks using 0.1 M bis-tris (pH 5.5), 0.3 M $MgCl_2$, 20% (w/v) PEG 3,350 as reservoir condition. They were cryo-protected with 20% (v/v) glycerol. Crystals were harvested on cryo-loops, and flash-cooled in a liquid N_2 containing dewar for further X-ray diffraction at 100K. Some harvested crystals were additionally analyzed by Glycine-SDS-PAGE in order to confirm the protein integrity. Several hundreds of crystals were tested for ΔCa, most of them diffracting no better than 5-6 Å. Two complete datasets from the best crystal were collected to 3.10 Å resolution on a Pilatus 6M detector at ESRF beamlines ID30A-3 and ID23-1 and further merged together. Crystals were orthorhombic with 47% solvent content, which corresponds to a half dimer per asymmetric unit. The structure of this protein was solved by Dr. Joan Lopez Arolas by molecular replacement using *Eh*Actn2 WT as a search model and final refinement was done by Dr. Nikos Pinotsis.

4 RESULTS

4.1 Construct design and protein preparation

The crystal structure of Ca^{2+}-bound *Eh*Actn2 WT was the starting point to design a collection of *Eh*Actn2 constructs for further structural biology and biochemical studies. *Eh*Actn2 domain boundaries and design of the constructs used in this work are shown in **Fig. 17**. ΔCa (Ca^{2+}-insensitive construct) was designed and cloned by Dr. Eirini Gkougkoulia (Gkougkoulia, 2014). It bears three point mutations in the Ca^{2+}-coordinating loop (D497N+N499G+D501N).

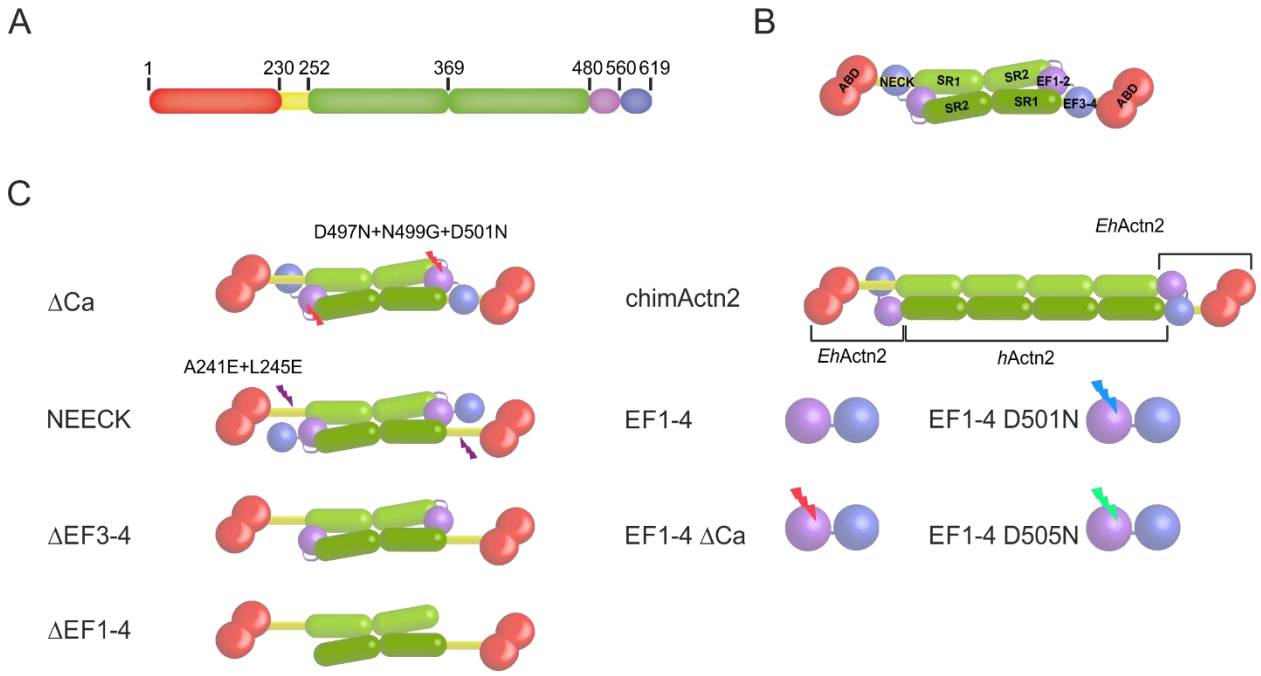

Figure 17. Design of constructs used in this work. (A) Domain boundaries in *Eh*Actn2. (B) Schematic representation of *Eh*Actn2 FL dimer. ABD is shown in red, neck region in yellow, rod in green, EF1-2 in violet, and EF3-4 in dark blue. (C) Schematics of the most important constructs used in this work.

NEECK constructs were designed in order to verify whether the hydrophobic interactions between the neck and EF-3-4 (see below) are important for protein function (**Fig. 17C**). Mutations disrupting the hydrophobic pocket were introduced based on the crystal structure of *Eh*Actn2 WT. Two protein variants

were designed, namely NEECK, with two point mutations (A241E, L245E), and NEECK$_b$, which carries only the first mutation (A241E). This residue was chosen for substitution based on the crystal structure of ΔCa mutant, where A241 is the last amino acid of the neck region that is clearly visible from the electron density map (see below).

A similar design was employed to generate ΔEF3-4 construct, where the whole CaM domain was removed (**Fig. 17C**) Like in the NEECK mutant, this variant is expected to have significantly increased mobility of ABD due to the lack of stabilizing interactions between EF3-4 and neck. This construct has also a closed rod domain due to the absence of EF1-2 (see below).

To address the functional importance of the insertion of EF1-2 in the rod of *Eh*Actn2 (see below), a chimeric construct was designed (**Fig. 17C**). In this chimera the rod from *Eh*Actn2 was replaced with the rod from *h*Actn2, for which the crystal structure had been previously reported (Ribeiro Ede et al., 2014) and in which the rod domain is closed. The construct was cloned using Gibson assembly resulting in a protein variant in which ABD and neck (residues 1-245) are from *Eh*Actn2, rod (residues 272-742) is from *h*Actn2, and the C-terminal CaM domain (residues 457-619) comes from *Eh*Actn2.

All of the constructs used in this work were obtained in high purity. Proteins were purified *via* affinity chromatography using a His-trap column (GE Healthcare), followed by anion exchange chromatography using Resource Q column (GE Healthcare), and size exclusion chromatography (SEC) using either Superdex 200 26/60 or Superdex 75 26/60 columns (both GE Healthcare). Last purification step (SEC) and respective SDS-PAGE gels are shown for the most relevant proteins in **Figs. 18A-F** and **19A-D**.

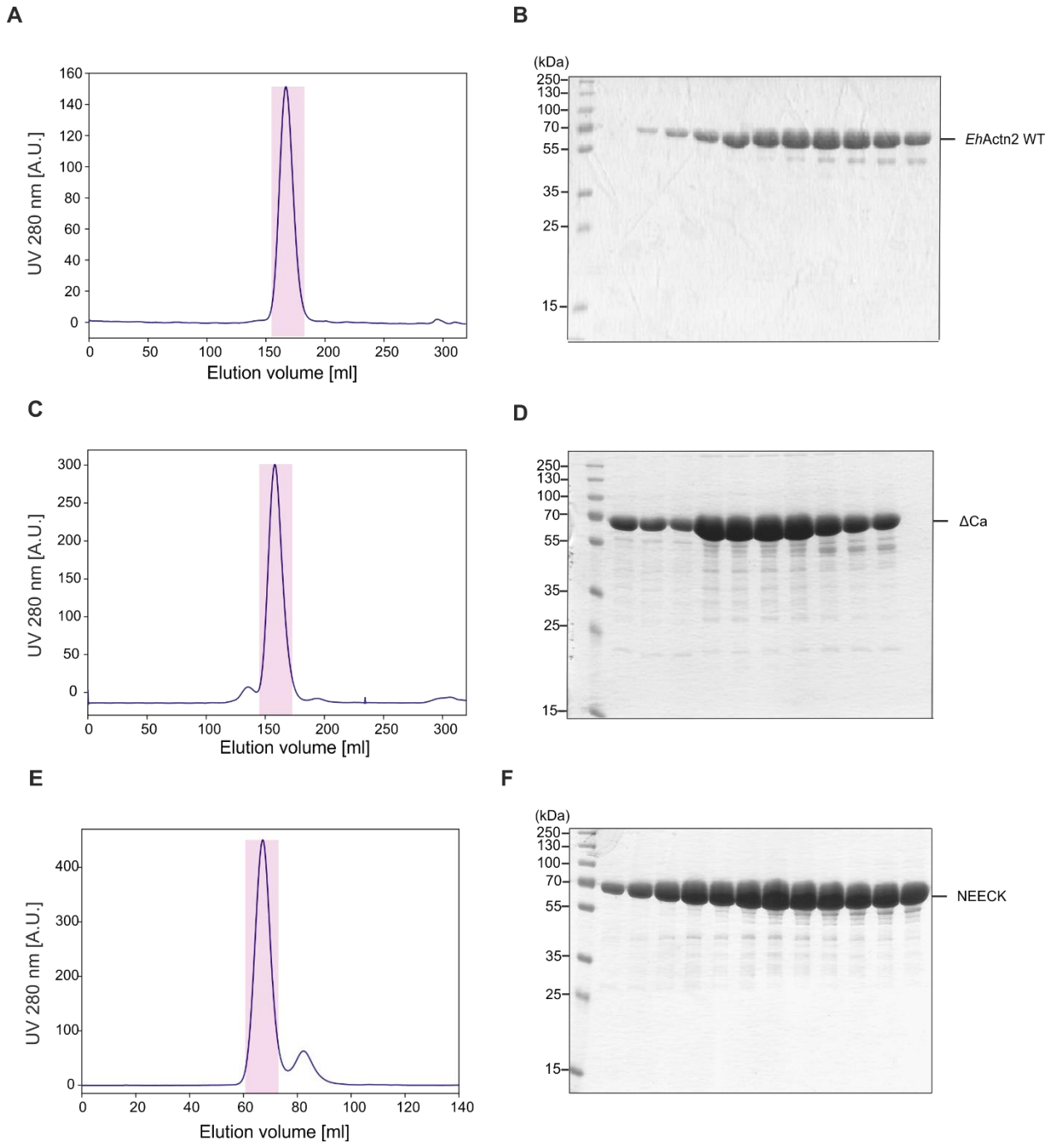

Figure 18. Purification of EhActn2 constructs (I). Size exclusion chromatography profiles of *Eh*Actn2 WT (A), lysine-methylated ΔCa (C) and NEECK (E) loaded onto a Superdex 200 26/60 or Superdex 16/60 column (GE Healthcare). (B), (D) and (F) 12.5% SDS-PAGE analysis of protein fractions from (A), (C) and (E), respectively (labeled in pink).

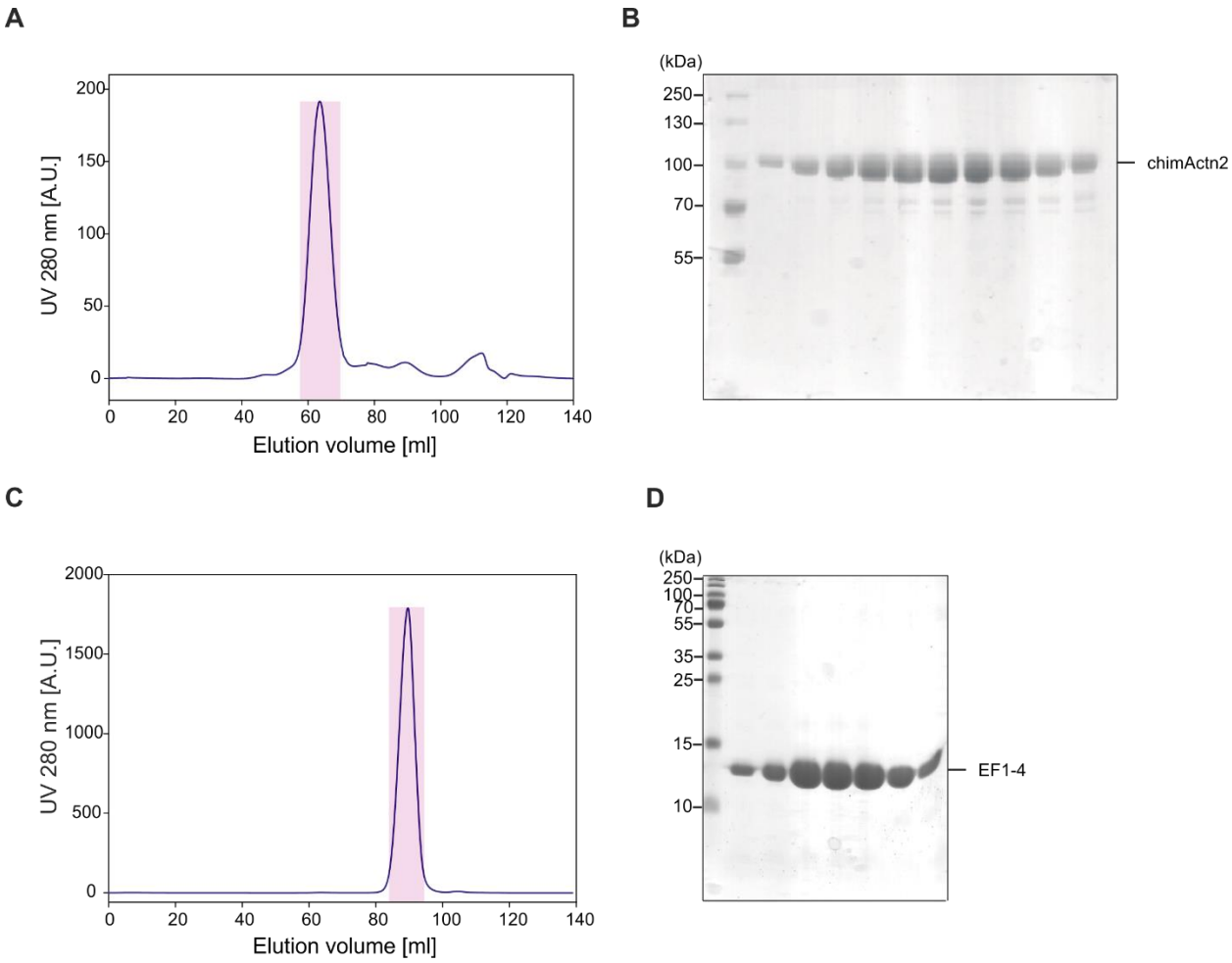

Figure 19. Purification of EhActn2 constructs (II). Size exclusion chromatography profiles of chimActn2 (A) and EF1-4 (C) loaded onto a Superdex 200 16/60 and Superdex 75 16/60 column, respectively (both GE Healthcare). (B) and (D) 12.5% SDS-PAGE analysis of protein fractions from (A) and (C), respectively (labeled in pink).

CD spectroscopy confirmed that all constructs were properly folded. All constructs displayed spectra typical of α-helical proteins, with two negative maxima at 208 and 222 nm (**Fig. 20**).

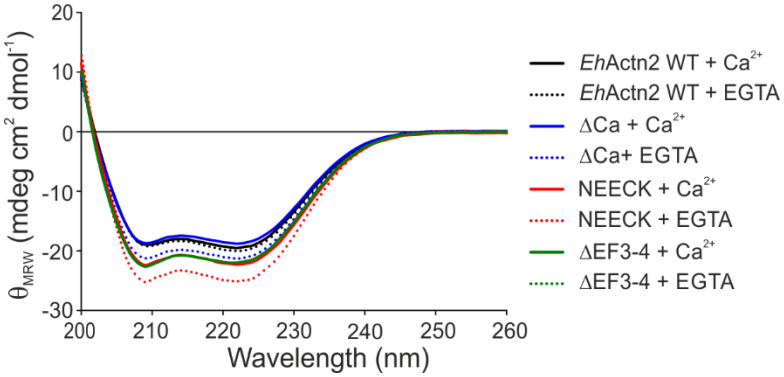

Figure 20. Circular dichroism spectroscopy of selected EhActn2 constructs. Circular dichroism spectra of *Eh*Actn2 WT, ΔCa, ΔEF3-4 and NEECK in the presence and absence of Ca^{2+}.

4.2 Structure of Ca^{2+}-bound *Eh*Actn2

4.2.1 Overall structure of *Eh*Actn2

Crystals of Ca^{2+}-bound *Eh*Actn2 WT in tetragonal space group ($P4_22_12$) were obtained by Dr. Muhammad Bashir Khan who also solved the crystal structure that was further refined by Dr. Nikos Pinotsis. Ca^{2+}-bound *Eh*Actn2 WT was also crystallized in orthorhombic space group ($P222_1$) by Dr. Eirini Gkougkoulia and the crystal structure solved by Dr. Nikos Pinotsis. Both structures were refined to a similar resolution (3.31 and 3.17 Å and R_{work}/R_{free} of 25.91/32.34% and 26.14/32.40%, respectively). Further crystallographic details are reported in the PhD thesis of Dr. Eirini Gkougkoulia (Gkougkoulia, 2014) and in Table I of the Appendix (see below). Details of Author Contributions can be found in Table II of the Appendix.

Overall, the crystal structure reveals that *Eh*Actn2 molecule forms an antiparallel dimer, where ABDs are opposite to each other (**Fig. 21**).

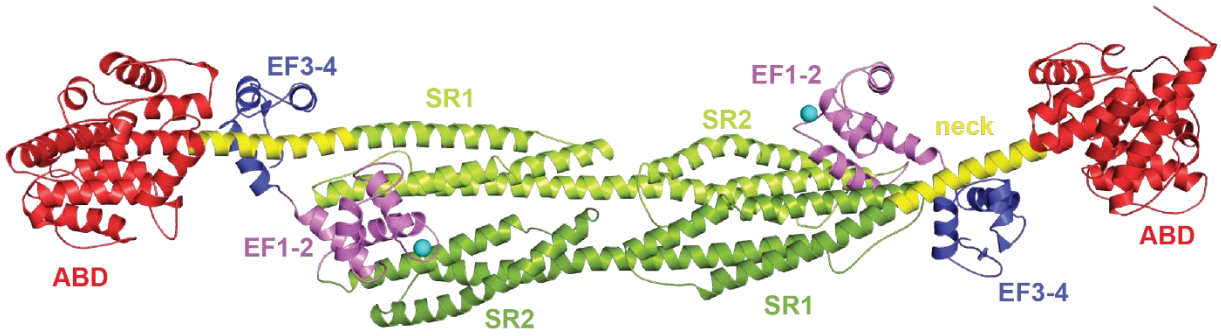

Figure 21. Crystal structure of Ca^{2+}-bound EhActn2. Protein was crystallized in orthorhombic space group ($P222_1$) and the structure was refined to a final resolution of 3.17 Å. ABDs are colored in red, neck in yellow, SRs in green, EF-hands 1-2 in violet, and EF3-4 in dark blue. Ca^{2+} ions are shown as cyan spheres.

Since ABDs are not bound to F-actin, they are seen in a 'closed' state in the crystal structure, with extensive contacts between both CH domains. *Eh*Actn2 ABD contains a long N-terminal helix, starting from Ser4, which is predicted to be unfolded in ABDs from other ABPs (**Fig. 22**).

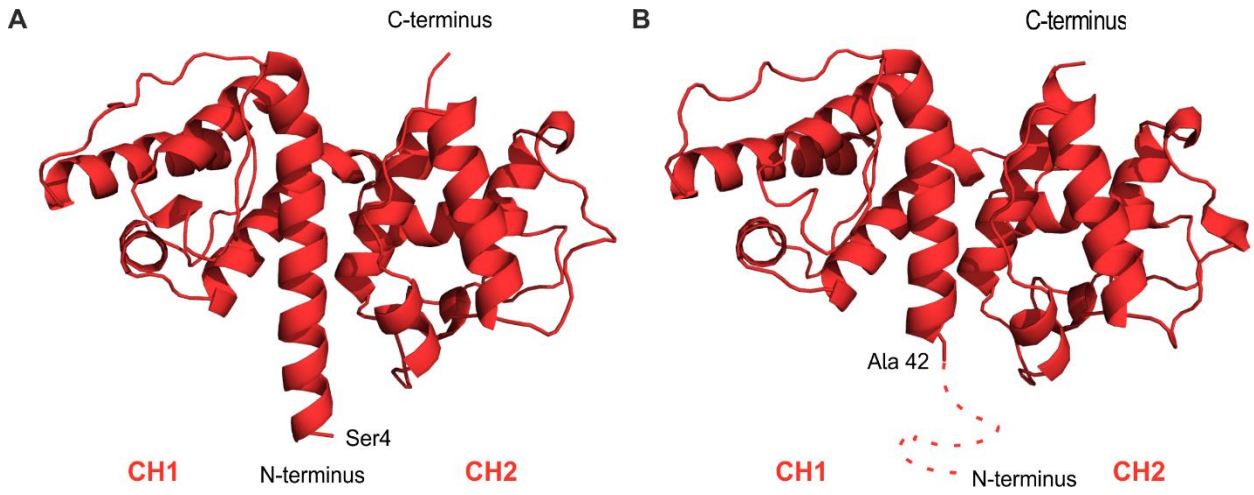

Figure 22. Actin binding domain of EhActn2. ABD in *Eh*Actn2 (A) has an extended N-terminal α-helix. (B) ABD from *h*Actn3. Crystallized domain lacked the first 26 amino acids which were predicted to be unstructured. Additionally residues 27-41 are not seen in electron density and are shown as a dashed line. Figure was generated in PyMOL using pdb code 1WKU (Franzot et al., 2005). Rmsd between both structures equals 1.062 Å (for 192 equivalent Cα atoms).

ABD continues to the α-helical neck region (residues 229-247), which connects ABD with SR1. Rod domain in *Eh*Actn2 forms a dimer interface involving 14 hydrogen bonds and 12 salt bridges. Moreover, there is a torsional twist in this domain (**Fig. 23**), which results in ABDs being oriented with respect to each other by 90° (**Fig. 23**), a feature critical for the modulation of α-actinin/F-actin interactions.

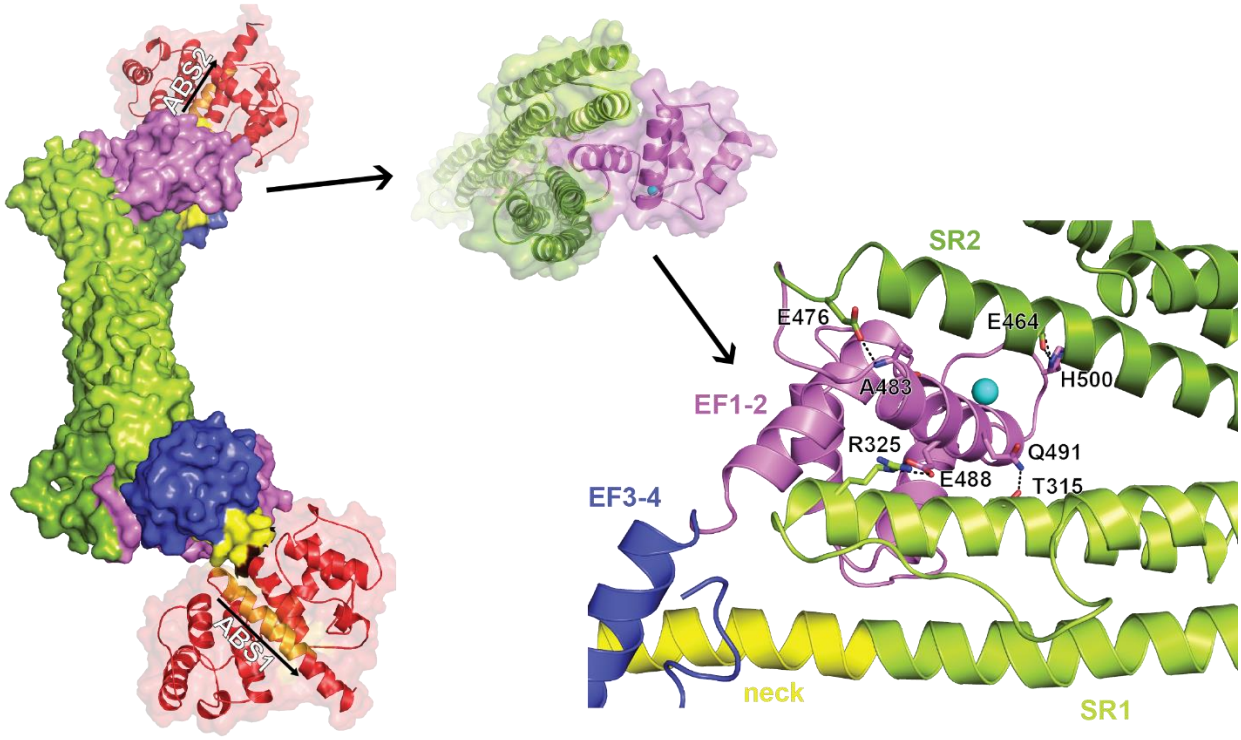

Figure 23. Rod domain in EhActn2 is open and shows a torsional twist. Torsional twist in *EhActn2* rod positions actin binding domains on both ends of the molecule perpendicular to each other in the presence of Ca^{2+}. EF1-2 is sandwiched within the rod domain, which additionally stabilizes protein structure.

*Eh*Actn2 C-terminal CaM domain is the source of additional stabilization in the protein due to its interactions with other protein domains. CaM is divided into two distinguished lobes: an N-terminal lobe (EF1-2) that binds one Ca^{2+} ion (in EF-1) and is partially inserted within the rod domain (**Fig. 23**), plus a C-terminal lobe (EF3-4) interacting with the neck region, restricting the mobility of ABD (**Fig. 24**).

4.2.2. EF1-2 is uniquely sandwiched within the rod

In *Eh*Actn2, EF1-2 is inserted between SRs, resulting in an open rod domain, which is strikingly different than that in *h*Actn2 structure, where the rod domain is closed (Ribeiro Ede et al., 2014). In *Eh*Actn2, the N-terminal helix of EF1-2 intercalates between SRs from both protomers. Although *a priori* such structural arrangement should destabilize the protein, this insertion introduces four hydrogen bonds formed between EF1-2 and SRs (between residues A483:E476, E488:R325, Q491:T315, H500:E464, respectively) (**Fig. 23**). The Ca^{2+}-binding loop remains solvent accessible and is additionally stabilized in this conformation due to a hydrogen bond formed between H500 from the loop and E464 from SR2. This interaction is not maintained in the ΔCa variant. The mode of binding of EF1-2 with the rod is different to the conventional binding of CaM-interacting peptides to EF-hands, where the latter slightly opens in order to accommodate the peptide in the cleft formed between neighbouring EF-hands. Here EF1-2 remains in a closed conformation and uses mainly charged residues to create additional structural stabilization for the rod architecture.

4.2.3. EF3-4 /neck interaction regulates the position of ABD

EF3-4 wraps itself around the neck region. The interaction between EF3-4 and the neck is similar to the one described for EF3-4 and neck in *h*Actn2 and to the interaction between EF3-4 from *h*Actn2 with titin Z-repeat 7 (Atkinson, Joseph et al., 2001). In both cases EF3-4 displays a semi-open conformation, where the neck region is inserted within the cleft formed between helix1 and helix 3 of the C-terminal lobe of the CaM domain. Despite the amphipathic nature of the neck, it uses only hydrophobic residues to engage in intimate contact with EF3-4 (**Fig. 24**). Neck amino acids participating in the formation of the hydrophobic pocket (G238, A241, G242 and L245) follow an earlier described 1-4-5-8 motif seen in *h*Actn2 (Ribeiro Ede et al., 2014). Accordingly, A241E mutation was chosen to create $NEECK_b$ variant, whereas NEECK mutant bears an additional L245E mutation.

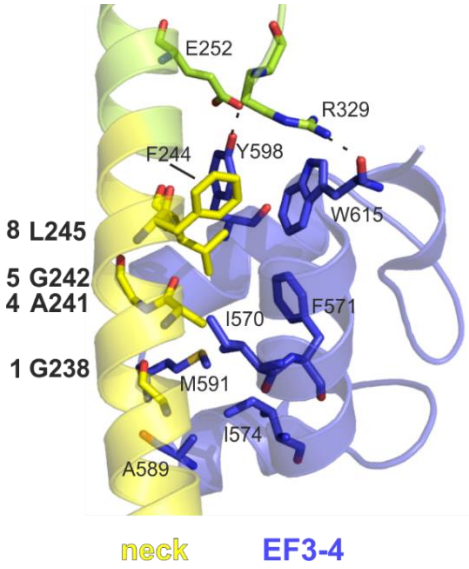

Figure 24. EF3-4/neck interaction in EhActn2. Hydrophobic interactions between EF3-4 and the amphipathic neck region follow the 1-4-5-8 motif (residues G238, A241, L245 and L245 in the NECK), previously described for *h*Actn2 (Ribeiro Ede et al., 2014).

4.2.4 ΔCa variant displays increased flexibility of ABD, neck and EF-hands

ΔCa (Ca^{2+}-insensitive) variant designed by Dr. Eirini Gkougkoulia (Gkougkoulia, 2014) was crystallized in orthorhombic space group ($P222_1$) and diffracted to a final resolution of 3.38 Å. Details of refinement of this structure are shown in Table I of the Appendix. Since Ca^{2+}-bound *Eh*Actn2 WT was also crystallized in orthorhombic group and diffracted to a similar resolution (3.17 Å), it was possible to directly compare both structures. In comparison with *Eh*Actn2 WT, ΔCa is more flexible (**Fig. 25A,B**). Flexible regions encompass not only the Ca^{2+}-binding loop, but also other parts of EF-hands (i.e. helix 3 of EF-1 and helix 2 of EF3-4), neck and some parts of ABD. The latter domain has different position in both structures. Structural differences between *Eh*Actn2 WT and ΔCa are reflected in increased B-factors for ΔCa structure in comparison to *Eh*Actn2 WT (**Fig. 25B**). In both structures the rod domain is rigid and open, with EF1-2 inserted between SRs (**Fig. 25A,B**).

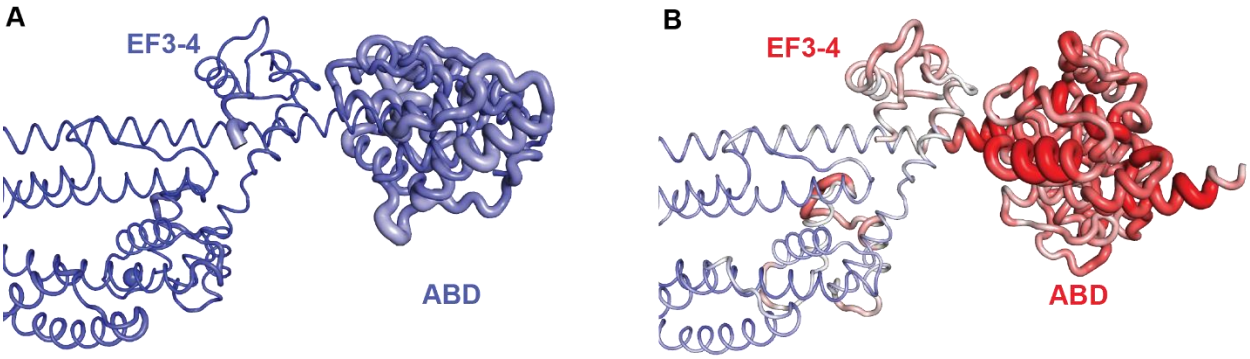

Figure 25. Comparison between Ca^{2+}-bound and Ca^{2+}-free EhActn2 crystallized in orthorhombic space group ($P222_1$). (A) Representation of B-factors in the half-dimer of *Eh*Actn2 WT. (B) Representation of B-factors in the half-dimer of ΔCa. Thickness of the ribbon and color intensity correlates positively with increased mobility. Figure made by Dr. Nikos Pinotsis.

4.3 Is *Eh*Actn2 a truly Ca^{2+}-regulated α-actinin?

4.3.1 Native mass spectrometry and Quin-2 assay demonstrate high affinity of *Eh*Actn2 for Ca^{2+}

Based on bioinformatics predictions (Mazumder, Padhan et al., 2014), *Eh*Actn2 EF-1 should bind one Ca^{2+} ion. By contrast, the other three EF-hands should be Ca^{2+}-insensitive, as they do not contain enough residues able to coordinate a divalent cation (**Fig 26**).

Figure 26. EF-hands of EhActn2. (A) Sequence alignment of EF-hands loops from *Eh*Actn2. X axis is shown in green, Y axis in orange, Z axis in violet.

Ca^{2+} binding was initially intended to be measured using ITC. FL protein was used in the preliminary experiments (data not shown), but no Ca^{2+} binding was observed. This prompted us to investigate whether *Eh*Actn2 can co-purify with bound Ca^{2+} ions. Quin-2 is a fluorescent dye with nanomolar affinity for Ca^{2+} and thus allow for detection of Ca^{2+} ions potentially co-purifying with the protein of interest upon thermal

denaturation of the latter. Indeed, Quin-2 detects Ca^{2+} ions bound to both EF1-4 and *Eh*Actn2 WT upon protein purification, suggesting that the Ca^{2+} affinity of *Eh*Actn2 must be very high. Ca^{2+}-insensitive variants (ΔCa and EF1-4 ΔCa) were used here as controls and both showed negative values of fluorescence at 500 nm, indicating that they did not co-purify with Ca^{2+} ions, as expected (**Table 5**).

Table 5. Ca^{2+} occupancy of EhActn2 constructs measured with Quin-2

construct	Ca^{2+} occupancy (%)
*Eh*Actn2 WT	73.2 ± 16.5
EF1-4	101 ± 24.3
ΔCa	N/A
EF1-4ΔCa	N/A

Each measurement was performed at least in triplicate.

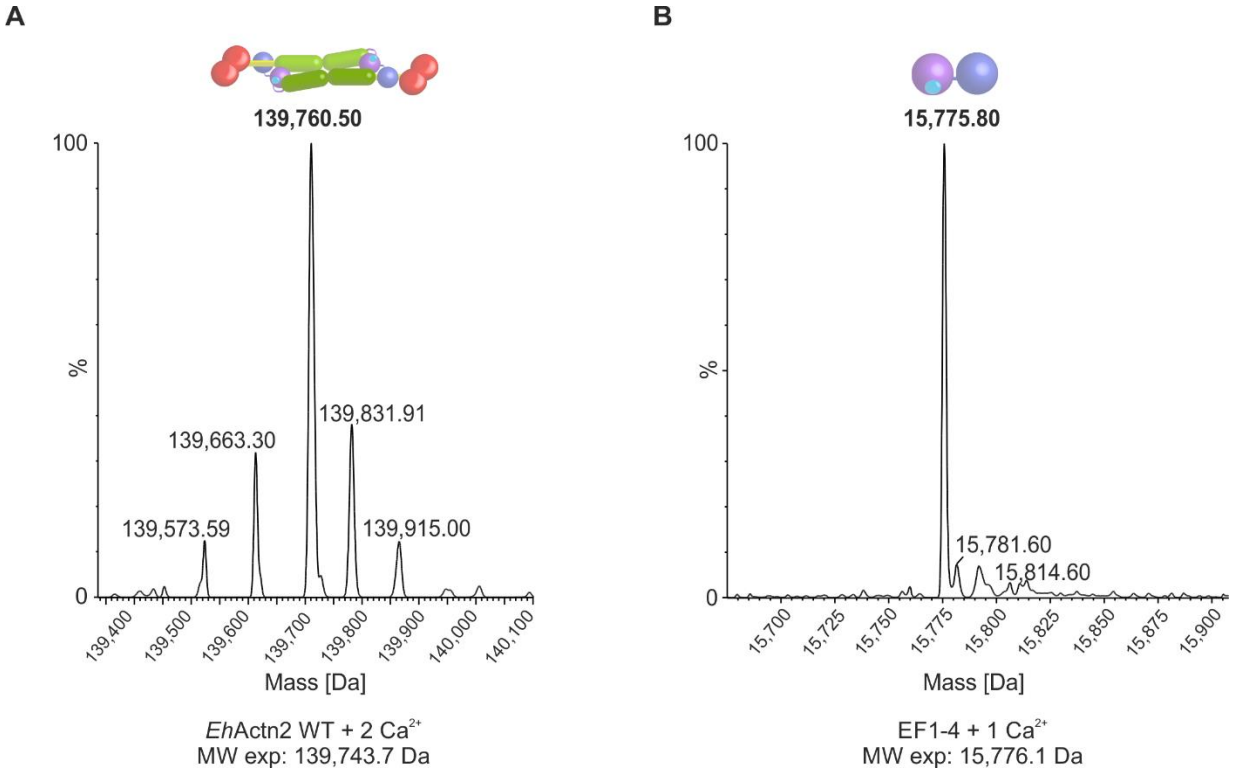

Figure 27. Intact mass spectrometry of EhActn2 constructs. Molecular mass of *Eh*Actn2 WT (A) and EF1-4 (B) from which Ca^{2+} ions were not removed after purification.

Intact mass spectrometry (MS) performed at the Mass Spectrometry Facility (MFPL, Vienna) revealed the presence of two Ca^{2+} ions bound to FL protein dimer (molecular mass of 139,760.5 Da) and one Ca^{2+} ion bound to EF1-4 *Eh*Actn2 (molecular mass of 15,775.8 Da) (**Fig. 27**). However, it is worth mentioning that this result alone cannot directly discriminate between Ca^{2+} and e.g. K^{+} ions (40.08 *vs.* 39.10 Da, respectively). Based on the result of Quin-2 assay we concluded that the bound ion is indeed Ca^{2+}.

4.3.2 Competition assay with BAPTA Oregon Green dye proves high affinity of *Eh*Actn2 for Ca^{2+}

Ca^{2+} binding to FL protein could not be measured using ITC, as this construct is less soluble than the CaM domain alone. Intact mass spectrometry and Quin-2 assay had previously indicated that *Eh*Actn2 WT should have the same high affinity for Ca^{2+} as EF-hands. To corroborate these findings, a competition assay with Oregon-Green-BAPTA dye was used. This fluorescent dye, unlike Quin-2, binds Ca^{2+} with a low affinity (K_d measured in our experimental conditions was 20 µM) and therefore a protein with higher affinity for Ca^{2+} should be able to compete with the dye for binding of Ca^{2+} ions. *Eh*Actn2 WT and EF1-4 were able to displace Ca^{2+} from the dye, whereas Ca^{2+}-insensitive variants of both constructs could not, confirming the specificity of our assay (**Fig. 28A,B**) . Moreover, and as expected, the stoichiometry of Ca^{2+} binding to EF-hands was close to 1 (log EC_{50} equals to 2.01, $CaCl_2$ concentration used in the assay was 2 µM) and was about 2-fold lower for FL protein, which is a constitutive dimer, which is consistent with the MS results.

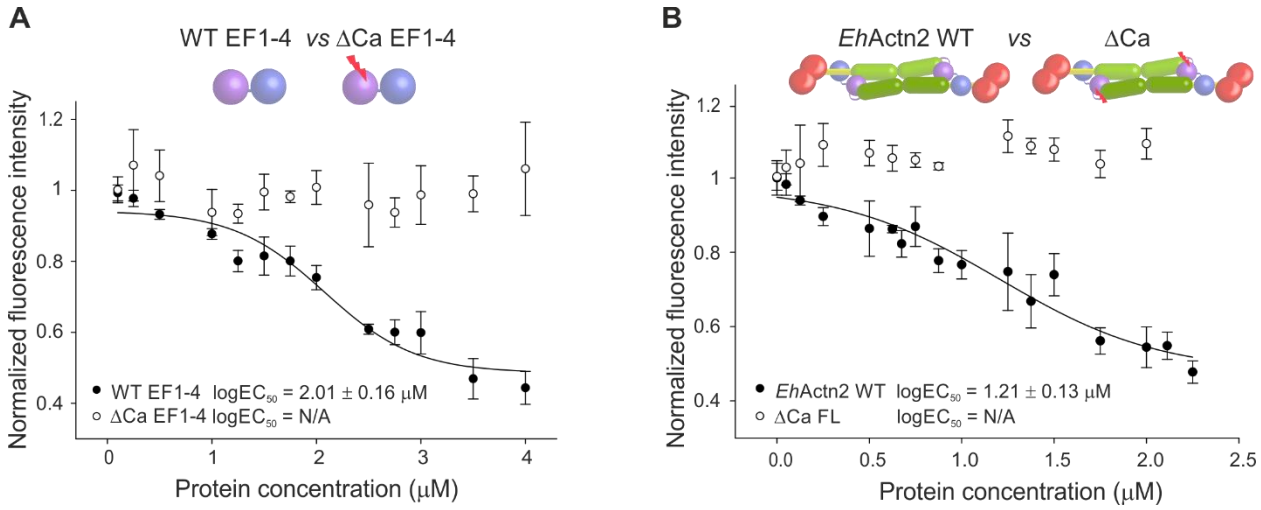

Figure 28. Ca^{2+} binding to EhActn2 WT and EF1-4 assessed by Oregon-Green-BAPTA dye. Ca^{2+} competition between EF1-4 (A) or *Eh*Actn2 WT (B) and Oregon-Green-BAPTA dye for binding of Ca^{2+} ions. Ca^{2+}-insensitive variants were used as a negative control. Protein concentration was calculated taking into account the oligomeric state of the proteins (i.e. monomer or dimer, respectively). Experiments were done at least in triplicate. R^2 for EF1-4 competition equals to 0.96, and 0.95 for *Eh*Actn2 WT, with a significance level of 0.05.

4.3.3 Isothermal titration calorimetry experiments demonstrate that *Eh*Actn2 binds Ca^{2+} with nanomolar affinity

After the results obtained from intact MS and dye competition assays, protein purification procedures were further optimized in order to remove Ca^{2+} ions from the protein. Accordingly, 10 mM EGTA was added to *Eh*Actn2 constructs just before the last SEC polishing step which was always carried out in Chelex-treated buffers (Bio-Rad). Titration of Ca^{2+} into FL protein did not yield significant heat to measure binding by isothermal titration calorimetry (ITC); therefore EF-hands were used, as these constructs are smaller and more soluble. In agreement with intact MS and Quin-2 assays, ITC experiments demonstrated that there is one Ca^{2+} binding site in EF1-4 (**Fig. 29B**). This site is located in EF1-2 in line with bioinformatics predictions (Mazumder et al., 2014), since this construct also binds stoichiometrically one Ca^{2+} ion (**Fig. 29D**). *Eh*Actn2 EF-hands showed exceptionally high affinity for Ca^{2+} (low nanomolar range, see Table 5), a surprising result when compared with *h*Actn1 CaM domain, which binds Ca^{2+} with affinity of only 50-100 μM (Drmota Prebil et al., 2016). The Ca^{2+}-insensitive mutant did not bind Ca^{2+} ions (**Fig. 29C**), as expected, confirming that the introduced mutations indeed abolished coordination of this ion.

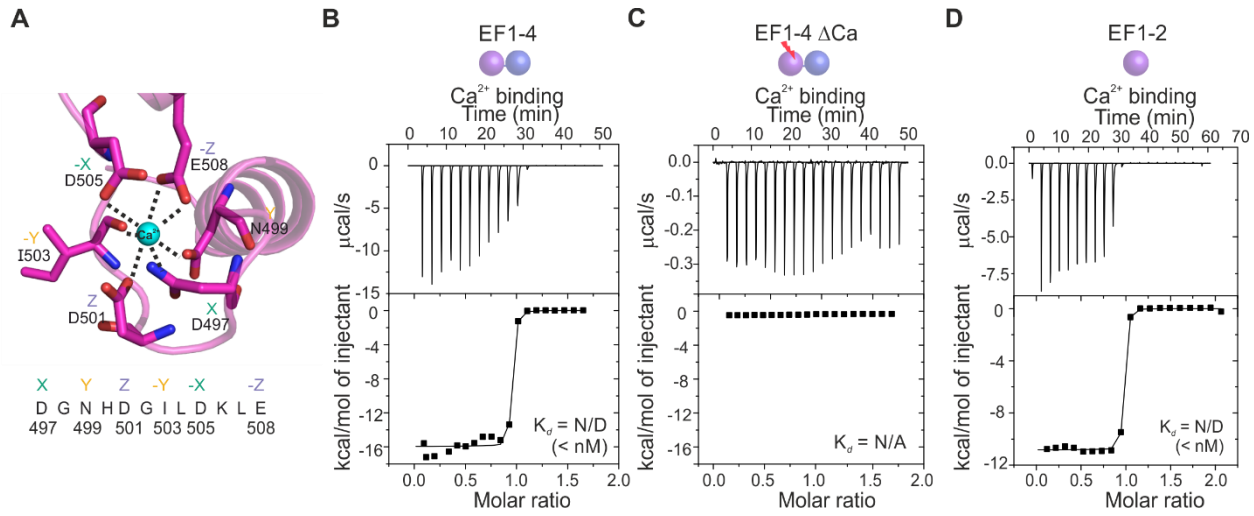

Figure 29. Ca^{2+} binding to EhActn2 EF-hands. (A) Ca^{2+}-binding loop from *Eh*Actn2. Ca^{2+}-coordinating residues are indicated (X axis is shown in green, Y axis in orange and Z axis in violet (B-D) ITC experiments of Ca^{2+} binding to different EF-hands constructs.

4.3.4 The acid pair hypothesis explains why *Eh*Actn2 has an exceptionally high affinity for Ca^{2+}

The high affinity of *Eh*Actn2 EF-hands for Ca^{2+} is surprising, particularly in contrast to the relatively low affinity of *h*Actn1 for this ion. Also when taking into account that there are not many proteins with nanomolar affinity for Ca^{2+}, and those that bind Ca^{2+} ion very tightly usually display a buffering and not a regulatory role (Falke et al., 1994). Moreover, according to CaIB server (Mazumder et al., 2014) *Eh*Actn2 EF-1 was predicted to be a weak Ca^{2+}-binder. Previous report demonstrated that *Eh*Actn2 bound Ca^{2+} very weakly (Virel et al., 2007). However, *Eh*Actn2 EF-1 follows the so-called acid pair hypothesis, which states that when negatively charged residues directly coordinating a Ca^{2+} ion lie axially opposite to each other, they create a high affinity Ca^{2+}-binder (Black et al., 2000, Reid, 1990). In *Eh*Actn2 EF-1 there are indeed acid pairs on both X (between D497 and D505) and Z (D501 and E508) axes, respectively (**Fig. 29A,**), like in other strong Ca^{2+}-binders. To verify whether this particular arrangement of acidic residues in the loop contributes to high Ca^{2+} affinity, residues on X (D501) and Z axes (D505) were substituted with asparagines in order to abrogate the acid pairs. Upon mutating the X axis, K_d increased to 0.20± 0.04 µM (**Fig. 30A, Table 6**), whereas upon disruption of charge on the Z axis K_d reached 0.28 ± 0.20 µM (**Fig. 30B, Table 6**), confirming that acidic pairs in the Ca^{2+}-coordinating loops are essential for the exceptionally high affinity of *Eh*Actn2 EF-hands for Ca^{2+} ions.

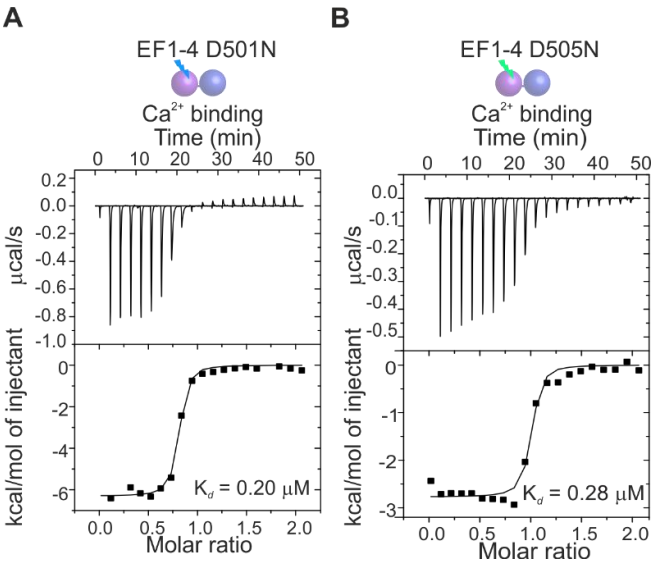

Figure 30. Ca^{2+} binding to EhActn2 EF-hands variants. (A,B) ITC experiments of Ca^{2+} binding to EF-hands variants verifying acid pair hypothesis.

4.3.5 Does *Eh*Actn2 bind Mg^{2+}?

The observed nanomolar affinity of *Eh*Actn2 for Ca^{2+} (see above) would preclude any possibility of the regulation of this protein *in vivo*. Consistently, a Ca^{2+} concentration in the cell around 100 nM (in resting conditions) would imply that *Eh*Actn2 would be constantly bound to these ions. However, many Ca^{2+}-binding proteins acting as Ca^{2+} buffers (that is, having high affinity for Ca^{2+}) are also able to bind Mg^{2+}, albeit with much lower affinity. *Eh*Actn2 is one of these proteins and binds Mg^{2+} with the affinity of roughly 10 µM (**Fig. 31A, Table 6**).

4.3.6 Mg^{2+} compete with Ca^{2+} for binding to *Eh*Actn2

Taking into account that in resting eukaryotic cells the concentration of Mg^{2+} exceeds that of Ca^{2+} around 1,000-fold (Romani & Scarpa, 1992), it is reasonable to think that there would be a competition between both ions. Therefore, in a resting state most *Eh*Actn2 would be Mg^{2+}-bound, simply due to the higher concentration of this ion. However, during the signaling event, when Ca^{2+} concentration rises, Ca^{2+} would compete Mg^{2+} off. To mimic the *in vivo* conditions, Ca^{2+} titration was conducted in the presence of 1 mM $MgCl_2$, which is considered to be physiological (Romani, 2011). In this Mg^{2+} concentration, K_d of EF1-4 for

Ca^{2+} is reduced to 0.49 ± 0.13 µM (**Fig. 31B,**), allowing *Eh*Actn2 to be regulated by Ca^{2+} in the cellular milieu. This competition assay also allowed to quantify the K_d of EF1-4 for Ca^{2+} ions, which was 5.3 ± 0.3 nM (**Table 6**).

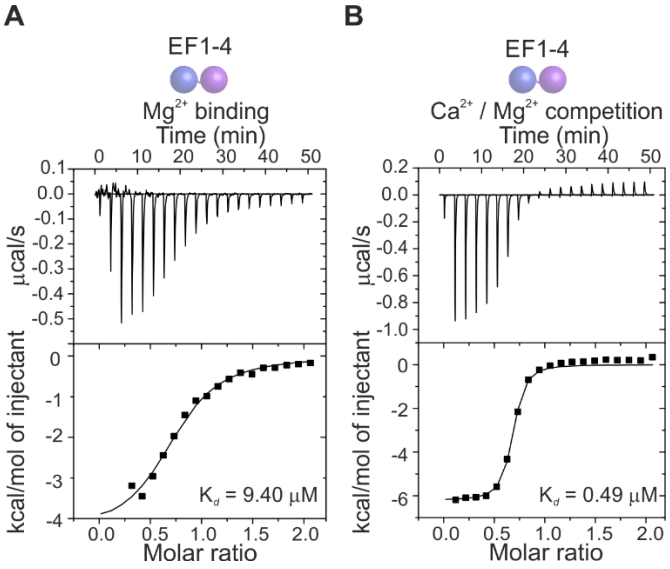

Figure 31. Mg^{2+} and Ca^{2+} binding to EhActn2 EF-hands. (A) ITC experiment of Mg^{2+} binding to *Eh*Actn2 EF-hands (B) ITC experiment of Ca^{2+} binding to EF1-4 in the presence of 1 mM $MgCl_2$.

4.3.7 Thermodynamic analysis of *Eh*Actn2 interactions with divalent ions

According to ITC experiments, all reactions of ions binding to *Eh*Actn2 EF-hands are exothermic (**Figs. 29B-D 30, 31** and **Table 6**). Direct thermodynamic analysis of Ca^{2+} binding to *Eh*Actn2 EF-hands was not possible due to very low K_d values, which impair the proper readout of the entropy values. In case of Mg^{2+} binding, such analysis was straightforward and showed that binding of this ion is enthalpically driven, which is in agreement with the formation of new coordinating bonds upon Mg^{2+} binding. The competition assay where binding of Ca^{2+} was performed in the presence of Mg^{2+} was also an enthalpically driven reaction (ΔH value of -26.12 kJ *vs.* ΔTS of 9.92 kJ). D501N mutant also bound Ca^{2+} in an enthalpically driven reaction, whereas D505N mutation had a slightly higher entropic contribution to Ca^{2+} binding (ΔH value of –16.87 kJ versus ΔTS of 20.87 kJ) (**Fig. 32** and **Table 6**).

Table 6. Thermodynamic parameters of protein-ion interaction assessed by isothermal titration calorimetry.

Protein	Ligand	N	K_d (μM)	ΔH (cal/mol)	ΔS (cal/mol/deg)
WT EF1-4	Ca^{2+}	0.93 ± 0.02	0.0053 ± 0.003*	-14,559 ± 2,576	N/D
WT EF1-4	Mg^{2+}	0.74 ± 0.09	9.39 ± 0.87	-4,217 ± 197	8.86 ± 0.84
WT EF1-4	Ca^{2+} + Mg^{2+}	0.65 ± 0.04	0.49 ± 0.13	-6,246 ± 165	7.95 ± 1.09
D501N EF1-4	Ca^{2+}	0.93 ± 0.14	0.20 ± 0.04	-6,093 ± 232	10.20 ± 1.05
D505N EF1-4	Ca^{2+}	0.89 ± 0.08	0.28 ± 0.20	-4,031 ± 224	16.73 ± 1.92
ΔCa EF1-4	Ca^{2+}	N/A	N/A	N/A	N/A

*Each experiment was performed at least in triplicate. Data were analyzed with Origin software (OriginLab Corporation). K_d for Ca^{2+} binding to EF1-4 was calculated based on a competition assay using AFFINIMeter software (Malvern Instruments LTD).

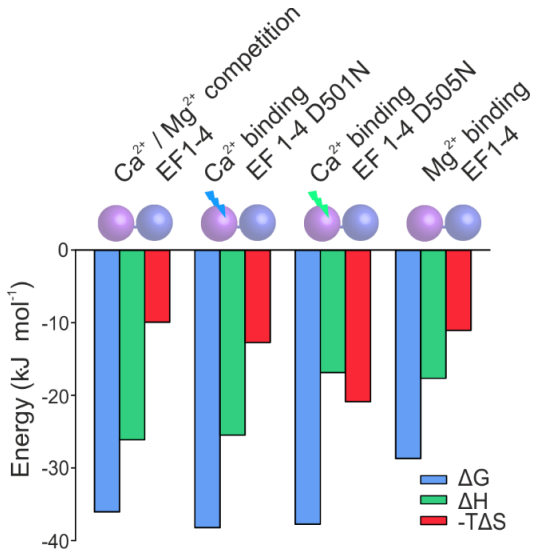

Figure 32. Thermodynamic analysis of Ca^{2+} and Mg^{2+} binding to EhActn2 EF-hands assessed by isothermal titration calorimetry. Parameters were calculated from averaged isothermal titration calorimetry experiments done in triplicate (see **Table 6**).

4.4 Ca^{2+} and Mg^{2+} stabilize *Eh*Actn2, albeit differently

4.4.1 Limited proteolysis experiments show that Ca^{2+} and Mg^{2+} stabilize *Eh*Actn2 structure

Comparison of the crystal structures of Ca^{2+}-bound and Ca^{2+}-free *Eh*Actn2 revealed that Ca^{2+} binding reduces flexibility of selected protein domains, particularly ABD, neck and EF-hands (**Fig. 25**). Limited proteolysis was used to further corroborate this finding and assess the effect of Mg^{2} ions on protein stability. Since many proteolytic enzymes require Ca^{2+} for their optimal activity, direct comparison between proteolytic cleavage of *Eh*Actn2 WT in the presence of Ca^{2+} and EGTA was avoided. Instead, *Eh*Actn2 WT and ΔCa (in the presence of either Ca^{2+} or Mg^{2+}) were used (**Fig. 33**). Regardless of the proteolytic enzyme used, ΔCa was digested more efficiently than *Eh*Actn2 WT, proving that this protein variant is more flexible (i.e. more accessible to proteolytic cleavage). Proteolytic stability of *Eh*Actn2 WT was significantly increased in the presence of Ca^{2+} and Mg^{2+}, with similar cleavage patterns for both ions. It is worth mentioning that during the cleavage with Mg^{2+} thermolysin was not efficient due to the presence of small amounts of EGTA used to remove Ca^{2+}.

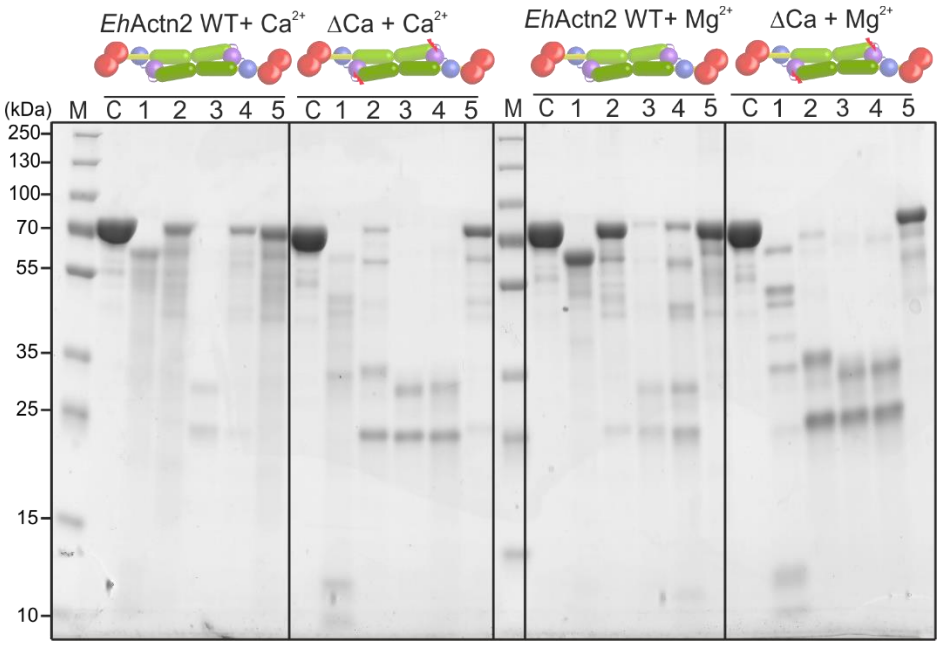

Figure 33. Limited proteolysis of EhActn2 WT and ΔCa in the presence of Ca^{2+} or Mg^{2+}. Proteins were digested in the presence of either 5 mM $CaCl_2$ or 0.5 mM EGTA plus 5 mM $MgCl_2$ using bovine pancreatic trypsin (lane 1), bovine pancreatic chymotrypsin (lane 2), proteinase K from *Engyodontium album* (lane 3), subtilisin from *Bacillus licheniformis* (lane 4), and thermolysin from *B. thermoproteolyticus* (lane 5). Samples were precipitated with trichloroacetic acid and run on gradient SDS-PAGE.

4.4.2 Ca^{2+} and Mg^{2+} stabilize *Eh*Actn2, as shown by differential scanning fluorimetry

Thermal stability of *Eh*Actn2 WT and ΔCa was measured by differential scanning fluorimetry (DSF) showing that they both have very similar melting temperatures (Tm) in the absence of Ca^{2+} (57.2 ± 0.2 and 57.1 ± 0.2°C, respectively) (**Fig. 34A,B**). However, thermal stability of the latter was increased in the presence of Mg^{2+} (58.3 ± 0.2°C) and even more in the presence of Ca^{2+} (60.1 ± 0.5°C). This effect was not observed for ΔCa. It can be therefore concluded that both ions increase thermal stability of *Eh*Actn2 WT, with Ca^{2+} having a significantly stronger effect than Mg^{2+}.

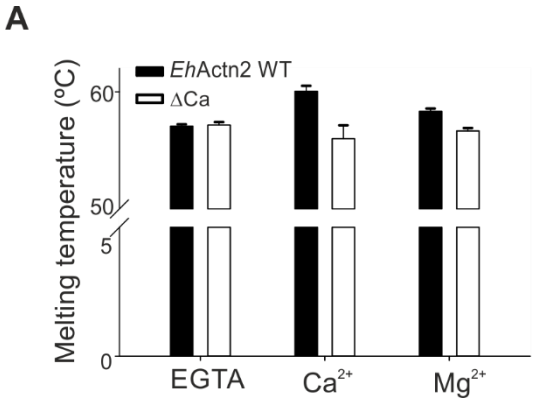

B

Construct	Tm (˚C)
*Eh*Actn2 WT+ Ca^{2+}	60.1 ± 0.5
ΔCa + Ca^{2+}	56.0 ± 1.1
*Eh*Actn2 WT + Mg^{2+}	58.3 ± 0.2
ΔCa + Mg^{2+}	56.7 ± 0.2
*Eh*Actn2 WT + EGTA	57.1 ± 0.2
ΔCa + EGTA	57.2 ± 0.2

Figure 34. Thermal stability of EhActn2 in the presence of Ca^{2+} and Mg^{2+}. (A,B) Differential scanning fluorimetry results comparing the melting temperatures of *Eh*Actn2 WT and ΔCa in the absence and presence of 1 mM Ca^{2+} and 1 mM Mg^{2+}.

4.4.3 Ca^{2+} induces subtle changes in *Eh*Actn2 structure according to static light scattering and fluorescence anisotropy

Altogether, limited proteolysis and DSF experiments demonstrate that Ca^{2+} binding exerts a stabilizing effect on *Eh*Actn2 structure. However, the conformational changes caused by Ca^{2+} binding are very subtle. Thus, the hydrodynamic radius of *Eh*Actn2 WT and ΔCa (used here as a control) did not change upon Ca^{2+} binding, as assessed by static light scattering (SLS) (**Fig. 35A,B**).

NEECK and $NEECK_b$ displayed an increased Stokes radius with respect to *Eh*Actn2 WT, as shown by SLS (**Fig. 35A,B**), indicating that ABD is more flexible in these constructs.

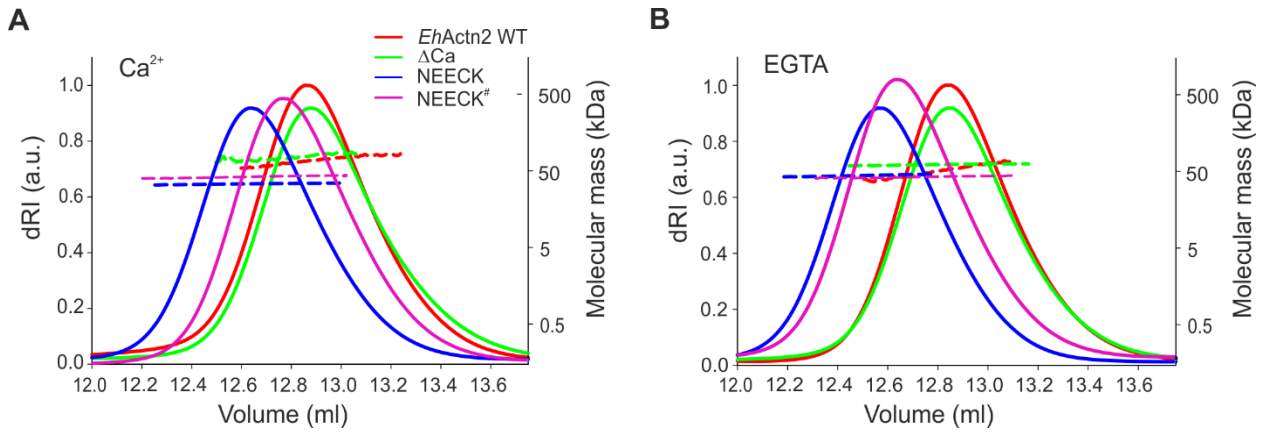

Figure 35. Hydrodynamic properties of EhActn2 constructs. Static light scattering (SLS) results of *Eh*Actn2 constructs in the presence (A) and absence (B) of Ca^{2+}.

4.5 To bundle or not to bundle? Effect of divalent ions on *Eh*Actn2 function

4.5.1 Binding of Ca^{2+} to *Eh*Actn2 affects its interaction with F-actin

Binding of *Eh*Actn2 constructs to F-actin was assessed by high-speed co-sedimentation assays using a fixed concentration of α-actinin and increasing concentration of F-actin and assuming a 1:1 stoichiometry.

*Eh*Actn2 WT binds F-actin with a similar apparent K_d in the absence and presence of Ca^{2+} (6.37 ± 0.79 µM *vs.* 4.19 ± 0.85 µM, respectively). Although the presence of Ca^{2+} did not affect significantly the dissociation constant, it affected the B_{max} values, which are 2.5-times reduced in case of Ca^{2+}-bound *Eh*Actn2 WT (**Fig. 36A**). This effect was not observed for ΔCa variant, which has very similar B_{max} values in the presence and absence of Ca^{2+} (2.0 ± 0.11 µM and 2.4 ± 0.14 µM, respectively) (**Fig. 36B**).

Notably, constructs exhibiting a highly flexible ABD, i.e. NEECK and ΔEF3-4, have a nearly 1-fold lower K_d. Despite their increased ability to associate with actin filaments, these constructs display drastically reduced B_{max} values (**Fig. 36C,D**).

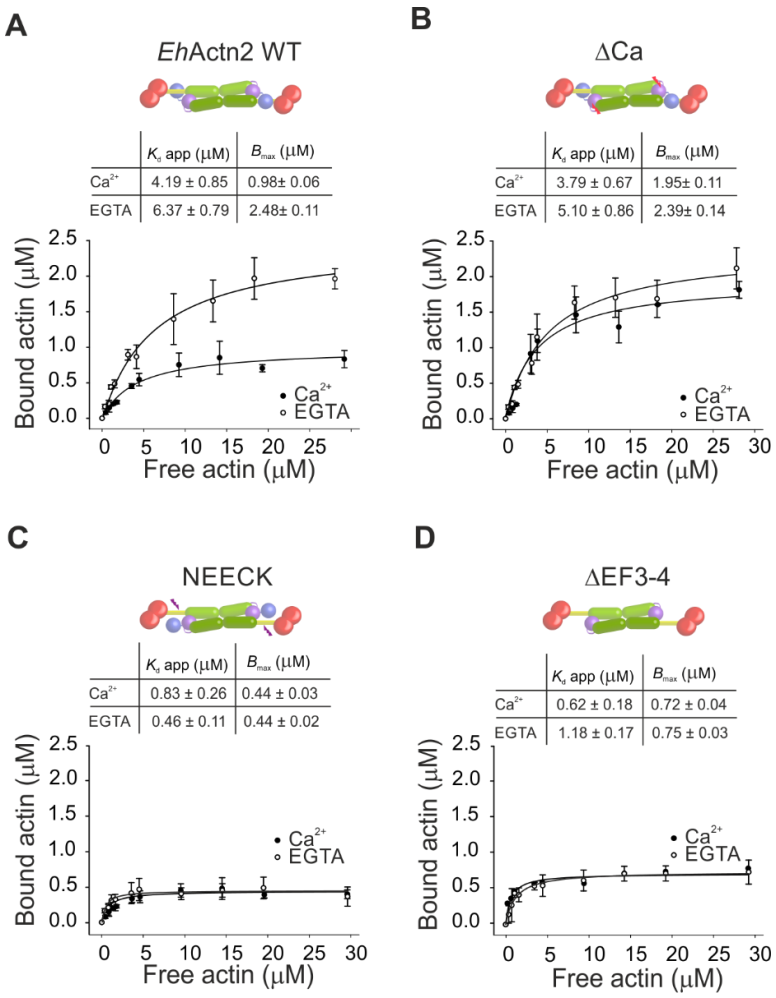

Figure 36. High-speed co-sedimentation assays of EhActn2 constructs. (A-D) Binding of *Eh*Act2 constructs to F-actin assessed by high speed co-sedimentation assays in the absence and presence of 1 mM Ca^{2+}.

4.5.2 Ca^{2+} inhibits *Eh*Actn2 bundling activity

α-Actinin function in the cell is to cross-link actin filaments, which is crucial for the regulation of actin cytoskeleton. Bundling of F-actin by *Eh*Actn2 was assessed by low-speed co-sedimentation assays using a fixed concentration of F-actin and increasing concentrations of *Eh*Actn2 construct. Ca^{2+} inhibited actin bundling, especially when the molar ratio of F-actin to *Eh*Actn2 WT was below 4:1 (**Fig. 37A**). Reduced B_{max} values found in binding assays in the presence of Ca^{2+} translated into a reduction in bundles formation (**Fig. 36A**). As expected, ΔCa did not respond to Ca^{2+} treatment. NEECK and ΔEF3-4 were completely deficient in bundling activity despite having K_d values much lower than *Eh*Actn2 WT (**Fig. 37C,D**). The

same defect in bundling was observed for NEECK$_b$ bearing only one mutation (A241E) (**Fig. 39A**). These results imply that the crucial parameter controlling *Eh*Actn2 bundling activity is in this case the B_{max} and that an increased flexibility of the ABD is detrimental for actin bundling. Therefore, the molecular mechanism regulating *Eh*Actn2bundling activity is very delicate and is determined by proper interactions between EF3-4 and the neck. At this point, we attempted to create a constitutively closed construct. This was achieved by introducing cysteine residues in EF3-4 and the neck in order to create disulfide bridges between both domains (V234C+A589C and A237C+T573C, respectively). However, the formation of disulfide bonds was not observed, most likely due to the fact that the distance between EF3-4 and neck is too long for their formation.

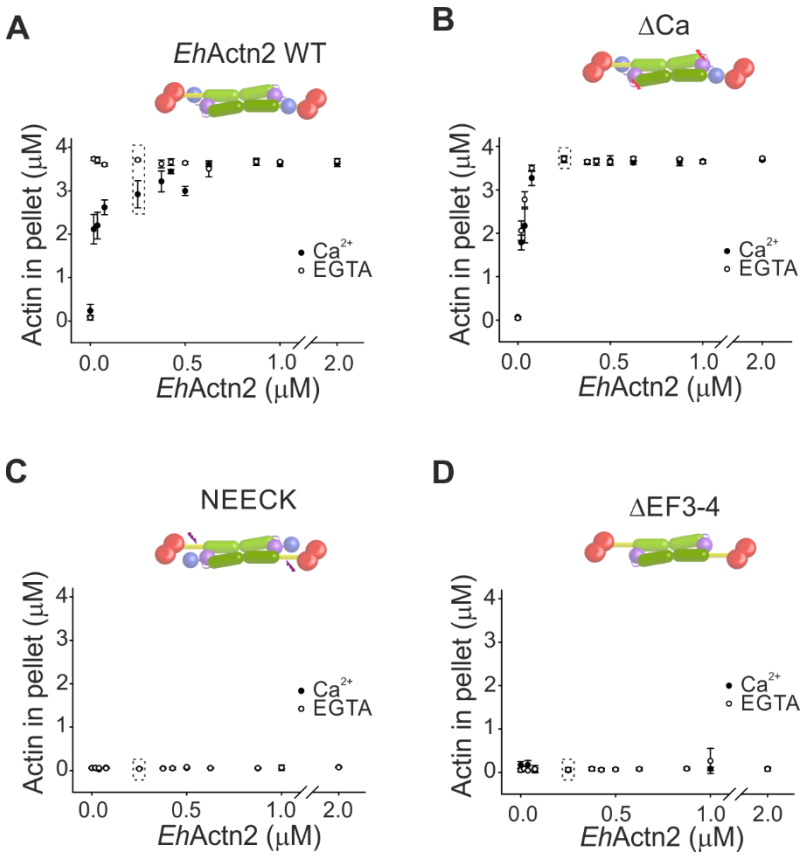

Figure 37. Low-speed co-sedimentation assays of EhActn2 constructs. (A-D) F-actin bundling activity of different *Eh*Actn2 constructs assessed by low-speed centrifugation assay in the absence and presence of 1 mM Ca^{2+}. Selected concentrations of α-actinin/F-actin complexes were additionally visualized by negative staining electron microscopy (see below).

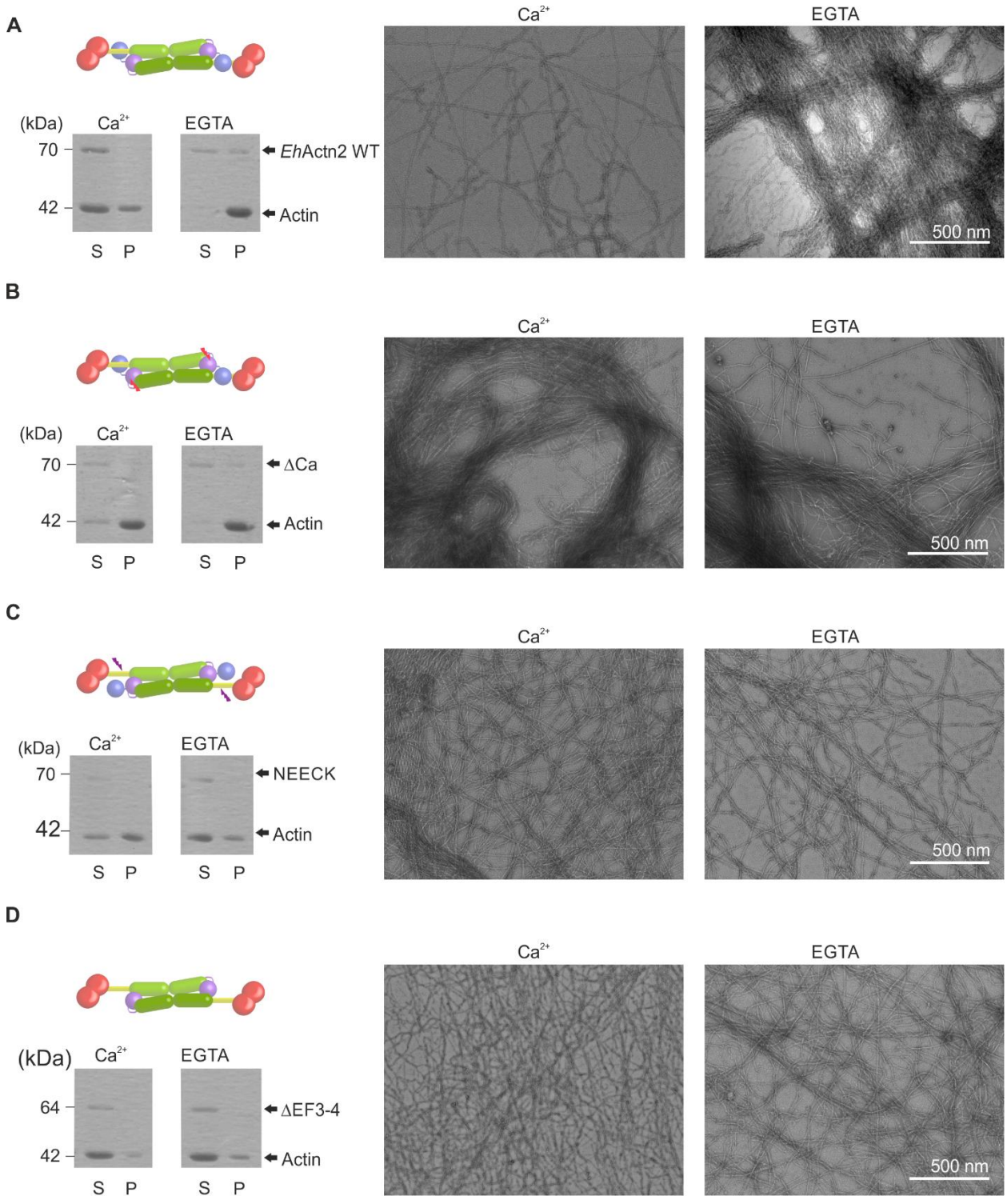

Figure 38. Bundling activity of EhActn2 constructs assessed by SDS-PAGE and negative staining electron microscopy. (A-D) Samples visible on SDS-PAGE were visualized by negative staining electron microscopy (image magnification of 56,000x). S, supernatant; P, pellet.

The results obtained from bundling experiments were verified by negative staining electron microscopy at the concentration of α-actinin/F-actin in which the biggest difference in bundles formation was seen in the absence and presence of Ca^{2+}(**Fig. 38EA-D**). Images were collected by Dr. Luciano Ciccarelli (Thomas Marlovits lab, IMBA, Vienna).

Since Mg^{2+} is more abundant in the cellular environment than Ca^{2+}, and both ions can compete for binding to *Eh*Actn2 WT, low-speed co-sedimentation assays were also used to test whether the presence of Mg^{2+} could affect the bundling activity of *Eh*Actn2 WT. No reduction of bundling efficiency was observed in the presence of Mg^{2+}, which means that *Eh*Actn2 is a truly Ca^{2+}-regulated α-actinin (**Fig. 39B**). The bundling assay was additionally performed under more physiological conditions, with 1 mM Mg^{2+} and 1.5 µM Ca^{2+}. (**Fig. 39C**). Under these conditions, *Eh*Actn2 WT still showed reduction in bundling, even though the concentration of Ca^{2+} used in this assay was lower than the highest *Eh*Actn2 WT concentration (2 µM) which proves that this protein can be indeed regulated by Ca^{2+} *in vivo*.

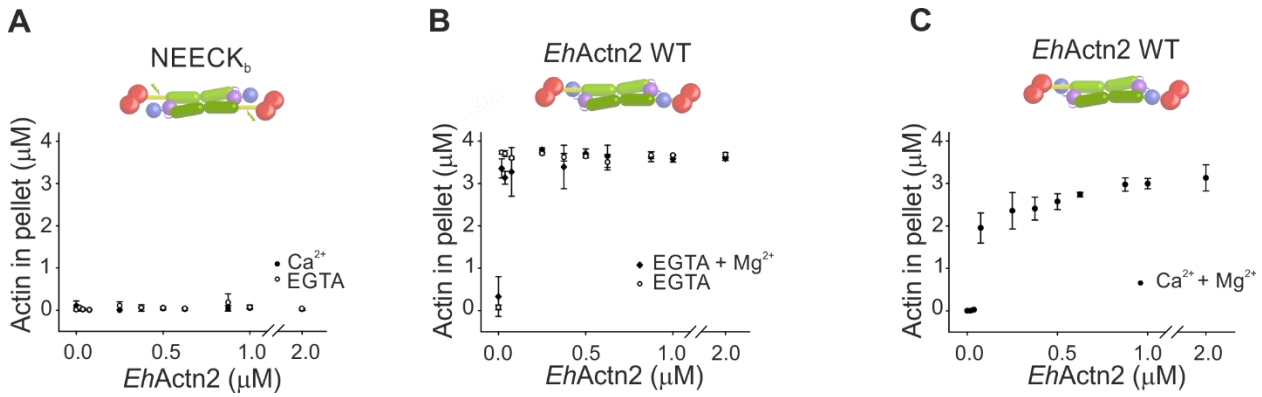

Figure 39. Low-speed co-sedimentation assays of EhActn2 constructs. (A) F-actin bundling activity of $NEECK_b$ construct in the absence and presence of 1 mM Ca^{2+} (B) F-actin bundling of *Eh*Actn2 in the presence of 0.5 mM EGTA (to remove Ca^{2+} traces) plus 2 mM $MgCl_2$. (C) Same as in (B) but in the presence of 1.5 µM Ca^{2+} plus 1 mM Mg^{2+}.

4.6 Integrity of the CaM domain drives the regulation of *Eh*Actn2 actin bundling

4.6.1 ΔEF1-4 can be rescued by the presence of EF1-4

ΔEF3-4 and NEECK constructs cannot bundle F-actin, which indicates that interactions between the C-terminal lobe of CaM domain and the neck region are crucial for protein function. Therefore, it can be expected that the function of ΔEF3-4 could be restored by the presence of EF3-4. This hypothesis was tested in bundling assays. However, ΔEF3-4 F-actin bundling activity could not be rescued even in the presence of 20-fold molar excess of EF3-4 (**Fig. 40A**).

As found for ΔEF3-4 in the presence of EF3-4, excess of EF3-4 did not restore the bundling activity of ΔEF1-4 (**Fig. 40B**), which means that the contact between EF3-4 and the neck region is not the only determinant behind the regulation of *Eh*Actn2 F-actin bundling function.

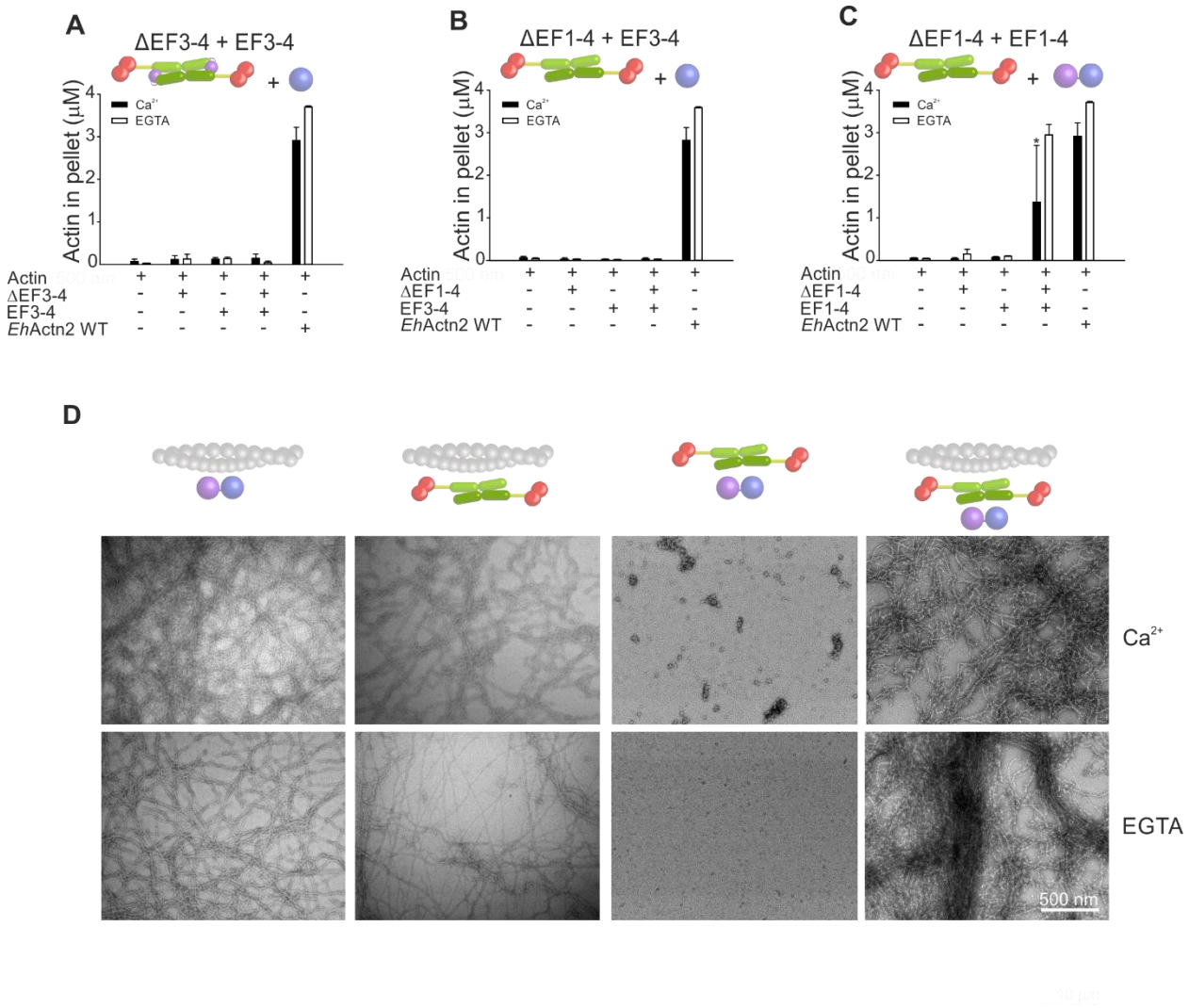

Figure 40. Rescue of F-actin bundling activity of* ΔEF3-4 and ΔEF1-4 *constructs by the presence of EF-hands. (A) F-actin bundling activity of ΔEF3-4 in the presence of 20-fold molar excess of EF3-4. (B) Same as (A) but ΔEF1-4 was used instead. (C) F-actin bundling activity of ΔEF1-4 in the presence of 20-fold molar excess of EF1-4. In all cases the outcome was compared with the bundling of *Eh*Actn2 WT. (D) Results from (C) imaged in negative staining electron microscopy (image magnification of 56,000x). All experiments were conducted in triplicate in the presence and absence of 1 mM Ca^{2+}.

Previous results demonstrated that the presence of EF3-4 alone is not sufficient to restore the bundling activity of ΔEF3-4 or ΔEF1-4. Therefore, we tested whether the function of the latter construct could be rescued in the presence of the whole CaM domain. In the absence of Ca^{2+} rescue was almost complete, while it was only partially restored in its presence (**Fig. 40**).

This result is significant (p = 0.033) despite the variability of the assay in the presence of Ca^{2+} and proves that the proper interaction between EF3-4 and the neck region requires the integrity of the CaM domain. These findings were further corroborated by negative staining electron microscopy, where the formation of F-actin bundles by ΔEF1-4 was only visible in the presence of EGTA upon addition of EF1-4 (**Fig. 40D**).

4.6.2 Thermodynamic analysis of interactions between EF3-4 and neck region

To better understand why successful rescue of ΔEF1-4 F-actin bundling activity requires the presence of the intact CaM domain, we investigated the interactions between EF3-4 and the neck region by ITC. For this purpose, neck was produced in the context of a longer construct (ABD-SR1) in order to ensure its proper folding and stability. EF1-4 interacts with the neck region with a K_d of 3.68 ± 1.65 and 8.30 ± 1.72 µM in the presence and absence of Ca^{2+}, respectively (**Fig. 41A,D**). The affinity of EF3-4 for the same construct is, however, five to 10-times weaker (**Fig. 41B,E**). Binding of EF1-4 to the neck region is more favorable in the presence of Ca^{2+}, as evidenced by a higher enthalpic contribution than in the presence of EGTA, where the interaction has higher unfavorable (positive) entropic contribution, resulting in a 5-times smaller ΔG (**Fig. 41G**). Results of the ITC experiments are shown in **Table 7**. Overall, these results demonstrate that the crosstalk between the N-and C-terminal lobes of CaM is vital for an optimal interaction between EF3-4 and neck, which subsequently controls the position of ABD in the context of the FL protein.

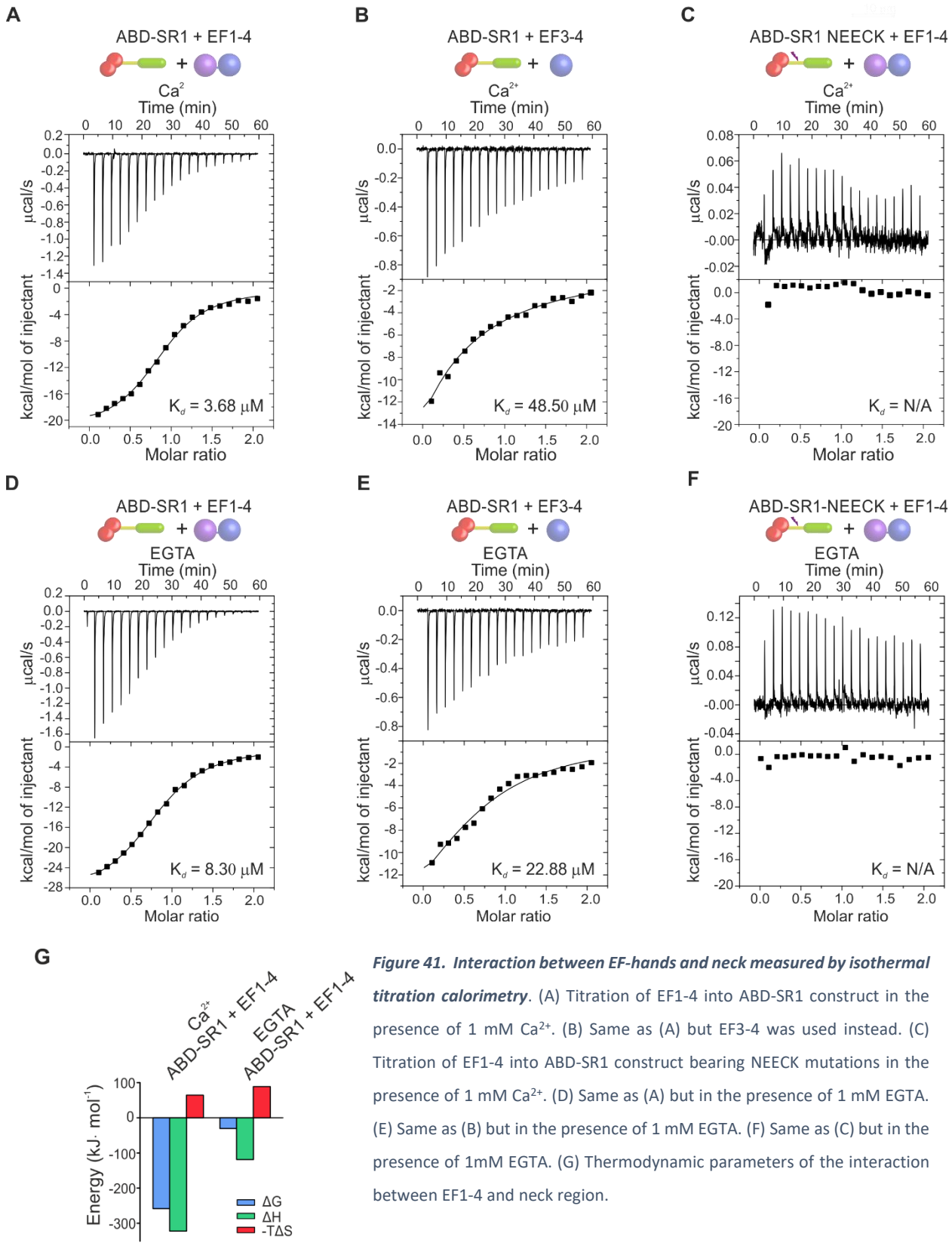

Figure 41. Interaction between EF-hands and neck measured by isothermal titration calorimetry. (A) Titration of EF1-4 into ABD-SR1 construct in the presence of 1 mM Ca^{2+}. (B) Same as (A) but EF3-4 was used instead. (C) Titration of EF1-4 into ABD-SR1 construct bearing NEECK mutations in the presence of 1 mM Ca^{2+}. (D) Same as (A) but in the presence of 1 mM EGTA. (E) Same as (B) but in the presence of 1 mM EGTA. (F) Same as (C) but in the presence of 1mM EGTA. (G) Thermodynamic parameters of the interaction between EF1-4 and neck region.

Table 7. Thermodynamic parameters of protein domains interactions assessed by isothermal titration calorimetry.

Protein	Ligand	N	K_d (μM)	ΔH (cal/mol)	ΔS (cal/mol/deg)
WT ABD-SR1 + Ca^{2+}	EF1-4	0.90 ± 0.05	3.68 ± 1.65	-77,700 ± 9,722	51.40 ± 5.85
WT ABD-SR1 + Ca^{2+}	EF3-4	N/D	48.50 ± 12.07	N/D	-145.28 ± 114.26
NEECK ABD-SR1 + Ca^{2+}	EF1-4	N/A	N/A	N/A	N/A
WT ABD-SR1 + EGTA	EF1-4	0.99 ± 0.11	8.3 ± 1.72	-28,400 ± 2,364	-71.00 ± 7.49
WT ABD-SR1 + EGTA	EF3-4	N/D	22.88 ± 2.90	N/D	-46.13 ± 18.01
NEECK ABD-SR1 + EGTA	EF1-4	N/A	N/A	N/A	N/A

4.7 Closed or open? Is rod opening essential for *Eh*Actn2 function?

4.7.1 Disulfide-bonded constructs help to verify whether rod is open or closed

The insertion of EF1-2 within the rod domain in *Eh*Actn2 is unique and distinguishes this α-actinin from *h*Actn2 where the rod domain is closed (Ribeiro Ede et al., 2014, Tang et al., 2001). To verify whether this structural arrangement seen in the crystal structure of *Eh*Actn2 is also observed in solution, we designed a series of disulfide-bonded constructs with introduced cysteine residues in the SRs of FL protein (SS1: S332C+Q473C and SS2: G326C+Q473C) and ΔEF3-4 construct (SS1: S332C+Q473C, SS2: G326C+Q473C and SS3: Q319C+Y469C) (**Fig. 42A**). Accordingly, disulfide bonds should form upon addition of oxidized glutathione (GSSG) in case the rod domain was open in solution. Equivalent mutations were introduced in the rod domain alone, which serves as a positive control, as it is constitutively closed due to the absence of EF1-2 (Gkougkoulia, 2014). There were disulfide bonds formed in the rod domain alone (**Fig. 42B**), but not in FL *Eh*Actn2 variants (Fig. 42D) nor in ΔEF3-4 constructs (**Fig. 42C**) under non-reducing conditions, which demonstrated that in the two latter constructs EF1-2 is sandwiched between SRs in solution, in agreement with *Eh*Actn2 crystal structure (**Fig. 21,23**).

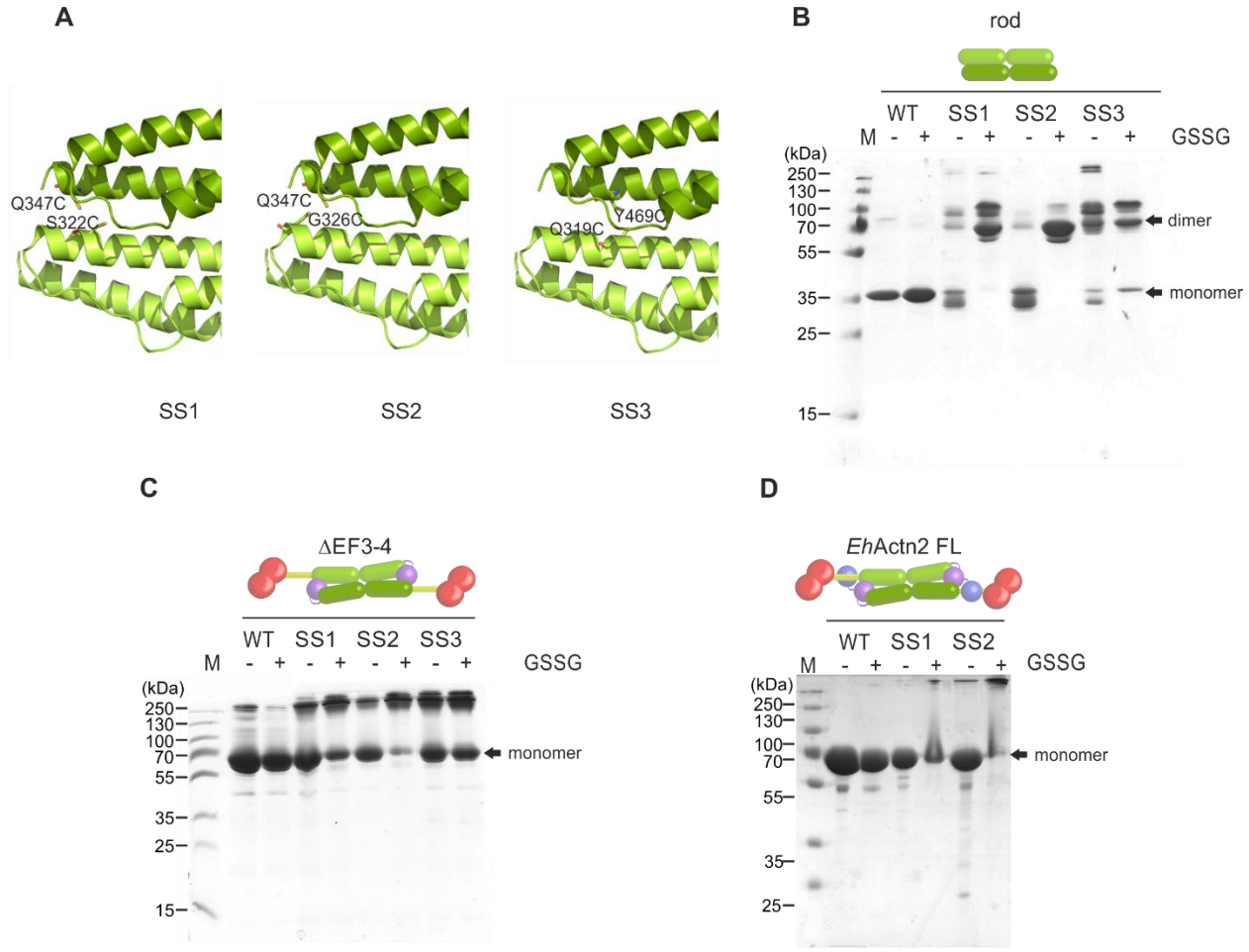

Figure 42. Rod domain in EhActn2 FL is open as assessed by designed disulfide-bonded constructs. (A) Design of disulfide bonds in *Eh*Actn2 FL was based on the structure of the rod domain alone. (B) SDS-PAGE disulfide-bonded constructs introduced in the rod under reducing (-GSSG) and oxidizing (+ 0.5 mM GSSG) conditions. (C) Same as in (B) but for ΔEF3-4. (D) Same as in (B and C), but for *Eh*Actn2 FL.

4.7.2 Insertion of EF1-2 within the rod is essential for *Eh*Actn2 Ca^{2+}-regulation

The intercalation of EF1-2 between SRs poses the question whether this particular molecular architecture might play an important functional role. To address this, it was initially attempted to disrupt the stabilizing interactions between SRs and EF1-2 by mutagenesis (**Fig. 23**). In order to exclude a possible negative influence from the introduced mutations on Ca^{2+} binding and regulation, only residues from rod domain were engineered resulting in a construct bearing four point mutations: T315A, R325E, E464K and E476K. These mutations were then introduced within a FL *Eh*Actn2 variant bearing additionally SS2 mutations

(G326C+Q473C), which would allow to verify whether EF1-2 was still inserted within the rod by means of disulfide-bond formation. No disulfide bond was found in this construct under oxidizing conditions, which indicates that EF1-2 was still intercalated in the rod (data not shown).

This result points out that the interaction between EF1-2 and SRs is very stable and is not only maintained by the four electrostatic interactions that we attempted to break. Therefore, another approach was necessary in order to interfere with the intercalation of EF1-2 in the rod domain; a chimeric variant was constructed in which the rod domain from *Eh*Actn2 was replaced with the rod domain from *h*Actn2, which is closed (Ribeiro Ede et al., 2014) (see Table 2 for details on this construct). Preliminary ITC experiments and Quin-2 assays (not shown) indicate that the chimeric variant showed unchanged Ca^{2+} binding affinity compared with EF1-4, but it displayed a surprising behavior in low-speed F-actin co-sedimentation assays, namely it behaved as a Ca^{2+}-insensitive variant (**Fig. 43**). Based on this finding, we envision that the insertion of EF1-2 within the rod domain mediates Ca^{2+} regulation of *Eh*Actn2.

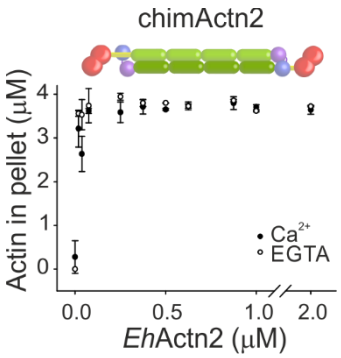

Figure 43. Low-speed co-sedimentation assay of chimActn2. F-actin bundling activity by chimActn2 in the absence and presence of 1 mM Ca^{2+}.

5 DISCUSSION

Until now the mechanism of Ca^{2+}-regulation of α-actinins has not been elucidated. In this thesis, I investigated this regulation in a model α-actinin, *Eh*Actn2, by using an integrative biophysical, biochemical and structural approach. The tetragonal structure of Ca^{2+}-bound *Eh*Actn2 solved by Dr. Nikos Pinotsis was the starting point for this project as it allowed us to design a collection of constructs in order to comprehensively study the Ca^{2+}-regulation mechanism of this protein. ΔCa variant designed by Dr. Eirini Gkougkoulia (Gkougkoulia, 2014) was subsequently crystallized in an orthorombic space group and compared with a second structure of Ca^{2+}-bound *Eh*Actn2 crystallized in the same space group and refined to a similar resolution. *Eh*Actn2 Ca^{2+}-bound and Ca^{2+}-free structures are the only high resolution structures of any Ca^{2+}-sensitive α-actinin reported thus far. Moreover, we were able to characterize in depth the Ca^{2} -binding to *Eh*Actn2, its impact on F-actin bundling activity and to elucidate the overall molecular mechanism behind the regulation in this protein, which involves multi-domain communication and the integrity of the CaM domain (see below).

5.1 Ca^{2+}-binding to *Eh*Actn2

It had been previously reported that *Eh*Actn2 binds Ca^{2+} ions (Virel et al., 2007). In contrast to published data (Karlsson, Persson et al., 2016), here it was demonstrated that *Eh*Actn2 displays exceptionally high affinity for Ca^{2+}, in fact too high to act as a regulatory protein. Therefore, we seeked to test whether it could also bind Mg^{2+}, which is a more ubiquitous cytoplasmic ion. We demonstrated that the Ca^{2+}-binding site in *Eh*Actn2 EF-1 is *de facto* a mixed Ca^{2+}/Mg^{2+} site, i.e. it is able to bind both ions, but with different affinities (**Figs. 29B,D, 31A**). Due to proven competition between both ions (**Fig. 31B**), *Eh*Actn2 is a truly Ca^{2+}-regulated α-actinin. The reason why this phenomenon has not been uncovered before might be due to the methodology used for protein purification, where Backman *et al* did not strip the protein from Ca^{2+} before accessing its Ca^{2+}-binding properties and moreover, used Mg^{2+}-containing buffer for radiography experiments (Karlsson et al., 2016).

We also provided the molecular basis for the unusually high affinity of *Eh*Actn2 for Ca^{2+} ions, which is driven by a privileged arrangement of residues involved in cation coordination (Black et al., 2000, Reid, 1990).

*Eh*Actn2 is different from most CaBPs because even though it contains four EF-hands, only EF-1 maintains the Ca^{2+}-binding properties (**Fig. 29D**). At first glance, having only one functional site out of four looks like a bad design. However, for this protein it suffices, as EF-1 shows extremely high affinity for Ca^{2+} and more importantly, binding of this ion to EF-1 affects the whole CaM domain (see below).

5.2 To bundle or not to bundle? Ca^{2+} binding affects the function and stability of *Eh*Actn2

We validated the published data where it was demonstrated that *Eh*Actn2 can bundle actin filaments *in vitro* in a Ca^{2+}-dependent manner (Virel et al., 2007)(**Figs. 37A, 38A**). The design of ΔCa variant allowed us to have a Ca^{2+}-free form of *Eh*Actn2, proving additionally that the Ca^{2+}-binding site is located in EF-1 of *Eh*Actn2 (**Fig. 29C**). It also proved that the physiologically abundant Mg^{2+} ion does not influence bundling of F-actin (**Fig. 39B,C**), which evinces that *Eh*Actn2 is a truly Ca^{2+}-regulated α-actinin.

How is Ca^{2+}-regulation of *Eh*Actn2 accomplished at the molecular level? Both ions, Ca^{2+} and Mg^{2+}, are able to increase the stability of the protein, albeit the first one exerting a more pronounced effect. Our limited proteolysis and DSF experiments (**Figs. 33**,**34**) are further supported by crystallographic data. Thus, B-factors of ABD, neck and EF-hands are increased in ΔCa variant, in comparison to Ca^{2+}-bound *Eh*Actn2 (**Fig. 25**). Therefore, subtle changes in the flexibility of these domains are the driving force for the regulation of *Eh*Actn2 function.

Notably, drastically increased flexibility of ABD is detrimental for *Eh*Actn2-dependent actin bundling, as shown by the behavior of NEECK and ΔEF3-4 constructs, which highlight the subtlety behind *Eh*Actn2 Ca^{2+} regulation.

5.3 Behind the scene: mechanism of Ca^{2+} regulation of *Eh*Actn2

As shown above, binding of Ca^{2+} to *Eh*Actn2 affects its function. In the next sections I will try to explain our understanding of the conformational changes occurring in the protein upon Ca^{2+} binding. The secret of the regulation of *Eh*Actn2 lies in the multi-domain composition and domain cross-talk within this protein.

5.3.1 Unique properties of *Eh*Actn2 calmodulin-like domain

The exact conformational changes occurring in EF-hands upon Ca^{2+} binding are only partially understood. The β-scaffold concept explains how dication binding to the EF-loop first affects its N-terminal part and subsequently causes rotation of the last Glu, which closes the Ca^{2+}-binding loop (Grabarek, 2006). However, how binding of Ca^{2+} to one EF-hand affects globally the whole CaM domain is still not understood in molecular detail. It has been demonstrated by NMR spectroscopy that when Ca^{2+} binds to the N-terminal EF-hand of calbindin D_{9k}, it clearly rigidifies the Ca^{2+}-binding loop in the neighboring EF-hand, although Ca^{2+}-binding site in the latter one was mutated (N56A) to abrogate the interaction with the ion. These findings help to explain cooperativity in the CaM domain of calbindin D_{9k}, namely Ca^{2+} binding to EF-1 already 'pre-orders' the EF-2 one and prepares it for ion binding (Maler, Blankenship et al., 2000). In our work, the low resolution of apo and holo structures of *Eh*Actn2 (3.38 and 3.17 Å, respectively) precludes a detailed analysis of amino acids interactions driving subtle conformational changes in CaM domain upon interaction with divalent ions, however it still allows to detect the mobility of protein domains through the comparison of B-factors. Moreover, the regulation of *Eh*Actn2 is more complex, as it is orchestrated by multi-domain interactions, as described in detail below.

The CaM domain in *Eh*Actn2 shows similarities with other published structures from α-actinin and spectrin families of proteins (Atkinson et al., 2001, Drmota Prebil et al., 2016, Ribeiro Ede et al., 2014, Trave, Lacombe et al., 1995). EF1-2 in *Eh*Actn2 is in a closed conformation, whereas EF3-4 adopts a semi-open structure due to the presence of the neck region. A similar feature is seen in *h*Actn2 and in the structure of *h*Actn2 EF3-4 bound to titin Z-repeat 7 (Atkinson et al., 2001, Ribeiro Ede et al., 2014). In all cases the interactions between C-lobe of CaM domain and the bound helical peptide (neck peptide and titin Z-repeat 7, respectively) accommodated in its cavity are hydrophobic and follow the so called 1-4-5-8 motif. The semi-open conformation of the C-lobe in *Eh*Actn2 and in *h*Actn2 represent a rare but distinct

mode of interaction between CaM domain and its target, as in those structures the peptide binding groove is more shallow than that seen in opened CaM so that the binding motif interacts only with the tip of the cavity. A semi-open conformation was reported for C-lobe of apo CaM bound to IQ motif of unconventional myosin V (Houdusse, Gaucher et al., 2006) and to the regulatory domain of scallop myosin, where the C-lobes of both essential and regulatory light chains adopt such structural arrangement (Houdusse & Cohen, 1996). It was proposed that in the apo state C-lobe of CaM exists already in semi-open conformation, pre-formed to interact with IQ motifs, which is driven by the presence of charged residues inside of the domain and lack of hydrophobic core, which is present in N-terminal domain and predisposes it to adopt closed conformation in the absence of Ca^{2+} (Swindells & Ikura, 1996). Importantly, adopting a semi-open conformation by CaM C-lobe prior and during the interaction with IQ motifs precludes Ca^{2+} coordination. I would dare to propose that Ca^{2+} binding would be in such a case redundant for *Eh*Actn2 EF3-4, as even if this domain would be Ca^{2+}-sensitive, adopting a semi-open conformation would preclude optimal metal ion chelation. Therefore, EF3-4 plays a different function in *Eh*Actn2, which is binding to the neck region and fixing the positon of ABD, like previously seen in *h*Actn2 (Ribeiro Ede et al., 2014). A similar role was suggested for β-spectrin EF3-4, where the deletion of the last 13 amino acids from the C-terminal EF-hand of α-spectrin abolished binding of β-spectrin ABD to F-actin in the presence of protein 4.1R. Based on this result the authors suggested that C-terminal EF-hand might bind to the linker connecting ABD with the first SR in β-spectrin (Korsgren & Lux, 2010). It might be therefore a common feature of the members of the spectrin family of cytoskeleton regulators.

Isolated apo and holo CaM domains from Ca^{2+}-sensitive *h*Actn1 reveal that ion binding rigidifies the Ca^{2+}-binding loop and triggers a moderate opening of the N-lobe; that is, there is a clockwise swing around the entering helix of EF-1 with minimal opening of the helices. In those structures the C-terminal lobe does not show significant changes upon ion binding. Similarly, in α-spectrin CaM domain, binding of Ca^{2+} results in domain opening and main conformational changes are seen in EF-1, whereas EF-2 is more static (Trave et al., 1995). In both proteins Ca^{2+} binding disrupts the hydrophobic core in EF-1. Notably, in contrast to the C-lobe of CaM, which adopts semi-open conformation before IQ motifs binding, EF3-4 is closed in both solution structures of CaM domain from *h*Actn1. Apparently, it opens in *Eh*Actn2 upon interaction with neck region, which is further supported by the NMR structure of isolated CaM domain from *Eh*Actn2 (Karlsson et al., 2016).

Binding of Ca^{2+} to *Eh*Actn2 does not cause any notable structural reorganization of the CaM domain, since the rmsd of EF1-4 is very similar (0.87 Å for 128 equivalent C-α atoms) in Ca^{2+}-bound and Ca^{2+}-free *Eh*Actn2 orthogonal structures.

It might be argued that EF1-2 does not change its conformation from closed to open upon Ca^{2+} binding due to its insertion between SRS and concomitant reduced mobility. In fact, only helix A penetrates the rod domain, which would still allow the rotation of other helices. To properly address this question, one would need to compare the structure of EF1-4 in solution in the presence and absence of Ca^{2+}. Karlsson *et al* claim they studied by NMR the Ca^{2+}-bound CaM domain from *Eh*Actn2 (Karlsson et al., 2016), however, since all measurements were performed in sodium phosphate buffer, it can be assumed that Ca^{2+} was most likely precipitated under those conditions and therefore the observed structure was actually Ca^{2+}-free, as the solubility of $(Ca^{2+})_3(PO_4)_2$ in water at 20°C is only up to 80 µM (Lide & Chemical Rubber Company., 1999) . This is additionally supported by the fact that titration of EGTA into this protein did not change the NMR spectrum (personal information, Lars Backman, Umea University, Sweden). In the reported solution structure, EF1-2 adopts a very similar conformation to the one seen in our crystal orthorhombic ΔCa structure (rmsd of 1.78 Å for 69 equivalent C-α atoms). EF3-4 in the NMR structure is also seen in a closed conformation, whereas in FL *Eh*Actn2 it prefers a semi-open structure due to its interaction with the NECK peptide (rmsd of 1.29 Å for 40 C-α atoms) (**Fig. 44**).

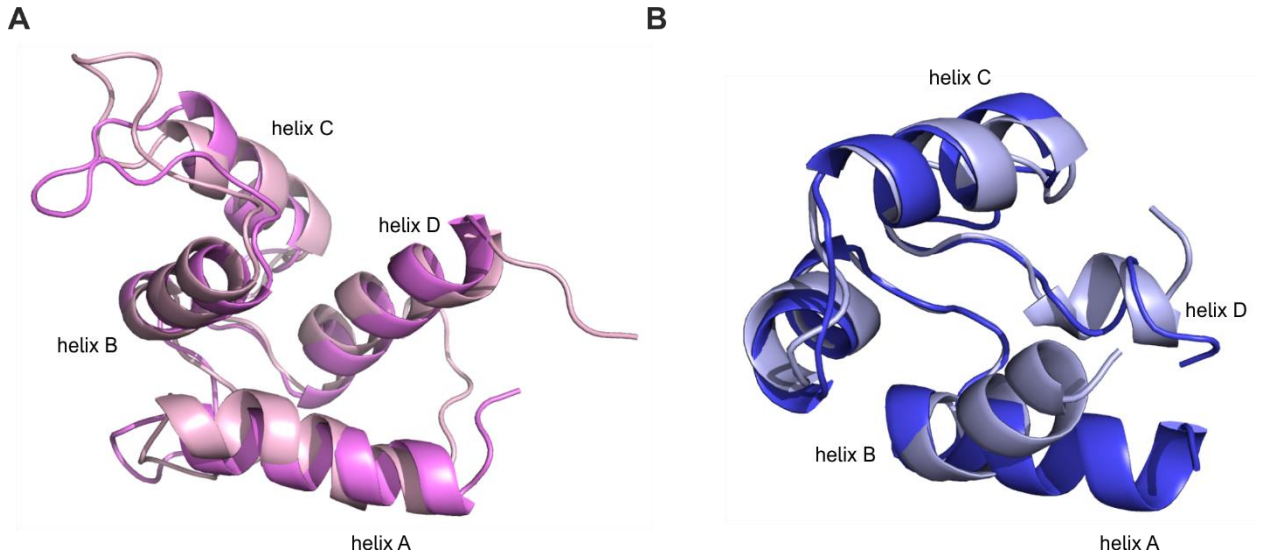

Figure 44. Superposition of ΔCa EhActn2 EF-hands with the NMR structure of EhActn2 CaM domain. (A) Superposition of EF1-2 from ΔCa (in violet) with EF1-2 from the NMR structure (in light pink; pdb code: 2ML7 (Karlsson et al., 2016)). (B) Superposition of EF3-4 from ΔCa (in dark blue) with EF3-4 from the NMR structure (in light blue; pdb code: 2ML7 (Karlsson et al., 2016)).

It is worth mentioning that in all published structures containing CaM domains of α-actinins, except from apo CaM domain of *h*Actn1 (Drmota Prebil et al., 2016), β-sheets which normally stabilize adjacent EF-loops are absent. So far it is not clear why this structural element is missing in *Eh*Actn2 and *h*Actn2 CaM domains. Also, in *Eh*Actn2 the linker between EF-1 and EF-2 is unusually long and contains 13 amino acids. Interestingly, this seems to be the case for other two Ca^{2+}-sensitive actinins – *h*Actn1 and *h*Actn4, with linker built by 12 amino acids, but not for Ca^{2+}-insensitive muscle human isoforms, where the linker has only seven amino acids. It is tempting to speculate that this linker might play a special regulatory role in Ca^{2+}-sensitive α-actinins.

Although we do not understand why other EF-hands lost their ability to bind Ca^{2+}, our results show that Ef-hands in *Eh*Actn2 function as an integral domain. Accordingly, in rescue experiments, the activity of ΔEF1-4 can only be restored when EF1-4 (and not EF3-4) is used (**Fig. 40C,D**), which means that the proper function of this protein relies on an effective communication between both CaM lobes. Comparison of crystal structures of *Eh*Actn2 WT and ΔCa shows that Ca^{2+} binding stabilizes not only EF-hands but also the neck region and ABD (**Fig. 25A,B**).

Therefore, *Eh*Actn2 EF-hands act most likely as function modulators. We postulate that Ca^{2+}-binding to EF1-2 is transmitted to EF3-4, which in turn regulates the position of ABD *via* its interaction with the neck region. EF1-2 acts as a molecular switch that drives a conformational change in EF3-4, which is Ca^{2+}-insensitive and exerts the function of the final tuner. Nonetheless, the conformation changes in CaM domain promoted by Ca^{2+} binding are very small.

5.3.2 Is rod participating in conformational cross-talk?

Based on the assumption that α-actinin, being an actin cross-linker, would be constantly subjected to mechanical stress enforced by the inherent dynamics of cytoskeleton, it was postulated that its rod domain may actually be more flexible than expected. Molecular dynamic simulations and normal mode analysis reveal that the rod domain of human α-actinin displays bending flexibility and increased dynamics of its termini with the central helical linkers being rigid, but displaying extensional rigidity (Golji, Collins et al., 2009). Although authors interpret increased dynamics of rod termini as a crucial factor determining flexibility of adjacent neck region, they did not take into account the stabilizing interaction between neck and CaM domain. Also, electron microscopy micrographs of actin-α-actinin bundles do not reveal flexibility within the rod domain, despite the fact that α-actinin crosslinks actin filaments in different orientations, presumably due to flexibility of ABD (Hampton, Taylor et al., 2007). Thus, it is unlikely that

the rod domain is directly involved in Ca^{2+}-induced conformational changes in the protein, but rather regulation is maintained and driven by the CaM domain.

5.3.3. Insertion of EF1-2 inside the rod has a special function

Another striking structural feature of *Eh*Actn2 is the insertion of EF1-2 within SRs, which adopts a unique conformation. EF1-2 conformation is indeed very unusual as it does not engulf the interacting peptide using hydrophobic residues like CaM domains usually do, but it is itself locked inside of the rod domain. *Eh*Actn2 EF1-2 is not actively involved in binding to target proteins, but rather adopts a role of a target itself. Moreover, EF1-2 utilizes only polar residues for the intercalation within the rod domain, which is also an unconventional mode of binding for EF-hands. Comparison of solvation free energy between the rod domain alone and rod/EF1-2 from FL *Eh*Actn2 implies that when EF1-2 is sandwiched between SRs it contributes positively to protein stability, with an increase in ΔG of additional -6.9 kcal/mol (Vangone & Bonvin, 2015). But does this conformation have a purely structural role? We addressed this question using a chimeric construct, where the rod domain of *Eh*Actn2 was replaced with that from *h*Actn2, which is closed, according to its published crystal structure (Ribeiro Ede et al., 2014). When EF1-2 is removed from its natural position, *Eh*Actn2 loses its ability to be regulated by Ca^{2+}, although it still binds the ion (**Fig. 43**). Therefore, insertion of EF1-2 within the rod has clearly an important regulatory function. This also helps to understand why the rescue of ΔEF1-4 by EF1-4 is more effective in the presence of EGTA. When EF1-2 is not embedded inside the rod, the Ca^{2+}-regulation is perturbed, which is reflected by high variability of the same experiment done in the presence of Ca^{2+} (**Fig. 40C**). Clearly, having EF1-2 sandwiched inside the rod helps to stabilize and orient the position of EF3-4 and impacts on its interaction with the neck region.

5.4 Subtlety behind the regulation of *Eh*Actn2

Ca^{2+}-bound and Ca^{2+}-free *Eh*Actn2 structures are very similar (rmsd of 1.14 Å for 712 eqivalent C-α atoms when both orthorhombic structures are compared) (**Fig. 25**). However, the latter shows increased flexibility of ABD, EF-hands and neck region, as reflected by increased B-factors for these protein domains. These differences in flexibility could not be detected by SLS (**Fig. 35**). Is this difference enough to regulate the function of such a large multi-domain protein?

A similar modulatory role of EF-hand on protein structure was reported for Ca^{2+}-binding protein 40 (CBP40) from slime mold *Physarum polycephalum*. This protein helps to close wounds in this organism by aggregating in a Ca^{2+}-dependent manner. It is composed of three domains: an N-terminal long coiled coil, an intervening domain, and a pair of EF-hands, where the two latter domains make an extensive contact (total area of 1,485 $Å^2$) (**Fig. 45A,B**).

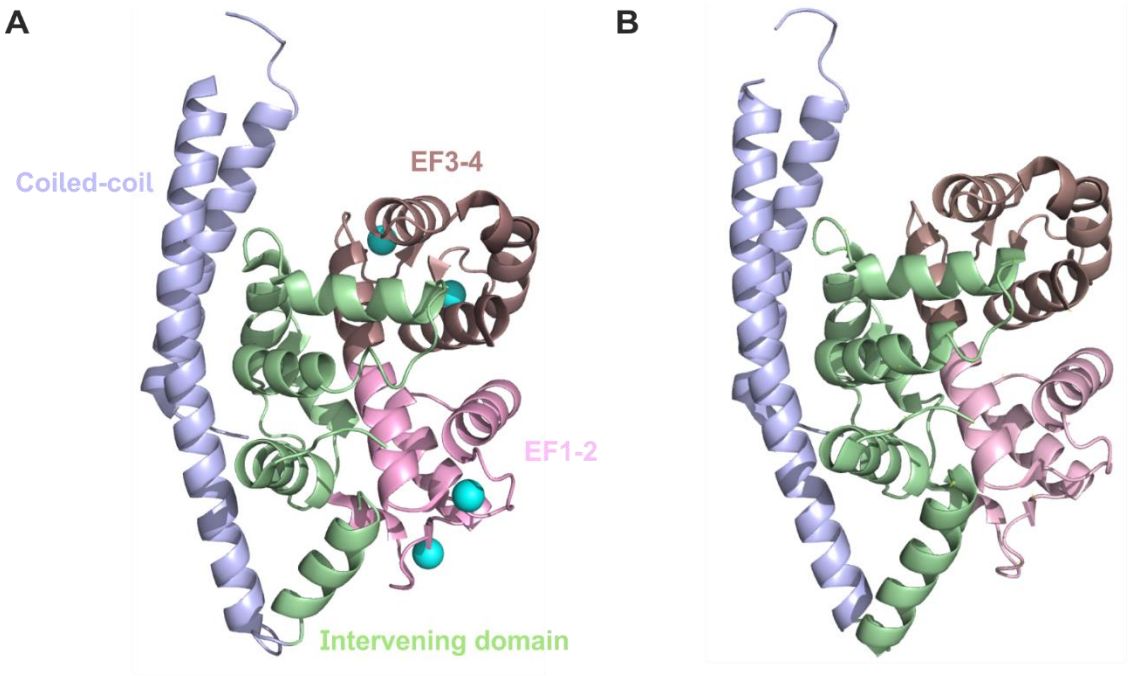

Figure 45. Structure of CBP40 from Physarum polycephalum. Ca^{2+}-bound (A) and Ca^{2+}-free (B) structures of CBP40. Figure was made in PyMOL using PDB entry 1IJ6 and 1IJ5, respectively (Iwasaki et al., 2003). Ca^{2+} ions are shown as cyan spheres.

Although the conformational change in CBP40 upon Ca^{2+} binding to EF-hands is very small (rmsd between Ca^{2+}-bound and Ca^{2+}-free structures equals 0.35 Å for 271 equivalent C-α atoms), it reduces the flexibility of other domains that are not directly involved in ion binding. The overall fold of the protein is not changed, but the structural changes are propagated from the EF-hands to the coiled-coil *via* the intervening domain, without direct contact between the CaM domain and the N-terminus of the protein (Iwasaki et al., 2003). This study shows a possible multi-domain regulation of a protein driven allosterically by EF-hands and in which the only indication of conformational changes caused by Ca^{2+} binding are reflected in higher B-factors in the domain not directly involved in ion binding, similar to what we observe for *Eh*Actn2.

Another example of a Ca^{2+}-binding protein in which conformational changes upon metal binding are very subtle is a cytoskeletal organizer EFhd2/Swissprosin-1 (hereafter EFhd2), a protein which (unlike α-

actinin) bundles F-actin only in the presence of Ca^{2+} ions and is involved in Ca^{2+}-dependent cell spreading and migration of epithelial cells. EFhd2 is a multidomain protein and contains an N-terminal disordered region, followed by a PxxP motif, two EF-hands displaying Ca^{2+}-affinity in nanomolar range, a ligand mimic helix (LM) and a C-terminal coiled-coil domain. Crystal structures of Ca^{2+}-bound EFhd2 core domain lacking the disordered N-terminus, and Ca^{2+}-insensitive mutants of EFhd2, with mutations abrogating metal binding in EF-1 and EF-2, (E116A and E152A, respectively), were reported (Park, Kwon et al., 2016). In this protein structural changes caused by Ca^{2+}-binding are very subtle (rmsd between WT EFhd2 and two variants (E116A and E152A) equals 0.34 Å for equivalent 102 C-α atoms for the former and 0.61 Å for equivalent 105 C-α atoms for the latter, respectively). Ca^{2+}-binding to EFhd2 rigidifies Ca^{2+}-binding loop in EF-hands and the C-terminal linker. Conformational flexibility of the latter in the absence of Ca^{2+} ions allows it to maintain F-actin binding ability, but impairs the bundling activity. In the opposite to *Eh*Actn2 F-actin bundling by EFhd2 requires that the core of the protein becomes more rigid. Similarly to *Eh*Actn2, though, the structural changes in EFhd2 upon Ca^{2+} binding are very subtle and are reflected mainly in the change in B-factors, which may be more common in Ca^{2+}-sensors as previously expected.

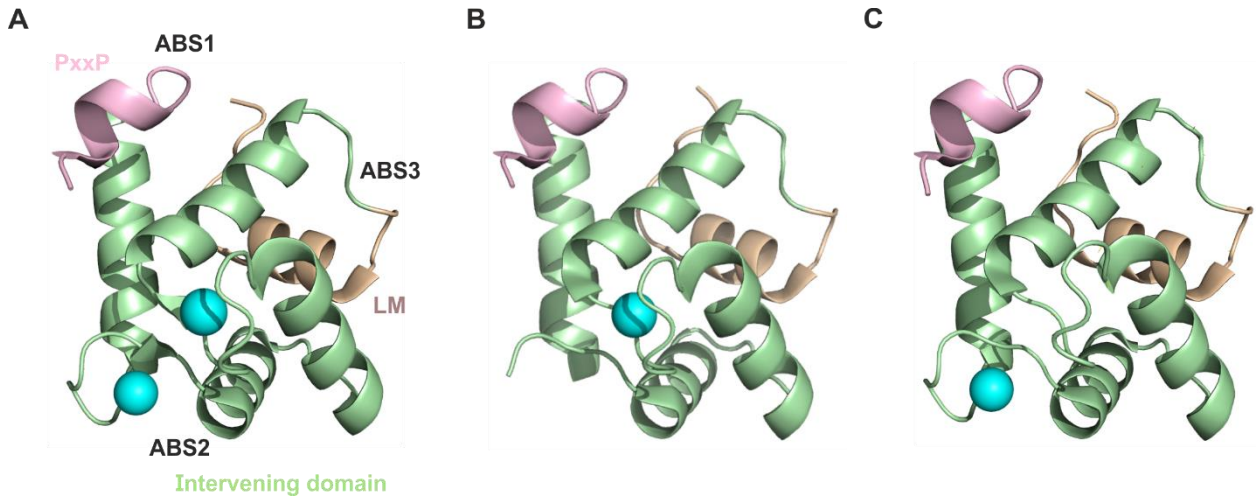

Figure 46. Crystal structures of EFhd2 variants. (A) Structure of wild-type EFhd2 core domain (B). Structure of Ca^{2+}-insenstive variant (E152A) of EFhd2 bearing a point mutation in EF-1. Ca^{2+}-binding loop in EF-1 is disordered. (C) Structure of Ca^{2+}-insenstive variant of EFhd2 core domain (E116A) bearing a point mutation in EF-2. Figures were generated in PyMOL using pdb codes: 5I2L (A), 5I2O (B) and5I2Q (C). (Park et al., 2016). Ca^{2+} ions are shown as cyan spheres.

5.5 Is *Eh*Actn2 a universal Ca^{2+}-sensitive α-actinin?

*Eh*Actn2 was proposed to be an ancestor of mammalian variants (Virel & Backman, 2007). It contains a shorter rod domain with only two SRs, whereas human α-actinins contain four. Therefore, *Eh*Actn2 might be considered as a model α-actinin. Is it so? Similarly to *h*Actn1 and *h*Actn2 (Ribeiro Ede et al., 2014, Tang et al., 2001), *Eh*Actn2 is an elongated molecule, where ABD is locked in a specific position due to the interaction between EF3-4 and the neck region. Unexpectedly, *Eh*Actn2 binds Ca^{2+} very tightly and is also able to bind Mg^{2+}, although the latter with a lower affinity (**Fig. 31A**). This is in sharp contrast with *h*Actn1, which has a micromolar affinity for Ca^{2+} (Backman, 2015, Drmota Prebil et al., 2016). Also, *Eh*Actn2 rod is open in order to accommodate EF1-2, which is not only contributing positively to protein stability but also has a functional role. Therefore, *Eh*Actn2 does not act like a prototypical α-actinin molecule, but rather has its own unique functional and structural properties. Accordingly, it might be postulated that α-actinins are regulated *via* different molecular mechanisms throughout the animal kingdom. However, more experiments are needed to test this, in particular, further structural information on Ca^{2+}-sensitive mammalian α-actinins is needed.

5.6 Is *Eh*Actn2 a Ca^{2+} sensor or a buffer?

*Eh*Actn2 EF-1 is designed to bind Ca^{2+} very tightly. Based on the comparison of the crystal structures of *Eh*Actn2 WT and ΔCa, there is no CaM domain opening observed in *Eh*Actn2 upon Ca^{2+} binding (**Fig. 25**). Both features are typical of Ca^{2+} binding proteins acting as buffers. However, *Eh*Actn2 is proposed to be involved in the remodeling of actin cytoskeleton and we prove that the orientation and flexibility of ABD are affected by Ca^{2+}-binding. Moreover, *Eh*Actn2 activity can be modulated by Mg^{2+} ions, which allows Ca^{2+} regulation *in vitro* and most likely also *in vivo* (**Fig. 39B,C**). *Eh*Actn2 EF1-4 has an intermediate content of methionine residues (five out of 140 residues; 3.5%), which does not allow to unambiguously classify this protein neither as a sensor nor as a buffer (Nelson & Chazin, 1998). Nevertheless, *Eh*Actn2 can be considered as a Ca^{2+} sensor if we take into account its multi-domain structure. Even though EF-hands do not act directly as Ca^{2+} sensors, they transmit conformational changes to the neighboring neck and ABD domains. If we define sensor as a protein in which Ca^{2+} binding can change the conformation of any protein

domain (and not only EF-hands), *Eh*Actn2 should be unambiguously categorized as such. A growing number of proteins considered before to act as Ca^{2+} buffers have been recently proposed, based on knockout mouse models, to have additional functional roles, particularly in the nervous system, which cannot be fully restored by other CaBPs (Schwaller, 2009). Therefore, it is not only the extend of the conformational change in the protein *per se*, but rather its molecular function what determines whether the actor in question plays a role of Ca^{2+} sensor or buffer. Taking all this into account, *Eh*Actn2 can be classified as Ca^{2+}-sensor.

5.7 Model of *Eh*Actn2 Ca^{2+} regulation

Based on our findings, we propose that there are two physiological states for *Eh*Actn2. Under resting conditions, *Eh*Actn2 will be Mg^{2+}-loaded, and during a signaling event, when Ca^{2+} levels are increased, it will be bound to Ca^{2+}. A situation in which *Eh*Actn2 is ion free is very unlikely to happen in a living cell.

Accordingly, we propose a model where the function of *Eh*Actn2 is regulated by Ca^{2+} in a very subtle manner (**Fig. 47A**). In the presence of Mg^{2+} ions (or in case of an artificial situation when no ion is bound, as for the ΔCa variant), ABDs at both ends of the molecule display flexibility, a situation optimal for F-actin bundling. When the Ca^{2+} ions are bound to EF-1, ABD flexibility is reduced due to the 90° twist embedded in the rod domain, ABDs at both ends of *Eh*Actn2 will be perpendicular to each other, which precludes parallel orientation and therefore bundling of F-actin (**Fig. 47A,B**). The ultimate position of ABDs is regulated by the cross-talk within the CaM domain, that is, EF1-2 needs to communicate with EF3-4 to transmit the Ca^{2+} regulation. Also, EF1-2 is required to be inserted within the rod domain for this to take place. The mechanism of Ca^{2+} regulation in *Eh*Actn2 is very subtly tuned, since allowing too much flexibility of ABDs is detrimental for protein function, like in NEECK mutant.

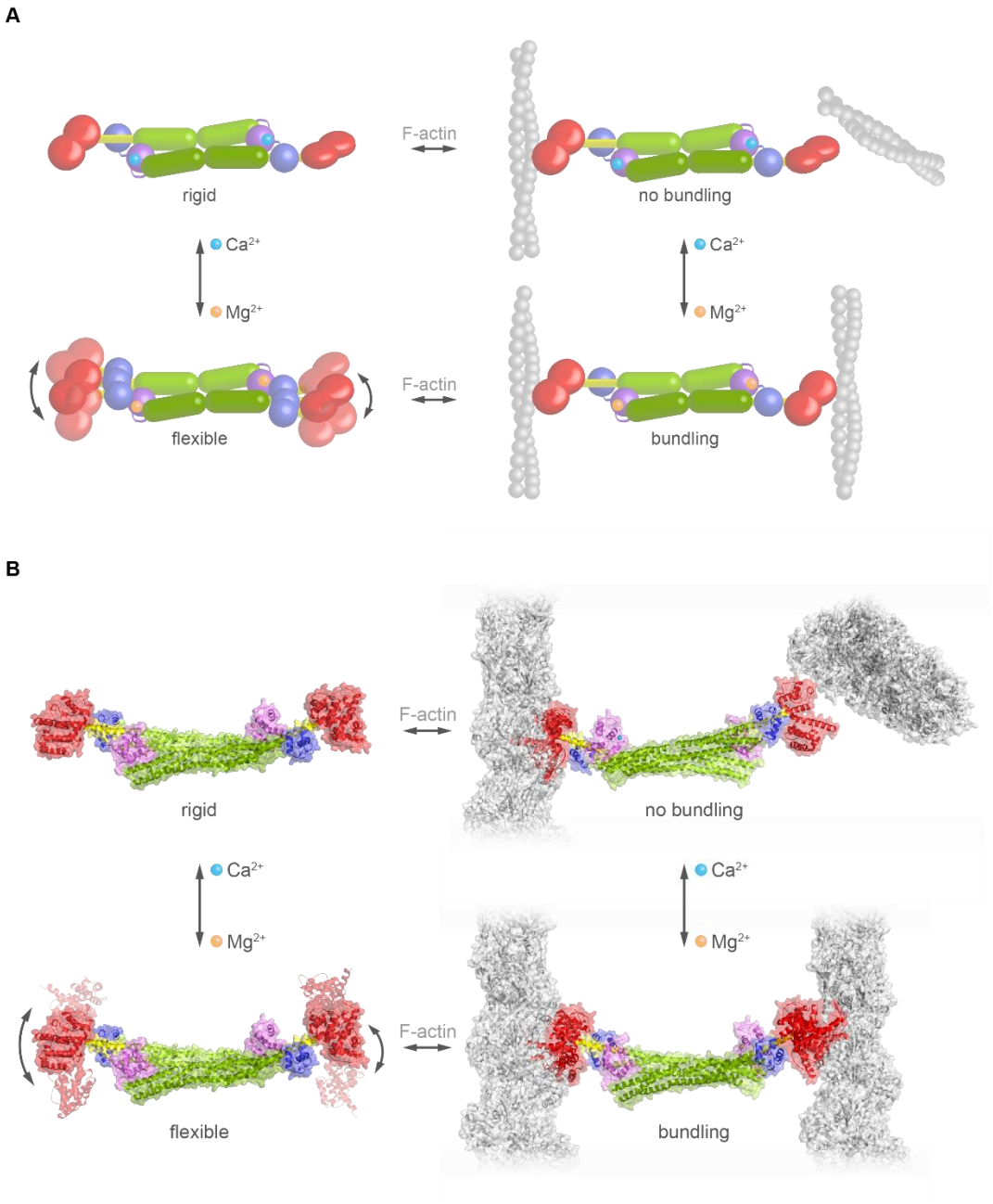

Figure 47. Proposed regulatory mechanism of EhActn2 by physiological divalent cations. (A) In the presence of Ca^{2+}, ABDs at the opposite ends of α-actinin are twisted by 90°, which precludes efficient F-actin bundling. In the presence of Mg^{2+}, ABDs are more flexible, an optimal situation for F-actin bundling, like in ΔCa mutant. (B) Same as (A) with fitted crystal structures of *Eh*Actn2 and F-actin. Figure was generated in PyMOL using pdb code 5JLF (von der Ecken et al., 2015). Figure made by Dr. Julius Kostan and Dr. Nikos Pinotsis.

5.8 Significance of our findings and future perspectives

This is the first time that Ca^{2+}-bound and Ca^{2+}-free structures of any FL Ca^{2+}-regulated α-actinin have been compared. This work has been complemented with an extensive biochemical and biophysical characterization of *Eh*Actn2.

Our research findings aid in the understanding of the regulation of actin cytoskeleton in eukaryotic cells. It is also a starting point to investigate the role of *Eh*Actn2 *in vivo* and to address its possible role in phagocytosis, a process crucial for amebic virulence.

There are still many unanswered questions related to this project. As mentioned in the "Introduction", it is possible that *Eh*Actn2 is the previously described 70-kDa spectrin-like protein that interacts with the cytoplasmic part of Gal/GalNac lectin (Marion, Tavares et al., 2004), having a vital role for virulence in *E. histolytica*. It would be interesting to see the effect of a knockout of *Eh*Actn2 *in vivo*. Is it possible to understand better the cross-talk between EF1-2 and 3-4 in *Eh*Actn2? Would our rescue experiment work *in vivo*? How does our findings translate to human Ca^{2+}-regulated α-actinins? How many different ways of α-actinin regulation are out there? Is the mechanism of actin bundling common in the members of spectrin family? Finally, are there more actin modulators in the cell which are regulated by such subtle molecular mechanisms?

6 REFERENCES

Ababou A, Desjarlais JR (2001) Solvation energetics and conformational change in EF-hand proteins. Protein Sci 10: 301-12

Addario B, Sandblad L, Persson K, Backman L (2016) Characterisation of Schizosaccharomyces pombe alpha-actinin. PeerJ 4: e1858

Allen JM (1962) The molecular control of cellular activity. McGraw-Hill, New York,

Andra J, Berninghausen O, Leippe M (2004) Membrane lipid composition protects Entamoeba histolytica from self-destruction by its pore-forming toxins. FEBS letters 564: 109-15

Aslam S, Bhattacharya S, Bhattacharya A (2012) The Calmodulin-like Calcium Binding Protein EhCaBP3 of Entamoeba histolytica Regulates Phagocytosis and Is Involved in Actin Dynamics. PLoS Pathogens 8: e1003055

Atkinson RA, Joseph C, Kelly G, Muskett FW, Frenkiel TA, Nietlispach D, Pastore A (2001) Ca2+-independent binding of an EF-hand domain to a novel motif in the alpha-actinin-titin complex. Nature structural biology 8: 853-7

Backman L (2015) Calcium affinity of human alpha-actinin 1. PeerJ 3: e944

Bailey GB, Shen PS, Beanan MJ, McCoomer NE (1992) Actin associated proteins of Entamoeba histolytica. Arch Med Res 23: 129-32

Banuelos S, Saraste M, Djinovic Carugo K (1998) Structural comparisons of calponin homology domains: implications for actin binding. Structure 6: 1419-31

Bennett V, Healy J (2009) Membrane Domains Based on Ankyrin and Spectrin Associated with Cell–Cell Interactions. Cold Spring Harbor Perspectives in Biology 1: a003012

Bharat TAM, Murshudov GN, Sachse C, Löwe J (2015) Structures of actin-like ParM filaments show architecture of plasmid-segregating spindles. Nature 523: 106

Bhattacharya A, Padhan N, Jain R, Bhattacharya S (2006) Calcium-binding proteins of Entamoeba histolytica. Arch Med Res 37: 221-5

Black DJ, Tikunova SB, Johnson JD, Davis JP (2000) Acid pairs increase the N-terminal Ca2+ affinity of CaM by increasing the rate of Ca2+ association. Biochemistry 39: 13831-7

Borrego-Diaz E, Kerff F, Lee SH, Ferron F, Li Y, Dominguez R (2006) Crystal structure of the actin-binding domain of alpha-actinin 1: evaluating two competing actin-binding models. J Struct Biol 155: 230-8

Bresnick AR, Janmey PA, Condeelis J (1991) Evidence that a 27-residue sequence is the actin-binding site of ABP-120. Journal of Biological Chemistry 266: 12989-12993

Burridge K, Feramisco JR (1981) Non-muscle alpha actinins are calcium-sensitive actin-binding proteins. Nature 294: 565-7

Carbajal ME, Manning-Cela R, Pina A, Franco E, Meza I (1996) Fibronectin-induced intracellular calcium rise in Entamoeba histolytica trophozoites: effect on adhesion and the actin cytoskeleton. Exp Parasitol 82: 11-20

Cates MS, Berry MB, Ho EL, Li Q, Potter JD, Phillips GN, Jr. (1999) Metal-ion affinity and specificity in EF-hand proteins: coordination geometry and domain plasticity in parvalbumin. Structure 7: 1269-78

Celio MR, Pauls TL, Schwaller B (1996) Guidebook to the calcium-binding proteins. Sambrook & Tooze Publication at Oxford University Press, Oxford

Chadee K, Petri WA, Jr., Innes DJ, Ravdin JI (1987) Rat and human colonic mucins bind to and inhibit adherence lectin of Entamoeba histolytica. J Clin Invest 80: 1245-54

Corrado K, Mills PL, Chamberlain JS (1994) Deletion analysis of the dystrophin-actin binding domain. FEBS letters 344: 255-260

Craig DH, Haimovich B, Basson MD (2007) α-Actinin-1 phosphorylation modulates pressure-induced colon cancer cell adhesion through regulation of focal adhesion kinase-Src interaction. American Journal of Physiology-Cell Physiology 293: C1862-C1874

Desai A, Mitchison TJ (1997) Microtubule polymerization dynamics. Annu Rev Cell Dev Biol 13: 83-117

Djinovic-Carugo K, Young P, Gautel M, Saraste M (1999) Structure of the alpha-actinin rod: molecular basis for cross-linking of actin filaments. Cell 98: 537-46

Dominguez R, Holmes KC (2011) Actin Structure and Function. Annual Review of Biophysics 40: 169-186

dos Remedios CG, Chhabra D, Kekic M, Dedova IV, Tsubakihara M, Berry DA, Nosworthy NJ (2003) Actin binding proteins: regulation of cytoskeletal microfilaments. Physiol Rev 83: 433-73

Drake SK, Lee KL, Falke JJ (1996) Tuning the equilibrium ion affinity and selectivity of the EF-hand calcium binding motif: substitutions at the gateway position. Biochemistry 35: 6697-705

Drmota Prebil S, Slapsak U, Pavsic M, Ilc G, Puz V, de Almeida Ribeiro E, Anrather D, Hartl M, Backman L, Plavec J, Lenarcic B, Djinovic-Carugo K (2016) Structure and calcium-binding studies of calmodulin-like domain of human non-muscle alpha-actinin-1. Sci Rep 6: 27383

Evenas J, Malmendal A, Thulin E, Carlstrom G, Forsen S (1998) Ca2+ binding and conformational changes in a calmodulin domain. Biochemistry 37: 13744-54

Evenas J, Thulin E, Malmendal A, Forsen S, Carlstrom G (1997) NMR studies of the E140Q mutant of the carboxy-terminal domain of calmodulin reveal global conformational exchange in the Ca2+-saturated state. Biochemistry 36: 3448-57

Fabbrizio E, Bonet-Kerrache A, Leger JJ, Mornet D (1993) Actin-dystrophin interface. Biochemistry 32: 10457-63

Falke JJ, Drake SK, Hazard AL, Peersen OB (1994) Molecular tuning of ion binding to calcium signaling proteins. Q Rev Biophys 27: 219-90

Falke JJ, Snyder EE, Thatcher KC, Voertler CS (1991) Quantitating and engineering the ion specificity of an EF-hand-like Ca2+ binding. Biochemistry 30: 8690-7

Fletcher DA, Mullins RD (2010) Cell mechanics and the cytoskeleton. Nature 463: 485-92

Flood G, Rowe AJ, Critchley DR, Gratzer WB (1997) Further analysis of the role of spectrin repeat motifs in α-actinin dimer formation. European Biophysics Journal 25: 431-435

Foley KS, Young PW (2013) An analysis of splicing, actin-binding properties, heterodimerization and molecular interactions of the non-muscle alpha-actinins. The Biochemical journal 452: 477-88

Franzot G, Sjoblom B, Gautel M, Djinovic Carugo K (2005) The crystal structure of the actin binding domain from alpha-actinin in its closed conformation: structural insight into phospholipid regulation of alpha-actinin. Journal of molecular biology 348: 151-65

Freeman SA, Grinstein S (2014) Phagocytosis: receptors, signal integration, and the cytoskeleton. Immunol Rev 262: 193-215

Gagné SM, Li MX, Sykes BD (1997) Mechanism of Direct Coupling between Binding and Induced Structural Change in Regulatory Calcium Binding Proteins. Biochemistry 36: 4386-4392

Galkin VE, Orlova A, Salmazo A, Djinovic-Carugo K, Egelman EH (2010) Opening of tandem calponin homology domains regulates their affinity for F-actin. Nature structural & molecular biology 17: 614-6

Galkin VE, Orlova A, VanLoock MS, Rybakova IN, Ervasti JM, Egelman EH (2002) The utrophin actin-binding domain binds F-actin in two different modes: implications for the spectrin superfamily of proteins. J Cell Biol 157: 243-51

Ghosh SK, Samuelson J (1997) Involvement of p21racA, phosphoinositide 3-kinase, and vacuolar ATPase in phagocytosis of bacteria and erythrocytes by Entamoeba histolytica: suggestive evidence for coincidental evolution of amebic invasiveness. Infect Immun 65: 4243-9

Gibson DG, Young L, Chuang RY, Venter JC, Hutchison CA, 3rd, Smith HO (2009) Enzymatic assembly of DNA molecules up to several hundred kilobases. Nature methods 6: 343-5

Gifford JL, Walsh MP, Vogel HJ (2007) Structures and metal-ion-binding properties of the Ca2+-binding helix-loop-helix EF-hand motifs. The Biochemical journal 405: 199-221

Gkougkoulia E (2014) Structural Studies on Calcium Regulation of α-Actinin. In University of Vienna

Godsel LM, Hobbs RP, Green KJ (2008) Intermediate filament assembly: dynamics to disease. Trends Cell Biol 18: 28-37

Golji J, Collins R, Mofrad MR (2009) Molecular mechanics of the alpha-actinin rod domain: bending, torsional, and extensional behavior. PLoS Comput Biol 5: e1000389

Grabarek Z (2005) Structure of a trapped intermediate of calmodulin: calcium regulation of EF-hand proteins from a new perspective. Journal of molecular biology 346: 1351-66

Grabarek Z (2006) Structural basis for diversity of the EF-hand calcium-binding proteins. Journal of molecular biology 359: 509-25

Hampton CM, Taylor DW, Taylor KA (2007) Novel Structures for α-Actinin:F-Actin Interactions and their Implications for Actin–Membrane Attachment and Tension Sensing in the Cytoskeleton. Journal of molecular biology 368: 92-104

Hemsley A, Arnheim N, Toney MD, Cortopassi G, Galas DJ (1989) A simple method for site-directed mutagenesis using the polymerase chain reaction. Nucleic Acids Res 17: 6545-51

Henzl MT, Tanner JJ (2008) Solution structure of Ca2+-free rat alpha-parvalbumin. Protein Sci 17: 431-8

Herrmann H, Bar H, Kreplak L, Strelkov SV, Aebi U (2007) Intermediate filaments: from cell architecture to nanomechanics. Nat Rev Mol Cell Biol 8: 562-73

Hirata KK, Que X, Melendez-Lopez SG, Debnath A, Myers S, Herdman DS, Orozco E, Bhattacharya A, McKerrow JH, Reed SL (2007) A phagocytosis mutant of Entamoeba histolytica is less virulent due to deficient proteinase expression and release. Experimental Parasitology 115: 192-199

Honda K, Yamada T, Endo R, Ino Y, Gotoh M, Tsuda H, Yamada Y, Chiba H, Hirohashi S (1998) Actinin-4, a novel actin-bundling protein associated with cell motility and cancer invasion. J Cell Biol 140: 1383-93

Houdusse A, Cohen C (1996) Structure of the regulatory domain of scallop myosin at 2 å resolution: implications for regulation. Structure 4: 21-32

Houdusse A, Gaucher JF, Krementsova E, Mui S, Trybus KM, Cohen C (2006) Crystal structure of apo-calmodulin bound to the first two IQ motifs of myosin V reveals essential recognition features. Proc Natl Acad Sci U S A 103: 19326-31

Ikura M (1996) Calcium binding and conformational response in EF-hand proteins. Trends Biochem Sci 21: 14-7

Iwasaki W, Sasaki H, Nakamura A, Kohama K, Tanokura M (2003) Metal-free and Ca2+-bound structures of a multidomain EF-hand protein, CBP40, from the lower eukaryote Physarum polycephalum. Structure 11: 75-85

Izore T, Kureisaite-Ciziene D, McLaughlin SH, Lowe J (2016) Crenactin forms actin-like double helical filaments regulated by arcadin-2. Elife 5

Jayadev R, Kuk CY, Low SH, Murata-Hori M (2012) Calcium sensitivity of α-actinin is required for equatorial actin assembly during cytokinesis. Cell Cycle 11: 1929-1937

Karlsson G, Persson C, Mayzel M, Hedenstrom M, Backman L (2016) Solution structure of the calmodulin-like C-terminal domain of Entamoeba alpha-actinin2. Proteins 84: 461-6

Katz AK, Glusker JP, Beebe SA, Bock CW (1996) Calcium Ion Coordination: A Comparison with That of Beryllium, Magnesium, and Zinc. Journal of the American Chemical Society 118: 5752-5763

Katz U, Ankri S, Stolarsky T, Nuchamowitz Y, Mirelman D (2002) Entamoeba histolytica expressing a dominant negative N-truncated light subunit of its gal-lectin are less virulent. Mol Biol Cell 13: 4256-65

Kawasaki H, Kretsinger RH (2012) Analysis of the movements of helices in EF-hands. Proteins 80: 2592-600

Kawasaki H, Nakayama S, Kretsinger RH (1998) Classification and evolution of EF-hand proteins. Biometals 11: 277-95

Kollman JM, Merdes A, Mourey L, Agard DA (2011) Microtubule nucleation by gamma-tubulin complexes. Nat Rev Mol Cell Biol 12: 709-21

Korsgren C, Lux SE (2010) The carboxyterminal EF domain of erythroid α-spectrin is necessary for optimal spectrin-actin binding. Blood 116: 2600-2607

Kos CH, Le TC, Sinha S, Henderson JM, Kim SH, Sugimoto H, Kalluri R, Gerszten RE, Pollak MR (2003) Mice deficient in α-actinin-4 have severe glomerular disease. The Journal of Clinical Investigation 111: 1683-1690

Kretsinger RH, Nockolds CE (1973) Carp muscle calcium-binding protein. II. Structure determination and general description. The Journal of biological chemistry 248: 3313-26

Kuhlman PA, Hemmings L, Critchley DR (1992) The identification and characterisation of an actin-binding site in α-actinin by mutagenesis. FEBS letters 304: 201-206

Kumar S, Aslam S, Mazumder M, Dahiya P, Murmu A, Manjasetty BA, Zaidi R, Bhattacharya A, Gourinath S (2014) Crystal structure of calcium binding protein-5 from Entamoeba histolytica and its involvement in initiation of phagocytosis of human erythrocytes. PLoS Pathog 10: e1004532

Lee FXZ, Houweling PJ, North KN, Quinlan KGR (2016) How does α-actinin-3 deficiency alter muscle function? Mechanistic insights into ACTN3, the 'gene for speed'. Biochimica et Biophysica Acta (BBA) - Molecular Cell Research 1863: 686-693

Lek M, MacArthur DG, Yang N, North KN (2010) Phylogenetic analysis of gene structure and alternative splicing in alpha-actinins. Molecular biology and evolution 27: 773-80

Levine BA, Moir AJG, Patchell VB, Perry SV (1990) The interaction of actin with dystrophin. FEBS letters 263: 159-162

Levine BA, Moir AJG, Patchell VB, Perry SV (1992) Binding sites involved in the interaction of actin with the N-terminal region of dystrophin. FEBS letters 298: 44-48

Lide DR, Chemical Rubber Company. (1999) CRC handbook of chemistry and physics : a ready-reference book of chemical and physical data. CRC Press, Boca Raton ; London

Liem RK (2016) Cytoskeletal Integrators: The Spectrin Superfamily. Cold Spring Harb Perspect Biol 8

Lodish HF, Berk A, Kaiser C, Krieger M, Bretscher A, Ploegh HL, Amon A, Scott MP (2013) Molecular cell biology. W.H. Freeman and Company, New York

Loftus B, Anderson I, Davies R, Alsmark UC, Samuelson J, Amedeo P, Roncaglia P, Berriman M, Hirt RP, Mann BJ, Nozaki T, Suh B, Pop M, Duchene M, Ackers J, Tannich E, Leippe M, Hofer M, Bruchhaus I, Willhoeft U et al. (2005) The genome of the protist parasite Entamoeba histolytica. Nature 433: 865-8

MacArthur DG, Seto JT, Raftery JM, Quinlan KG, Huttley GA, Hook JW, Lemckert FA, Kee AJ, Edwards MR, Berman Y, Hardeman EC, Gunning PW, Easteal S, Yang N, North KN (2007) Loss of ACTN3 gene function alters mouse muscle metabolism and shows evidence of positive selection in humans. Nature genetics 39: 1261

Makioka A, Kumagai M, Ohtomo H, Kobayashi S, Takeuchi T (2001) Effect of calcium antagonists, calcium channel blockers and calmodulin inhibitors on the growth and encystation of Entamoeba histolytica and E. invadens. Parasitol Res 87: 833-7

Maler L, Blankenship J, Rance M, Chazin WJ (2000) Site-site communication in the EF-hand Ca2+-binding protein calbindin D9k. Nature structural biology 7: 245-50

Malmendal A, Linse S, Evenas J, Forsen S, Drakenberg T (1999) Battle for the EF-hands: magnesium-calcium interference in calmodulin. Biochemistry 38: 11844-50

Mansuri MS, Bhattacharya S, Bhattacharya A (2014) A novel alpha kinase EhAK1 phosphorylates actin and regulates phagocytosis in Entamoeba histolytica. PLoS Pathog 10: e1004411

Marion S, Guillen N (2006) Genomic and proteomic approaches highlight phagocytosis of living and apoptotic human cells by the parasite Entamoeba histolytica. Int J Parasitol 36: 131-9

Marion S, Tavares P, Arhets P, Guillén N (2004) Signal transduction through the Gal–GalNAc lectin of Entamoeba histolytica involves a spectrin-like protein. Molecular and biochemical parasitology 135: 31-38

Martin SR, Linse S, Johansson C, Bayley PM, Forsen S (1990) Protein surface charges and Ca2+ binding to individual sites in calbindin D9k: stopped-flow studies. Biochemistry 29: 4188-93

Mazumder M, Padhan N, Bhattacharya A, Gourinath S (2014) Prediction and analysis of canonical EF hand loop and qualitative estimation of Ca(2)(+) binding affinity. PloS one 9: e96202

Merino F, Raunser S (2016) The mother of all actins? eLife 5: e23354

Meza I, Sabanero M, Cazares F, Bryan J (1983) Isolation and characterization of actin from Entamoeba histolytica. The Journal of biological chemistry 258: 3936-41

Meza I, Talamas-Rohana P, Vargas MA (2006) The cytoskeleton of Entamoeba histolytica: structure, function, and regulation by signaling pathways. Arch Med Res 37: 234-43

Murphy AC, Young PW (2015) The actinin family of actin cross-linking proteins - a genetic perspective. Cell Biosci 5: 49

Nelson MR, Chazin WJ (1998) An interaction-based analysis of calcium-induced conformational changes in Ca2+ sensor proteins. Protein Sci 7: 270-82

Nickel R, Jacobs T, Urban B, Scholze H, Bruhn H, Leippe M (2000) Two novel calcium-binding proteins from cytoplasmic granules of the protozoan parasite Entamoeba histolytica. FEBS letters 486: 112-6

Nozaki T, Bhattacharya A Amebiasis : biology and pathogenesis of entamoeba. In p 1 online resource.

Oda T, Iwasa M, Aihara T, Maeda Y, Narita A (2009) The nature of the globular- to fibrous-actin transition. Nature 457: 441-5

Ohki S-y, Ikura M, Zhang M (1997) Identification of Mg2+-Binding Sites and the Role of Mg2+ on Target Recognition by Calmodulin. Biochemistry 36: 4309-4316

Okada M, Huston CD, Mann BJ, Petri WA, Jr., Kita K, Nozaki T (2005) Proteomic analysis of phagocytosis in the enteric protozoan parasite Entamoeba histolytica. Eukaryot Cell 4: 827-31

Orozco E, Guarneros G, Martinez-Palomo A, Sanchez T (1983) Entamoeba histolytica. Phagocytosis as a virulence factor. J Exp Med 158: 1511-21

Otey CA, Carpen O (2004) Alpha-actinin revisited: a fresh look at an old player. Cell motility and the cytoskeleton 58: 104-11

Park KR, Kwon MS, An JY, Lee JG, Youn HS, Lee Y, Kang JY, Kim TG, Lim JJ, Park JS, Lee SH, Song WK, Cheong HK, Jun CD, Eom SH (2016) Structural implications of Ca(2+)-dependent actin-bundling function of human EFhd2/Swiprosin-1. Sci Rep 6: 39095

Pascual J, Castresana J, Saraste M (1997) Evolution of the spectrin repeat. Bioessays 19: 811-7

Peersen OB, Madsen TS, Falke JJ (1997) Intermolecular tuning of calmodulin by target peptides and proteins: differential effects on Ca2+ binding and implications for kinase activation. Protein Sci 6: 794-807

Petri WA, Jr., Smith RD, Schlesinger PH, Murphy CF, Ravdin JI (1987) Isolation of the galactose-binding lectin that mediates the in vitro adherence of Entamoeba histolytica. The Journal of Clinical Investigation 80: 1238-1244

Petry S, Groen AC, Ishihara K, Mitchison TJ, Vale RD (2013) Branching microtubule nucleation in Xenopus egg extracts mediated by augmin and TPX2. Cell 152: 768-77

Pidcock E, Moore GR (2001) Structural characteristics of protein binding sites for calcium and lanthanide ions. J Biol Inorg Chem 6: 479-89

Potter JD, Gergely J (1975) The calcium and magnesium binding sites on troponin and their role in the regulation of myofibrillar adenosine triphosphatase. The Journal of biological chemistry 250: 4628-33

Ralston KS (2015) Chew on this: Amoebic trogocytosis and host cell killing by Entamoeba histolytica. Trends in parasitology 31: 442-452

Ralston KS, Solga MD, Mackey-Lawrence NM, Somlata, Bhattacharya A, Petri WA, Jr. (2014) Trogocytosis by Entamoeba histolytica contributes to cell killing and tissue invasion. Nature 508: 526-30

Rauert W, Eddine AN, Kaufmann SH, Weiss MS, Janowski R (2007) Reductive methylation to improve crystallization of the putative oxidoreductase Rv0765c from Mycobacterium tuberculosis. Acta crystallographica Section F, Structural biology and crystallization communications 63: 507-11

Ravdin JI, Moreau F, Sullivan JA, Petri WA, Jr., Mandell GL (1988) Relationship of free intracellular calcium to the cytolytic activity of Entamoeba histolytica. Infect Immun 56: 1505-12

Ravdin JI, Murphy CF, Guerrant RL, Long-Krug SA (1985a) Effect of antagonists of calcium and phospholipase A on the cytopathogenicity of Entamoeba histolytica. J Infect Dis 152: 542-9

Ravdin JI, Murphy CF, Salata RA, Guerrant RL, Hewlett EL (1985b) N-Acetyl-D-galactosamine-inhibitable adherence lectin of Entamoeba histolytica. I. Partial purification and relation to amoebic virulence in vitro. J Infect Dis 151: 804-15

Ravelli RBG, Gigant B, Curmi PA, Jourdain I, Lachkar S, Sobel A, Knossow M (2004) Insight into tubulin regulation from a complex with colchicine and a stathmin-like domain. Nature 428: 198

Reid RE (1990) Synthetic fragments of calmodulin calcium-binding site III. A test of the acid pair hypothesis. The Journal of biological chemistry 265: 5971-6

Renner M, Danielson MA, Falke JJ (1993) Kinetic control of Ca(II) signaling: tuning the ion dissociation rates of EF-hand Ca(II) binding sites. Proc Natl Acad Sci U S A 90: 6493-7

Ribeiro Ede A, Jr., Pinotsis N, Ghisleni A, Salmazo A, Konarev PV, Kostan J, Sjoblom B, Schreiner C, Polyansky AA, Gkougkoulia EA, Holt MR, Aachmann FL, Zagrovic B, Bordignon E, Pirker KF, Svergun DI, Gautel M, Djinovic-Carugo K (2014) The structure and regulation of human muscle alpha-actinin. Cell 159: 1447-60

Rodriguez MA, Orozco E (1986) Isolation and characterization of phagocytosis- and virulence-deficient mutants of Entamoeba histolytica. J Infect Dis 154: 27-32

Romani A, Scarpa A (1992) Regulation of cell magnesium. Arch Biochem Biophys 298: 1-12

Romani AM (2011) Cellular magnesium homeostasis. Arch Biochem Biophys 512: 1-23

Roostalu J, Surrey T (2017) Microtubule nucleation: beyond the template. Nat Rev Mol Cell Biol 18: 702-710

Rupp B, Marshak DR, Parkin S (1996) Crystallization and preliminary X-ray analysis of two new crystal forms of calmodulin. Acta crystallographica Section D, Biological crystallography 52: 411-3

Sabanero M, Meza I (1982) [Localization of actin in trophozoites of Entamoeba histolytica (HMI)]. Arch Invest Med (Mex) 13 Suppl 3: 37-42

Sahoo N, Labruyère E, Bhattacharya S, Sen P, Guillén N, Bhattacharya A (2004) Calcium binding protein 1 of the protozoan parasite Entamoeba histolytica interacts with actin and is involved in cytoskeleton dynamics. Journal of Cell Science 117: 3625-3634

Sateriale A, Huston CD (2011) A Sequential Model of Host Cell Killing and Phagocytosis by Entamoeba histolytica. J Parasitol Res 2011: 926706

Schwaller B (2009) The continuing disappearance of "pure" Ca2+ buffers. Cellular and molecular life sciences : CMLS 66: 275-300

Sen S, Dong M, Kumar S (2009) Isoform-Specific Contributions of α-Actinin to Glioma Cell Mechanobiology. PloS one 4: e8427

Shih YL, Rothfield L (2006) The bacterial cytoskeleton. Microbiol Mol Biol Rev 70: 729-54

Singh Surinder M, Mallela Krishna MG (2012) The N-Terminal Actin-Binding Tandem Calponin-Homology (CH) Domain of Dystrophin Is in a Closed Conformation in Solution and When Bound to F-actin. Biophysical Journal 103: 1970-1978

Stanley SL, Jr. (2003) Amoebiasis. Lancet 361: 1025-34

Stossel TP, Chaponnier C, Ezzell RM, Hartwig JH, Janmey PA, Kwiatkowski DJ, Lind SE, Smith DB, Southwick FS, Yin HL, et al. (1985) Nonmuscle actin-binding proteins. Annu Rev Cell Biol 1: 353-402

Strynadka NC, James MN (1989) Crystal structures of the helix-loop-helix calcium-binding proteins. Annu Rev Biochem 58: 951-98

Studier FW (2005) Protein production by auto-induction in high density shaking cultures. Protein expression and purification 41: 207-34

Swindells MB, Ikura M (1996) Pre-formation of the semi-open conformation by the apo-calmodulin C-terminal domain and implications binding IQ-motifs. Nature structural biology 3: 501-4

Tang J, Taylor DW, Taylor KA (2001) The three-dimensional structure of alpha-actinin obtained by cryoelectron microscopy suggests a model for Ca(2+)-dependent actin binding. Journal of molecular biology 310: 845-58

Tee YH, Shemesh T, Thiagarajan V, Hariadi RF, Anderson KL, Page C, Volkmann N, Hanein D, Sivaramakrishnan S, Kozlov MM, Bershadsky AD (2015) Cellular chirality arising from the self-organization of the actin cytoskeleton. Nature Cell Biology 17: 445

Trave G, Lacombe PJ, Pfuhl M, Saraste M, Pastore A (1995) Molecular mechanism of the calcium-induced conformational change in the spectrin EF-hands. EMBO J 14: 4922-31

Vangone A, Bonvin AM (2015) Contacts-based prediction of binding affinity in protein-protein complexes. Elife 4: e07454

Verkhratskiĭ AN, Toescu EC (1998) Integrative aspects of calcium signalling. Plenum Press, New York ; London

Viel A (1999) Alpha-actinin and spectrin structures: an unfolding family story. FEBS letters 460: 391-4

Virel A, Addario B, Backman L (2007) Characterization of Entamoeba histolytica alpha-actinin2. Molecular and biochemical parasitology 154: 82-9

Virel A, Backman L (2007) A comparative and phylogenetic analysis of the alpha-actinin rod domain. Molecular biology and evolution 24: 2254-65

von der Ecken J, Muller M, Lehman W, Manstein DJ, Penczek PA, Raunser S (2015) Structure of the F-actin-tropomyosin complex. Nature 519: 114-7

Wilson MA, Brunger AT (2000) The 1.0 A crystal structure of Ca(2+)-bound calmodulin: an analysis of disorder and implications for functionally relevant plasticity. Journal of molecular biology 301: 1237-56

Winder SJ (1996) Structure-function relationships in dystrophin and utrophin. Biochem Soc Trans 24: 497-501

Winder SJ, Ayscough KR (2005) Actin-binding proteins. Journal of Cell Science 118: 651-654

Wu JQ, Bahler J, Pringle JR (2001) Roles of a fimbrin and an alpha-actinin-like protein in fission yeast cell polarization and cytokinesis. Mol Biol Cell 12: 1061-77

Yang N, MacArthur DG, Gulbin JP, Hahn AG, Beggs AH, Easteal S, North K (2003) ACTN3 Genotype Is Associated with Human Elite Athletic Performance. The American Journal of Human Genetics 73: 627-631

Yap KL, Ames JB, Swindells MB, Ikura M (1999) Diversity of conformational states and changes within the EF-hand protein superfamily. Proteins 37: 499-507

Ye Y, Lee HW, Yang W, Shealy S, Yang JJ (2005) Probing site-specific calmodulin calcium and lanthanide affinity by grafting. J Am Chem Soc 127: 3743-50

Ylanne J, Scheffzek K, Young P, Saraste M (2001) Crystal structure of the alpha-actinin rod reveals an extensive torsional twist. Structure 9: 597-604

Zhang M, Tanaka T, Ikura M (1995) Calcium-induced conformational transition revealed by the solution structure of apo calmodulin. Nature structural biology 2: 758-67

7 APPENDIX

Table I. X-ray crystallographic data collection and refinement statistics.

	***Eh*Actn2 (tetragonal)**	***Eh*Actn2 (orthorombic)**	**ΔCa (orthorombic)**
Data collection			
Beamline	I03 (Diamond)	ID29 (ESRF)	ID23-1 and ID30-A3 (ESRF)
Wavelength (Å)	0.97860	1.00576	0.968620
Resolution Range (Å)	41.65 – 3.10	46.24 – 3.10	46.85 – 3.30
	(3.31 – 3.10)*	(3.17 – 3.10)	(3.38 – 3.30)
Space group	P 4_2 2_1 2	P 2 2 2_1	P 2 2 2_1
Cell parameters a, b, c (Å	192.3, 192.3, 57.17	43.21, 71.84, 241.70	40.74, 75.53, 234.25
Total reflections	174,399	100,558	49,197
Unique reflections	20,112	14,460	10,696
Multiplicity	8.7 (7.6)	7.0 (6.8)	4.6 (4.1)
Completeness (%)	100.0 (99.9)	99.1 (95.3)	97.8 (77.0)
Mean I/Sigma(I)	13.6 (1.3)	8.57 (0.48)	11.57 (1.66)
Wilson B-factor (Å^2)	114.0	126.6	120.1
R_{merge} (%)	10.9 (143.6)	13.3 (555.4)	8.4 (85.0)
CC1/2 (%)	98.4 (71.4)	99.9 (43.3)	99.8 (76.9)
Software	XDS/Aimless	XDS/XSCALE	XDS/XSCALE
Refinement			
R_{work}/R_{free} (%)	21.49/25.14	25.91/32.45	26.14/32.40
CC_{work}/CC_{free} (%)	96.3 / 95.7	95.1 / 87.7	94.0 / 92.0
Protein atoms	4,852	4,730	4,792
Solvent molecules			
Other atoms	1 Ca^{2+}	1 Ca^{2+}	
B-factor (Å^2)			
Protein	117.2	82.7	210.8
Solvent			
Ramachandran Plot			
Favored (%)	97.06	94.81	94.97
Allowed (%)	2.76	4.38	4.54
Outliers (%)	0.17	0.81	0.49
Clashscore	7.82	20.51	10.93
Rmsd			
Bonds (Å)	0.003	0.013	0.010
Angles (grad)	0.573	1.745	1.682
Software	PHENIX	Refmac5	Refmac5

*Values in parentheses refer to the outermost resolution shell.

Table II. Author contribution list

Mag. Karolina Zielinska	Molecular cloning of all constructs used in this work (except *Eh*Actn2 WT, ΔCa, ΔEF3-4, ΔEF1-4 and rod) Expression and purification of all proteins used for biophysical and biochemical assays Crystallization of ΔCa ITC experiments Oregon-Green-BAPTA competition assays SLS experiments DSF experiments Limited proteolysis CD experiments Analysis of ΔEF3-4 and rod disulfide-bonded mutants F-actin bundling and binding experiments Preparation of samples for negative-staining EM
Dr. Joan Lopez Arolas	Determination of ΔCa crystal structure
Dr. Muhammad Bashir Khan	Crystallization and structure determination of *Eh*Actn2 ABD, rod and tetragonal Ca^{2+}-bound *Eh*Actn2 WT
Dr. Eirini Gkougkoulia	Expression, purification and crystallization of orthogonal Ca^{2+}-bound *Eh*Actn2 WT
Dr. Nikos Pinotsis	Final refinement of all crystal structures
Ing. Claudia Schreiner	Purification and crystallization of *Eh*Actn2 ABD and rod Purification of rabbit actin used for biochemical assays
Dr. Martin Gerald Puchinger	Time-resolved FA experiments
Dr. Luciano Ciccarelli	EM imaging of negatively-stained grids
Dr. Mrigya Babuta	*In vivo* experiments (generation of amebic stable cell lines, confocal microscopy, co-localization studies, erythrocyte uptake assay, mobility assays)